INVESTIGATION OF AERODYNAMIC CHARACTERISTICS OF SUBSONIC WINGS

by

Fred R. DeJarnette and Neal T. Frink

Mechanical and Aerospace Engineering
North Carolina State University
Raleigh, North Carolina 27650

(NASA-CR-158661) INVESTIGATION OF AERODYNAMIC CHARACTERISTICS OF SUBSONIC WINGS Final Report (North Carolina State Univ.) 148 p HC A07/MF A01 CSCL 01A

N79-23921

Unclas
G3/02 22124

FINAL TECHNICAL REPORT

on

NASA Grant NSG 1437

with

NASA Langley Research Center
Hampton, Virginia 23665

June 11, 1979

JUN 1979
RECEIVED
NASA STI FACILITY
ACCESS DEPT.

FOREWORD

The Final Technical Report for NASA Grant NSG 1437 is embodied in the attached M.S. thesis by Mr. Neal T. Frink entitled "Water Tunnel and Analytical Investigation of the Effect of Strake Design Variables on Strake Vortex Breakdown Characteristics in the Presence of Wing-Body". This grant covered the period from July 25, 1977 to May 15, 1979. Principal Investigator was Dr. Fred R. DeJarnette of North Carolina State University and the NASA Technical Officer was Dr. James F. Campbell, Mail Stop 287, NASA Langley Research Center, Hampton, Virginia 23665.

WATER TUNNEL AND ANALYTICAL INVESTIGATION OF THE EFFECT OF STRAKE DESIGN VARIABLES ON STRAKE VORTEX BREAKDOWN CHARACTERISTICS IN THE PRESENCE OF WING-BODY

by

NEAL T. FRINK

A thesis submitted to the Graduate Faculty of
North Carolina State University
in partial fulfillment of the
requirements for the Degree of
Master of Science

DEPARTMENT OF MECHANICAL AND AEROSPACE ENGINEERING

RALEIGH

1 9 7 9

Approved by

Fred R. DeJarnette

Chairman of Advisory Committee

J. M. A. Danby

James F. Campbell

ABSTRACT

FRINK, NEAL T. Water Tunnel and Analytical Investigation of the Effect of Strake Design Variables on Strake Vortex-Breakdown Characteristics In The Presence of Wing-Body. (Under the direction of Dr. F. R. DeJarnette.)

An analytical strake design procedure is investigated. A numerical solution to the governing strake design equation is used to generate a series of strakes which are tested in a water tunnel to study their vortex breakdown characteristics. The strakes are scaled for use on a half-scale model of the NASA-LaRC general research fuselage with a 44° trapezoidal wing. In addition, an analytical solution to the governing design equation is obtained.

The strake design procedure relates the potential-flow leading-edge suction and pressure distributions to vortex stability. Several suction distributions are studied and it is found that those which are more triangular and peak near the tip generate strakes that reach higher angles of attack before vortex breakdown occurs at the wing trailing edge. In addition, for the same suction distribution, a conical rather than three dimensional pressure specification results in a better strake shape as judged from its vortex breakdown characteristics.

Several techniques are investigated for reducing the chord of an existing strake while maintaining as much of the benefit of the

original design as possible. It is found that cutting along the trailing edge is the most favorable method for making moderate chord reductions.

Effects of initial sweep, slenderness ratio, and size are investigated. Though no relationship for initial sweep effects can be established, it is found that strakes with higher slenderness ratio have better vortex breakdown characteristics. Of all the strake shapes designed and tested, i.e. reflexive, gothic, and delta gothic, the gothic had the superior vortex breakdown characteristics.

BIOGRAPHY

NEAL TILSON FRINK was born in Asheville, North Carolina on November 23, 1953. He was reared in Asheville (Buncombe County) and graduated from A.C. Reynolds High School in May, 1972. He attended North Carolina State University, Raleigh, North Carolina as an Aerospace Engineering major while supplementing his education through a cooperative education program with NASA-Langley Research Center, Hampton, Virginia. He received a Bachelor of Science degree with a major in Aerospace Engineering in May, 1977.

In July, 1977 the author accepted a research assistantship from North Carolina State University to pursue a Masters degree in Aerospace Engineering. The research was funded by a grant from NASA-Langley Research Center. The grant included one-year of on campus scholastic study and an additional one-year of thesis research at NASA-Langley Research Center.

The author's major field of interest lies in the area of aerodynamics and fluid dynamics with a minor in mathematics. As a result of his co-op experience and thesis research work at NASA-Langley Research Center, Hampton, Virginia, the author received a variety of working experience in addition to his scholastic development ranging from experimental wind tunnel research to theoretical/analytical work.

ACKNOWLEDGEMENTS

The author wishes to express his deepest appreciation to the people who made this work possible. First, he would like to extend his very special thanks to Dr. F. R. DeJarnette, chairman of his advisory committee, whose assistance, guidance, and personal interest has been invaluable. A special thanks is also extended to Dr. J. E. Lamar for his expert advice, encouragement and many hours of council throughout this research and its writing.

Particular appreciation is extended to Dr. J. F. Campbell for making this work possible, and expressing his confidence in the author. Also, special thanks are extended to A. M. Skow and G. E. Erikson of Northrop Corporation/Aircraft Division, Los Angeles, California for making this effort a reality by allowing the use of Northrop's 16 x 24 inch diagnostic water tunnel facility and providing personnel for assisting in the tests.

TABLE OF CONTENTS

Page

LIST OF TABLES viii

LIST OF FIGURES ix

LIST OF SYMBOLS xii

INTRODUCTION 1

STRAKE DESIGN PROCEDURE 3

General 3

Criterion 4

Description of Method 4

$c_s c$-η Description 5

ΔC_p Specification 7

Characteristics of the Solution 8

STRAKE SHAPES STUDIED 9

Configurations Selected 9

Parametric Selections 10

Basic Strake Series 11

Snagged Strakes 12

Strake III 13

BASIC FUSELAGE-WING DESCRIPTION 15

TEST FACILITY AND PROCEDURE 16

RESULTS AND DISCUSSION 17

CORRELATION WITH WIND TUNNEL DATA 25

TABLE OF CONTENTS (Continued)

Page

CONCLUSIONS 26

APPENDICES

Appendix A. Basic Equations Used in Strake Shape Development 29

Appendix B. Analytical Solution to the Basic Strake Design Equation 34

REFERENCES 41

LIST OF TABLES

Page

1. Pertinent geometric properties of basic strake series 43

2. Basic data presentation and pertinent suction characteristics 44

3. Qualitative evaluation of strake vortex stability - by groups 45

LIST OF FIGURES

Page

1. Water tunnel photograph of wing, flow field at $\alpha = 20^{\circ}$ 46

2. Photograph of vortex flow generated by highly swept maneuver strakes on the General Dynamics YF-16 lightweight fighter 47

3. Delta wing vortex breakdown angle correlation with leading-edge suction distribution 48

4. Design parameters and resulting strake shape - Original gothic shape of ref. 1 49

5. Leading edge suction distributions studied 50

6. Lifting pressure distributions studied 53

7. Design parameters and resulting strake shape - Reflexive group 54

8. Design parameters and resulting strake shape - Gothic group 65

9. Design parameters and resulting strake shape - Limiting case 74

10. Area scaling of original strake/SA-1: SA Series 75

11. Chordwise scaling of original strake/SX-10: SX Series 76

12. Addition of trailing edge area/side edge length to the SX-3 strake: SE Series 77

13. Generation of apex cut strakes from the original strake: SC-A Series 78

14. Generation of trailing edge cut strakes from the original strake: SC-T Series 79

15. Generation of spanwise cut strakes from the original strake: SC-S Series 80

16. Snagged variations of the SX-3 strake 81

17. Strake III of reference 7 82

Page

18. Drawing of water tunnel wing-fuselage model with wing in forward position 83

19. Northrop 16 x 24 inch diagnostic water tunnel 84

20. Group 3 water tunnel photographs and strake vortex breakdown characteristics 85

21. Group 4, 5, and 6 water tunnel photographs and strake vortex breakdown characteristics 87

22. Group 8 water tunnel photographs and strake vortex breakdown characteristics 89

23. Group 10 water tunnel photographs and strake vortex breakdown characteristics 91

24. Group 11 water tunnel photographs and strake vortex breakdown characteristics 93

25. Group 12 water tunnel photographs and strake vortex breakdown characteristics 95

26. Group 13 water tunnel photographs and strake vortex breakdown characteristics 97

27. SA series water tunnel photographs and strake vortex breakdown characteristics 99

28. SX series water tunnel photographs and strake vortex breakdown characteristics 101

29. Apex cut series water tunnel photographs and strake vortex breakdown characteristics 103

30. Trailing edge cut series water tunnel photographs and strake vortex breakdown characteristics 105

31. Spanwise cut series water tunnel photographs and strake vortex breakdown characteristics 107

32. SE series water tunnel photographs and strake vortex breakdown characteristics 109

33. Snagged strake series water tunnel photographs and strake vortex breakdown characteristics 111

34. Strake III of ref. 7 water tunnel photograph and strake vortex breakdown characteristics 113

Page

35. Summary of strake vortex breakdown position for the "better" strakes from the suction distribution group study 115

36. Effect of suction distribution on vortex breakdown position for two strakes with $[\ell/b/2)]_s = 7.0$ and $[(b/2)_s/(b/2)_w]_{exp} = 0.212$ 117

37. Summary of vortex breakdown characteristics for area scaling: SA series 118

38. Effect of strake geometry on vortex breakdown position for a fixed ratio of strake area to wing reference area 119

39. Summary of trailing edge breakdown angle for the various chord modification techniques 121

40. Summary of strake vortex breakdown characteristics for chord modification by chordwise scaling: SX series 122

41. Summary of strake vortex breakdown characteristics for chord modification by apex cutting: SC-A series 123

42. Summary of strake vortex breakdown characteristics for chord modification by trailing edge cutting: SC-T series . . . 124

43. Summary of strake vortex breakdown characteristics for chord modification by spanwise cutting: SC-S series 125

44. Summary of strake vortex breakdown characteristics for chord modification by addition of trailing edge area/side edge length: SE Series 126

45. Effect of slenderness ratio on wing trailing edge breakdown angle for gothic strakes with $[(b/2)_s/(b/2)_w]_{exp} = 0.212$ 127

46. Effect of strake shape on wing trailing edge breakdown angle for a strake semispan of $[(b/2)_s/(b/2)_w]_{exp} = 0.212$ . . . 128

47. Effect of strake geometry on vortex breakdown position for a fixed slenderness ratio 129

48. Wind tunnel force and water tunnel vortex breakdown data for two wing-strake configurations; M = .2, .3 131

LIST OF SYMBOLS

A	parameter defined by eq. (B-14)
a_1	constant
$\bar{a}$	constant, $a_1/C_1^{\,2}$
B	parameter defined by eq. (B-15)
b	span, cm (in.)
b_1	constant
$\bar{b}$	constant, $b_1/C_1^{\,2}$
C	parameter defined by eq. (B-16)
C_L	lift coefficient, lift/$q_\infty S_{ref}$
$\Delta C_p(\theta,\eta)$	lifting pressure coefficient at θ,η
C_o	constant
C_1	constant
C_2	constant
C_3	constant
$c(\eta)$	local chord, cm (in.)
c_r	root chord along side of fuselage, cm (in.)
c_t	tip chord of strake, cm (in.)
$c_s c\|_\eta$	local suction force/q_∞, cm (in.)
F	parameter defined by eq. (B-10)
f	parameter defined by eq. (B-8)
G	parameter defined by eq. (B-11)
$\bar{G}$	parameter defined by eq. (A-4)

g	parameter defined by eq. (B-9)
$\bar{H}$	parameter defined by eq. (A-6)
K_1	$\tan \Lambda_t$, a constant
ℓ	exposed longitudinal length of strake, cm (in.)
$\ell/(b/2)$	slenderness ratio of exposed strake
M	Mach number
P_1	parameter defined by eq. (B-20)
P_2	parameter defined by eq. (B-21)
Q	parameter defined by eq. (B-13)
$q_o(\eta)$	coefficient of $\cot(\theta/2)$ lifting pressure function, N/m
$q_j(\eta)$	coefficient of $\sin(j\theta)$ lifting pressure function, N/m
q_∞	free stream dynamic pressure, N/m^2
R	parameter defined by eq. (B-12).
R_a	ratio of exposed strake area to wing reference area
S	area, m^2 (in^2)
U	free stream velocity, m/sec (feet/sec)
VLM	Vortex Lattice Method
x	longitudinal distance from wing trailing edge to vortex breakdown, cm (in.)
$x/(c_r)_w$	non-dimensionalized chordwise vortex breakdown position
z	$\tan \Lambda_\ell(\eta)$
α	angle of attack, deg
β	$\sqrt{1 - M^2}$
η	spanwise coordinate in fractions of exposed semispan

η^*	η value where $c_s c$ vs η changes slope
θ	angular distance along local chord, 0 at leading edge π at trailing edge
Λ	constant leading-edge sweep angle, deg
$\Lambda_\ell(\eta)$	leading edge sweep angle function, deg
Λ_t	constant trailing edge sweep angle, deg
ξ	strake chordwise scaling factor

Subscripts

BD	breakdown
exp	exposed
le	leading edge
max	maximum
ref	reference
s	strake
se	side edge
TE	trailing edge
w	wing
ws	wing-strake

INTRODUCTION

One measure of the superiority of today's high performance aircraft is their ability to maneuver. Transonic maneuverability is subject to a large extent on the availability of excess lift. For a basic wing-body configuration with no flow controlling devices, the wing flow field can be extremely disorganized within the maneuver angle-of-attack range as shown in figure 1. This disorganized flow field signifies a substantial loss in lift. In an attempt to recover this lift loss, new wing designs are sought which maintain an organized flow field throughout the maneuver angle-of-attack range.

One design that has received considerable attention in recent years, as evidenced by the F-16 and F/A-18 aircraft, is the use of a strake in combination with a wing (see figure 2). The increased lift on the strake-wing configuration is realized from separation-induced vortex-flow on the strake itself as well as from the favorable interference of the strake vortex on the wing. The strake vortex induces a spanwise flow on the wing which has the effect of organizing the wing flow field. This means that higher angles-of-attack can be reached and consequently more lift developed before the wing stalls. At very large angles-of-attack, the strake vortex starts to breakdown aft of the wing trailing-edge. This phenomenon is characterized by a trumpeting and subsequent dissipation of energy in the vortex core. When this vortex breakdown occurs over the wing, the favorable interference effects diminish and a decrease in lift results.

Over 100 strakes were tested by each company during the development of the F-16 and F/A-18 aircraft before final designs were selected. During their development, no analytical procedure was available for the design of strake shapes which would generate well organized vortex systems at high angles-of-attack or lift coefficients. Since then, a strake design procedure has been developed which relates the potential flow leading-edge suction and pressure distributions to vortex stability. This procedure was utilized in the design of a strake used in reference 1 and is described there as well as repeated in Appendix A here. In this thesis, the procedure is applied to design some 21 strakes and to explore the utility of the method and assess the validity of its assumptions. In addition, an analytical solution is found for the correlative equation given in reference 1 governing strake design. This solution is presented in Appendix B.

As a verification of the strake design procedure, it is necessary to test a variety of strake-wing combinations in the wind tunnel. However, in order to keep the effort within manageable proportions, a way was sought to eliminate from consideration those strakes which would most likely not perform well at high angles of attack. An economical way, which also has inherent excellent flow visualization features is to use a water tunnel. With it a study of the strake-and wing-vortex breakdown patterns with angle of attack can be easily accomplished. This thesis presents the results of a water tunnel investigation of a representative group of strake shapes designed by the analytical procedure.

STRAKE DESIGN PROCEDURE

General

The problem in designing a strake is to find a starting place. Does one pick conventional shapes that are known to have reasonably good vortex-flow characteristics and reach large angles of attack and lift coefficients before breakdown occurs ahead of the trailing edge, as with the highly-swept delta and low-aspect-ratio-rectangular wing; or does one try to find "better shapes," and, if so, by what means other than experimental?

It should be pointed out that the significance of vortex breakdown occurring ahead of the trailing edge is directly related to the α at which $C_{L,max}$ is developed as shown in figure 3 for a 70° delta wing. This is further documented by Wentz in reference 2 for other slender delta wings having $\Lambda > 70^{\circ}$.

It is recognized, of course, that "isolated" strake characteristics do not necessarily define the relative effectiveness of a strake-wing combination. Nevertheless, in order to make this initial design study more amenable to a theoretical approach, the designs were made on an isolated strake basis assuming that if the vortex breakdown could be delayed on the isolated strake then it might also provide improved strake-wing characteristics. Once a series of strakes has been designed and tested in combination with a wing, the experimental data can be analyzed with the aid of a strake-wing analysis theory to provide additional information on design techniques.

Criterion

This section describes a criterion which is used to try and establish "better strake shapes". The criterion is based on an observation that strakes which in attached flow would develop leading-edge suction distributions that are more triangular and reach a higher peak near the tip tend to maintain vortex stability to higher angles of attack. Reference 3 first noted this for simple delta wings and figure 3 shows the effect of increasing sweep on both the peak and α_{BD-TE}. Similar effects were noted for cropped planforms in reference 4. Although no attempt has been made to justify the criterion on a theoretical basis, the fact that the leading-edge suction analogy tends to relate the vortex feeding rate and axial pressure gradient to the suction distribution may add some additional credance with regard to vortex stability.

Description of Method

The present strake design method relates the potential-flow leading-edge suction and pressure distributions to the strake planform geometry. Appendix A presents the underlying assumptions and shows a development of the basic equations used in the method.

A strake planform geometry is generated from the design procedure by solving an initial value problem. Here, the local leading-edge sweeps are determined by numerically integrating eq. (A-5) in the spanwise direction from the tip to the root. The designer must specify a leading-edge suction distribution, a spanwise ΔC_p distribution, a

semispan, $\frac{b}{2}$, tip chord, c_t, trailing edge sweep, Λ_t, and subcritical Mach number, M.

The design method can be executed using either a conical or three-dimensional, polynomial, type ΔC_p distribution. Each is specified to occur at either a constant x/c or a constant Δx from the leading edge. (The examples employed in this thesis only use a constant x/c specification.) The leading-edge suction distribution can also be defined by either two linear segments or a more generalized 3-D distribution.

$c_s c$-η Description

As previously described, the potential-flow-suction distribution has an effect on the resulting strake shape. For example, in reference 1 the $c_s c$-η distribution for the 76° delta in a three dimensional flow, when used in the two dimensional design procedure, leads to a gothic shape (see figure 4). This difference in shape is not surprising due to one being associated with a three dimensional and the other a conical ΔC_p distribution. Wind tunnel tests of the gothic strake in combination with a wing-body showed it to perform well.

The successful test, however, raises a question concerning the criterion: Was the stability of the strake vortex to high α due to (1) the high tip suction peak or (2) the steep inboard slope of the suction curve? To answer this question in particular and others pertaining to the relationship between the $c_s c$-η distribution and resulting shape, a study was undertaken. In this study, the original suction distribution was perturbed to gain an understanding of which part, inboard or

outboard, is more important. In addition, other $c_s c-\eta$ variations were investigated including some that tended to violate the criterion set forth. In all, some thirteen groups of suction distributions were investigated. Figure 5 shows these groups and the following gives a brief description of the salient features of each.

Group 1 varies the outboard part while holding the inboard part fixed. Group 2 varies the inboard part while holding the outboard part fixed. Group 3 translates the inner part vertically and varies the outer slope to keep the suction continuous. Group 4 translates the outer part vertically and varies the inner slope to keep the suction distribution continuous. Group 5 varies the segment breakpoint while holding the two extremal values and the slope of the first part constant. Groups 6, 7, and 8 are vertical translations of an indicated distribution. Group 6 is a single segmented curve with positive slope. Group 7 is a two segmented curve with both parts having a positive slope. Group 8 is a two segmented curve with the inboard and outboard parts having negative and positive slopes, respectively. Group 9 varies the slope of a single segment curve holding the inboard extremal value constant. Group 10 is similar to group 8, but the magnitude of the slopes are decreased. As a limiting case, the lowest curve in group 10 is allowed to reach zero at the tip $\eta = 1$. Group 11 varies the outboard part while fixing the inboard part with negative slope. Group 12 holds the two external values constant, the outer being larger than the inner, while varying the path between the two points. Group

13 holds the two extremals equal at a constant value while varying the path of the curves between them.

ΔC_p Specification

In reference 1, the ΔC_p is specified to be constant along constant values of x/c near the leading edge or, in other words, the ΔC_p behaves in a conical manner. Even for the first application made using this variation of ΔC_p it was noted, in reference 1, that other ΔC_p forms near the leading edge could be used (see figure 6), among them a three-dimensional or polynomial one was specifically noted. The idea was that if a more representative type ΔC_p variation was used then the resulting strake shape would have more of the three-dimensional flow features in its solution and perhaps be a better strake.

The first attempt to verify this idea employed the three-dimensional ΔC_p distribution for a 76° delta wing near the leading edge and its corresponding $c_s c$-η distribution. Both distributions were obtained from the NASA-Vortex Lattice Method, VLM, (refs. 5 and 6). The resulting shape was close to that of the 76° delta wing used as input to the VLM as seen in sketch a. This served to validate the idea.

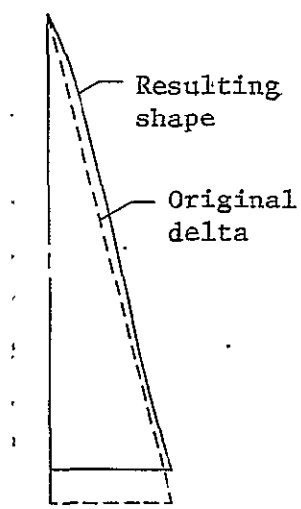

sketch a

Both the conical and three-dimensional pressure distributions were used to generate the strake shapes to be discussed later.

Characteristics of the Solution

It would be advantageous to know why certain strake shapes are generated by the design procedure for certain $c_s c-\eta$ and ΔC_p distributions. In particular, the designer should have some feeling for the type of strake shape to expect from the procedure for those $c_s c-\eta$ distributions which meet the design criterion stated in a previous section. Therefore, an analytical study of the basic strake design equation was performed to provide some understanding of the nature of the solution. Appendix B presents an analytical solution to the design equation. Here, a conical ΔC_p distribution is assumed. Also included in appendix B is an order of magnitude analysis of the solution which is useful in isolating the dominant terms.

The order of magnitude analysis reveals that the leading-edge sweep tends to increase logarithmically in the spanwise direction for those $c_s c-\eta$ distributions which meet the design criterion. Therefore for these suction distributions the designer can anticipate a gothic shaped strake to result from the design procedure.

STRAKE SHAPES STUDIED

Configurations Selected

The parametric study using the $c_s c-\eta$ and ΔC_p distributions previously described generated a large number of strake shapes. In order to reduce the study to more manageable proportions, the strakes were characterized according to resulting shapes (reflexive, gothic, almost delta) and other pertinent geometric features. From these shapes selections were made for water tunnel testing. Two types of strakes were basically chosen: the more promising ones, based on a general knowledge of those able to produce stable vortices, and the more unusual ones. With regard to the reflexive shaped strakes, eleven were chosen (figure 7) as being representative of the group and were tested. For the gothic-shaped strake a large number were produced by the code and nine were chosen (figure 8) to provide examples of representative slenderness ratio and initial sweep combinations. As a limiting case, the tip suction was allowed to reach zero for one strake. This case is shown in figure 9.

Designations are given to identify the strakes in figures 7 through 9 by their respective $c_s c-\eta$ group. For example, $c_s c-\eta$ distribution for the S3A-C in figure 8(a) is from group 3 of figure 5. The "A" distinguishes between distributions within the group and the "C" signifies a "conical" ΔC_p distribution. Similarly, the suction distribution for the S12B-P in figure 7(j) is from group 12 of figure 5. Here again, the "P" signifies a "polynomial", or three-dimensional ΔC_p distribution.

Parametric Selections

The strake design problem poses a number of questions which are critical in obtaining a good strake. They also provide important information with regard to the versatility and usability of the code. As pointed out earlier, a fundamental question is how good is the isolated $c_s c-\eta$ concept in strake generation when the strake is applied in a wing-strake combination? One of the objectives of the present investigation is to determine the validity of the concept.

Assuming the criterion is valid, how does the designer select a shape? For a group of gothic strakes, how important is the initial sweep? To study this parameter, initial sweeps varying from 46° to 77° were selected for study.

What are the effects of strake slenderness ratio, i.e. the ratio of length to semispan, $\ell/(b/2)$? To study this parameter, a variety of slenderness ratios ranging from 4.6 to 8.7 were chosen for the experimental investigation.

Once the designer has selected a shape, how much area should it have in relation to the wing? To study this effect, the original gothic strake from reference 1 was scaled to different area ratios of the wing reference area while retaining the strake shape. These strakes form the SA series to be discussed later.

If the strake is too long, how can it be shortened, i.e. scaled down in chord or cut off, without sacrificing its good performance qualities? If the chord is scaled down, then how much should it be scaled? To study this parameter, the original gothic shape of reference

1 was systematically scaled down in the chordwise direction while holding the semispan constant. These strakes form the SX series. If the strake is cut, then what regions are to be involved and how much area should be removed? To study these effects, the original gothic shape was cut in the apex and trailing edge regions, and along the inboard edge. These shapes form the SC-A, SC-T, and SC-S series, respectively.

Alternately, can strake performance be improved by adding a side edge to a too small strake? This effect was studied by adding a side edge to a shape which should exhibit early vortex breakdown. These strakes form the SE series.

Basic Strake Series

Additional details of the strake series just described are given herein. Table I is used to summarize pertinent geometric properties of the strakes.

The original gothic strake of reference 1 is designated the SA-1/SX-10. Strakes SA-2 and SA-3, shown in figure 10, are scaled down from the SA-1/SX-10 to have the same ratio of exposed strake area to wing reference area, R_a, as Strake II and Strake I of reference 7, respectively.

Strakes SX-7 and SX-3, shown in figure 11, were derived by scaling the SA-1/SX-10 70% and 30%, respectively, in the chordwise direction while holding the semispan constant. Strake SX-7 has the same slenderness ratio as Strake III of reference 7. Strake SX-3 is an extreme

case of small slenderness and provides an additional data point for the dependency of vortex breakdown on chordwise scaling.

It was anticipated that the SX-3 would exhibit poor vortex breakdown characteristics. In an attempt to improve its performance, a side edge extension of approximately the length of the strake was added to the SX-3. The side edge was progressively shortened and this series of strakes, shown in figure 12, are identified as SE-1, SE-2, and SE-3.

Strakes SC-A1 through SC-A4, shown in figure 13, are formed by cutting the SA-1/SX-10 in the chordwise direction at regular intervals from the apex. The 60° initial sweep corresponds to $\Lambda_{\ell}(\eta = 0)$ of the SA-1/SX-10. Strakes SC-A2 and SC-A4 have the same slenderness ratios as the SX-7 and SX-3, respectively.

Strakes SC-T1 through SC-T4, shown in figure 14, are formed by cutting the SA-1/SX-10 in the chordwise direction at regular intervals from the trailing edge. The strake SC-T2 has approximately the same slenderness ratio as the SX-7.

Strakes SC-S15, SC-S30, and SC-S45, shown in figure 15, are formed by cutting the SA-1/SX-10 parallel to the inboard edge. Cuts were made at 15%, 30%, and 45% of the original semispan, respectively, from the inboard edge.

Snagged Strakes

In another attempt to improve the performance of a strake with small slenderness ratio, a snag was added to the SX-3. The snag was

produced by altering the chord distribution over the inboard and outboard regions of the strake. Over the inboard region, the chord was reduced linearly from the root to the snag location. Over the outboard region, the chord was increased linearly from the tip to the snag location.

The idea was to use the snag to increase the local leading edge sweep across the span and thus enable the strake to generate a stronger vortex. However, it was anticipated that the counter-rotating snag side-edge vortex would impede the improved strake vortex and be detrimental to the overall performance gains.

Two snagged strakes, shown in figure 16, were tested. The snag on strake SCE-33 has a spanwise position of 1/3 semispan and a length of 1/8 semispan. The snag on strake SCE-66 has a spanwise position of 2/3 semispan and a length of 1/4 semispan.

Strake III

Strake III of reference 7 (shown in figure 17) was selected for water tunnel testing to provide additional data on the influence of geometric parameters such as area, slenderness ratio, and shape on the vortex breakdown phenomenon. For example, strakes SX-7 and SC-A2 were designed to have the same slenderness ratio as Strake III so that comparisons could be made for different strake shapes having the same slenderness ratio. In addition, wind tunnel force data is available for Strake III in reference 7. It was thought that a better

understanding of pertinent geometric parameters could be gained by attempting a correlation of water tunnel results with wind tunnel data.

BASIC FUSELAGE-WING DESCRIPTION

The basic fuselage-wing used was a one-half scaled model of the general research fighter configuration used extensively in the Langley 7 x 10 foot high speed tunnel. A drawing of the water tunnel configuration along with pertinent dimensions is given in figure 18. The 44° swept wing has a reference aspect ratio, taper ratio, and area of 2.5, 0.2, and $0.0258m^2$ (40 $inch^2$), respectively. All of the preceding are based on the reference wing which includes the area between the leading- and trailing-edges projected to the model centerline. The wing was tested in both a fore and aft position depending on the length of the strake.

TEST FACILITY AND PROCEDURE

The test facility used was the Northrop 16 x 24 inch Diagnostic Water Tunnel (shown in figure 19). It features a closed return with both a horizontal and vertical test section. Figure 19 shows a model mounted in the downward flow vertical test section. The test conditions were velocity $\approx$ .15 m/sec ($\approx$ 0.5 feet/sec), Reynolds number $\approx 1.76 \times 10^4$ based on the mean aerodynamic chord, with angle of attack variations from 0° to 50°. Sideslip could also be varied but was set to zero for the results reported herein.

The test procedure was to align the model so that at both high and low α it produced symmetrical strake vortex breakdown. Breakdown was determined by noting the behavior of the dye injected into the strake vortex core. When the dye trumpeted or exhibited reversal of direction, breakdown was said to have occurred. After symmetry was established, the α was increased from 10° in 2° increments until breakdown occurred near the trailing edge and then in 1° increments. After strake vortex breakdown occurs ahead of the wing trailing edge the α increment is increased to 2°. At each 5° increment after 10°, photographs were taken in both planview and side-view, with one exception, to establish the vortex patterns and, with the help of scribed lines on the wing and strake surfaces, estimates were made of vortex breakdown position. The results of the photography and breakdown estimation are given next.

RESULTS AND DISCUSSION

It must be kept in mind that the following analysis deals only with the vortex breakdown characteristics and that the actual aerodynamic performance can be determined only after wind tunnel force tests have been performed. In this section, both the strake vortex breakdown data for each configuration and sample top and side view photographs at $\alpha = 20^{\circ}$ are presented in figures 20 to 34. The results are organized according to: (1) the various $c_s c$-η groups, and (2) those obtained through variations of the original gothic strake of reference 1. Table II provides a listing of the strake designations with their respective data figure numbers and a description of the corresponding suction distributions.

The breakdown plots illustrate the progression of non-dimensional chordwise strake vortex breakdown location, $x/(c_r)_w$, with angle of attack, α. Since the wing is the main lifting surface, the strake vortex flow characteristics over the wing are of primary interest. Therefore, the chordwise vortex breakdown position, x, is non-dimensionalized by $(c_r)_w$ to make the results directly comparable over the wing. Vortex breakdown over the strake is not directly comparable between configurations but its absolute location can be observed relative to the generating strake shape shown at the right of the (b) part of each of these figures. Each type of line segment used to define the strake shapes in the planform sketch are the same as those used to connect the corresponding data points.

The photographs on the facing pages, the (a) part of these figures, reveal the influence of the wing pressure field on the path of the vortex. The strake vortex core is visible as a long heavy line emanating from the strake apex. The wing vortices are generally visible outboard of the strake vortices. In several of the top view photographs, the wing vortices have been enhanced by a grease pencil to increase their visibility.

Judgment of strake performance is based on (1) the angle of attack at which the strake vortex breakdown crosses the wing trailing edge, α_{BD-TE}, and (2) the rate at which the breakdown progresses forward over the wing. The "better strakes" are those which have a higher α_{BD-TE} and a lower rate of breakdown progression with α as illustrated in the following sketches

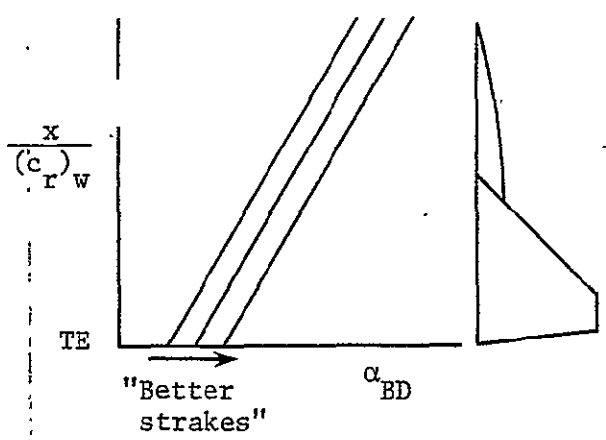

sketch b

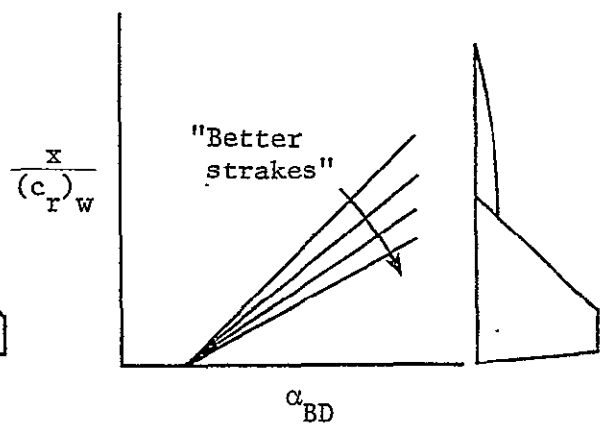

sketch c

A qualitative evaluation of vortex stability for the strakes organized by various $c_s c$-η groups is presented in Table III. Figure

35 summarizes the vortex breakdown data for the "better" strakes. Unanimously, the "better" strakes are those which have a high tip suction value and a high slope over the inboard region of the suction curve. This conclusion is further supported by comparing the S3A-C with the SA-2 in figure 36. Both strakes have the same slenderness ratio and semispan but the suction distribution for the S3A-C (see insert and figure 8(a)) has a high slope over the inboard region and a high suction value at the tip while the SA-2* has a tuncation of the suction distribution in the outboard region (see insert and figure 4). The remaining strakes listed in Table III exhibit inferior breakdown characteristics. Those strakes which have a negative slope over the inboard region of the suction curve show poor breakdown properties. These results would appear to confirm the validity of the original design criterion. They further show that even though the original suction distribution used could be modeled by truncation, as in the original example given in reference 1, this is not the best distribution.

Strakes S12B-C and S12B-P in figure 35(b) demonstrate the effects of modeling the spanwise ΔC_p distribution. The three-dimensional or polynomial form of ΔC_p for the S12B-P results in a reduction of α_{BD-TE} but adds stability to the vortex system by lowering the rate of breakdown progression over the wing. By contrast, the conical

---

*The $c_s c$-η distribution for the SA-2 and SA-3 is identical to that of the SA-1/SX-10.

ΔC_p distribution leads to a higher α_{BD-TE} than that of the three-dimensional form.

Figure 37 portrays the strake vortex breakdown properties for the SA series as a function of strake area. As might be anticipated, the reduction of strake area while holding the contour the same results in an earlier vortex breakdown across the wing trailing edge. As the vortex breakdown progresses forward over the wing, the adverse effects of area reduction become less pronounced. At the wing apex, the vortex breakdown position remains virtually unchanged as strake area is reduced.

Figure 38 shows the breakdown characteristics for strakes with equal area ratios but different leading edge shapes. Figure 38(a) compares the SA-2 with the SE-3 which both have a ratio of strake to wing reference area of $R_a = 0.166$. Figure 38(b) compares the SA-1/SX-10 with the SE-1 both of which have $R_a = 0.325$. In both cases, the gothic strake is obviously the superior of the two. This serves to emphasize that the strake shape is an important parameter.

Figure 39 presents the vortex breakdown characteristics across the wing trailing edge for those strakes which are chordwise variations of the SA-1/SX-10. The spanwise cut series, SC-S, yields an improvement in performance over the original SA-1/SX-10 though the benefits are limited to small chord reductions. Overall, the trailing edge cut series, SC-T, offers the most favorable technique for reducing the chord of an existing gothic strake while maximizing the vortex breakdown characteristics across the wing trailing edge.

The breakdown properties for the SX-series are presented in figure 40 as a function of chord. The results indicate that as the chord is scaled down in this series, there is a corresponding reduction in α_{BD} over the wing. Chordwise scaling requires that the leading edge sweep be reduced (see figure 11) resulting in a decrease in the strake vortex strength. Also, for strakes with lower leading edge sweeps particularly near the tip, the strake vortex tends to be steered outboard into the wing vortex, resulting in early wing-strake coalescence and a premature vortex breakdown. This phenomenon can be observed from the SX-3 photographs in figure 28(a).

The vortex breakdown characteristics as a function of chord for the SC-A series (see figure 13) are shown in figure 41. The vortex breakdown angle is sensitive to removal of area near the apex of the original strake as indicated by the large slopes to the right of the plot. As indicated by a decrease in the slopes to the left of the plot, additional area removal past that for the SC-A2 strake has a lesser impact on the breakdown angle. The planform of the SC-A series strakes is essentially a 60° delta leading edge with an attached gothic shaped side edge. The results illustrate that removing the apex region of an existing strake is a poor method for reducing the chord if good strake performance is to be maintained and that reshaping is required.

Figure 42 presents the vortex breakdown properties for the SC-T series as a function of chord. By cutting along the trailing edge and shifting the strake aft, chord reductions up to 30% can be made without

appreciably changing the angle at which the strake vortex breakdown point passes over the wing trailing edge. At angles of attack where the vortex breakdown occurs over the wing, a moderate depreciation in α_{BD} is observed as chord is decreased. As more of the trailing edge region is removed, the leading edge sweep near the tip decreases for the gothic strake. Again, this leads to the problem of premature vortex breakdown due to early wing-strake vortex coalescence. In addition, extreme chord reduction by this technique results in a significant span reduction, which leads to fuselage interference problems. Overall, the removal of trailing edge area appears to be a good method for moderately reducing the chord of an existing strake while maximizing the vortex breakdown characteristics across the wing trailing edge.

Figure 43 portrays the vortex breakdown properties for the SC-S series as a function of chord. The results show that strake vortex stability improves as spanwise cuts are used to make small chord reductions. As seen in this figure and also in figure 31, improvements are evident for spanwise cuts up to 30% of the semispan from the inboard edge. This technique is the most favorable for making small chord reductions without recontouring since it offers improvement to the vortex breakdown characteristics. However, in strake design the effects on total lift capability must also be considered.

Figure 44 presents the vortex breakdown characteristics as a function of chord for the SE-series. The addition of side edge increases the angle of attack at which the vortex breakdown crosses the

wing trailing edge by effectively increasing the average sweep of the strake. However, as the vortex breakdown progresses forward over the wing, additional side edge results in very little improvement to the breakdown characteristics (see figure 32). Adding side edge to a "too short" strake is an unsatisfactory method for improving its over-all performance.

Figure 33 presents the vortex breakdown characteristics for the snagged strakes which are variations of the SX-3. The SCE-66 shows a slight improvement over the SX-3. However, the SCE-33 shows a reduction in strake performance. This is more evident in the photograph of the SCE-33, figure 33(a), which reveals extensive disorder in the flow field around the snag region.

Figure 34 shows the vortex breakdown characteristics for Strake III of reference 7. This strake has a high α_{BD-TE} but is burdened with an extremely high rate of breakdown progression near the wing trailing edge.

Figure 45 addresses the question of initial sweep effects on the breakdown performance of gothic strakes with the same semispan. As the results signify, no consistent relationship can be established for these effects from this investigation. Since there was no attempt made in the experimental study to use only strakes from one $c_s c-\eta$ group, this may be clouding the establishment of a relationship for the initial sweep effects. The results do reveal however that strakes with higher slenderness ratios have better vortex breakdown characteristics.

Slenderness ratio effects on α_{BE-TE} are shown in figure 46 for strake shapes characterized by reflexive, gothic, and delta gothic. All strakes have an exposed strake span to wing span of 0.212. The data are faired and even though there is some scatter it is clear that the gothic shaped strakes reach larger angles of attack before breakdown occurs at the wing trailing edge than the reflexive and delta gothic strakes for $\ell/(b/2) > 5$.

Figure 47 shows the effect of strake geometry on vortex breakdown position for a fixed slenderness ratio. For very small slenderness ratios, fig. 47(a), the gothic shape gives better vortex breakdown properties than the smallest apex cut strake. The strakes in figure 47(b) have the same slenderness ratio but some have different semi-spans and consequently different lengths. The larger reflexive shaped strake III exhibits the best vortex breakdown properties of the four strakes followed by the gothic SX-7. The smaller gothic shaped SC-T2 yields better vortex breakdown characteristics than the larger cut strake SC-A2. Therefore, for the same slenderness ratio, about the only statement to be made is that strake size and shape are important overall design parameters in delaying vortex breakdown and its forward progression.

CORRELATION WITH WIND TUNNEL DATA

To this point, only the water tunnel data and photographs for each configuration have been presented. It would be interesting to see if the water tunnel data could be used in a correlative manner with available wind tunnel data. Strakes SA-1/SX-10 and Strake III are two configurations for which wind tunnel force data is available, as found in references 1 and 7, respectively.

Figure 48 presents the wind tunnel results from the references and repeats the water tunnel vortex breakdown data for the correlation attempt. The gentle rounding of the wing and strake lift curves at the peaks for the SA-1/SX-10 configuration, shown in figure 48(a), are reflective of the overall low rate of vortex breakdown progression for this strake (see figure 48(b)). For the Strake III configuration, the more abrupt wing C_L peak is characteristic of the high rate of vortex breakdown progression which occurs near the wing trailing edge. The leveling off for the C_L curve after the peak is indicative of the decrease in rate of vortex breakdown as the breakdown progresses forward over the wing. Hence, it has been demonstrated that a correlation exists and that water tunnel results can be useful in making a qualitative assessment of wind tunnel data.

CONCLUSIONS

A systematic water tunnel study is made to determine the vortex breakdown characteristics of 44 strakes, more than half of which were designed with a new analytical strake design method. The strakes were scaled for use on a half-scale model of the NASA-LaRC general research fighter fuselage with a 44° trapezoidal wing. The strakes are categorized by (1) the various suction distribution groups used in their design, and, (2) those obtained through variations of a gothic strake tested previously.

With regard to making a judgment of strake performance, the evaluation is based on (1) the angle of attack at which the strake vortex breakdown crosses the wing trailing edge, and (2) the rate at which the breakdown progresses forward over the wing. The "better strakes" are those which have a higher trailing edge breakdown angle and a lower rate of breakdown progression with angle of attack.

The following conclusions are drawn from this study:

1. Validity of the design criterion which is based on the correlation idea that "better shapes" are those which have potential-flow-suction distributions that are more triangular and peak near the tip is confirmed.

2. For the same suction distribution, the specification of a lifting pressure near the leading edge that is conical rather than three-dimensional is determined to result in a better strake shape as judged by its vortex breakdown characteristics, performance.

3. Decreasing strake area while holding the shape constant results in an over-all reduction in the angles of attack at which the strake vortex breakdown occurs over the wing.

4. For the same area, the gothic strake exhibits better vortex breakdown characteristics than a small strake with a long side edge.

5. With regard to seeking improvements in or not losing the benefits of a designed strake while making it smaller by selectively removing portions of the strake so as to reduce the chord, it has been found that:

(a) Removal of area from the apex region of an existing strake is a poor method for reducing the chord while maintaining good strake performance.

(b) Area removal from the trailing edge region appears to be a good technique for making moderate chord reductions to an existing gothic strake while maximizing the vortex breakdown characteristics across the wing trailing edge.

(c) Spanwise cutting of the inboard region of an existing gothic strake is the most favorable technique for making small chord reductions and can actually improve vortex stability.

(d) Scaling the chord for a given semispan leads to a corresponding angle of attack reduction for vortex breakdown occurring at the wing trailing edge.

6. Adding side edge to a "too short" strake is an unsatisfactory method for improving its overall performance, even though it does

increase the angle of attack reached before vortex breakdown occurs at the wing trailing edge.

7. Adding a snag to a strake yields no significant improvement to its overall performance.

8. No consistent relationship has been established for the effects of initial sweep on the performance of gothic strakes, however it is found that strakes with higher slenderness ratios have better vortex breakdown characteristics.

9. For the same semispan, the gothic shaped strakes reach larger angles of attack before breakdown occurs at the wing trailing edge than the reflexive and delta gothic strakes for slenderness ratios greater than 5.

10. For the same slenderness ratio, strake size and shape are important over-all design parameters in delaying vortex breakdown and its forward progression.

11. It has been demonstrated that a correlation exists between water tunnel and wind tunnel data and that water tunnel results can be useful in making a qualitative assessment of wind tunnel data.

APPENDIX A

Basic Equations Used in Strake Shape Development

Starting from an attached-flow-pressure distribution that is given by

$$\Delta C_p\ (\theta,\eta) = \frac{2q_o(\eta)}{q_\infty c(\eta)} \cot\frac{\theta}{2} + \sum_{j=1}^{N-1} \frac{2q_j(\eta)}{q_\infty c(\eta)} \sin j\theta$$

the local-suction distribution can be found from reference 7 to be

$$c_s c\big|_\eta = \frac{\sqrt{\beta^2 + \tan^2 \Lambda_\ell\ (\eta)}}{2\pi \cos \Lambda_\ell\ (\eta)} \left(\frac{2q_o(\eta)}{q_\infty c(\eta)}\right)^2 \bar{c}(\eta)$$

This equation relates the local leading-edge sweep angle, $\Lambda_\ell\ (\eta)$, and chord, $c(\eta)$ through the suction distribution, $c_s c\big|_\eta$, and coefficient of the $\cot(\theta/2)$ term in $\Delta C_p(\theta,\eta)$. Another relationship between $\Lambda_\ell(\eta)$ and $c(\eta)$ is the geometrical relationship

$$c(\eta) = c_r - (b/2) \int_o^\eta (\tan \Lambda_\ell(\bar{\eta}) - \tan \Lambda_t)\ d\bar{\eta}$$

However, to obtain a solution, some assumptions will be needed with regard to $c_s c|_\eta$ and $\Delta C_p(\theta,\eta)$. For example, the correlation between suction distributions which peak towards the tip and the resulting large values of α_{BD-TE} could be used. This can be done by assuming that

$$c_s c|_\eta = (a_1 + b_1\eta)\,\frac{b}{2}\,.$$

The second assumption would be that since the planar strakes are designed to produce separated flow with reattachment; i.e., vortex flow, the associated leading-edge pressures must conceptually, as well as in reality, exceed an unspecified limiting value beginning at some small angle of attack. This means that for the attached-flow-pressure distribution, the region of interest is near the leading edge; i.e., where θ and x/c are small. Hence, one approximation is to set

$$\Delta C_p(\theta,\eta) \approx \frac{2q_o(\eta)}{q_\infty c(\eta)} \cot\frac{\theta}{2}$$

If an additional assumption is made that across the span

$$\Delta C_p\ (\theta,\eta) = \text{constant} = C_o$$

at constant θ or x/c*, which means that the sectional lift contribution from the cot $\theta/2$ term is constant, then

$$\frac{2q_o(\eta)}{q_\infty c(\eta)} \approx \text{constant} = C_1$$

The preceding discussion implies that if the flow separates anywhere, it separates everywhere simultaneously. Putting all of the assumptions together yields

$$(a_1 + b_1\eta)\left(\frac{b}{2}\right) = \frac{\sqrt{\beta^2 + \tan^2 \Lambda_\ell(\eta)}\; c(\eta)}{2\pi \cos \Lambda_\ell(\eta)} (C_1)^2$$

$$(\bar{a} + \bar{b}\,\eta)\left(\frac{b}{2}\right) = \frac{\sqrt{\beta^2 + \tan^2 \Lambda_\ell(\eta)}}{2\pi \cos \Lambda_\ell(\eta)} \Big[c_r$$

$$- \frac{b}{2} \int_0^\eta (\tan \Lambda_\ell(\bar{\eta}) - \tan \Lambda_t)\, d\bar{\eta}\Big]$$

where

---

*Other assumptions concerning $\Delta C_p(\theta,\eta)$ and θ could be made. For example, $\Delta C_p(\theta,\eta)$ could take on a three-dimensional variation at constant θ.

$$\bar{a} = \frac{a_1}{C_1^2} \quad \text{and} \quad \bar{b} = \frac{b_1}{C_1^2}$$

at $\eta = 1$, the tip sweep of the strake can be determined by

$$\Lambda_\ell\ (\eta = 1) = \sin^{-1}\left[\left(\frac{c_t^2\ M^2}{2\pi b^2(\bar{a} + \bar{b})^2} + 1 - \sqrt{\frac{M^4\ c_t^4 + 4\pi^2 b^2 c_t^2(\bar{a} + \bar{b})^2}{2\pi^2 b^2(\bar{a} + \bar{b})^2}}\right)^{\frac{1}{2}}\right] \tag{A-1}$$

For $\eta < 1$, $\Lambda_\ell(\eta)$ can be solved for from the following initial value problem

$$c_r - \frac{(\bar{a} + \bar{b}\eta)(b/2)\ 2\pi}{\sqrt{\beta^2\ \sec^2\Lambda_\ell(\eta) + \sin^2\Lambda_\ell(\eta)\sec^4\Lambda_\ell(\eta)}} =$$

$$\frac{b}{2}\int_0^\eta (\tan\Lambda_\ell(\bar{\eta}) - \tan\Lambda_t)\ d\bar{\eta} \tag{A-2}$$

Differentiating eq. (A-2) yields

$$\frac{d\Lambda_\ell}{d\eta} = \frac{\bar{G}^{3/2}\left[1 - \frac{\tan\Lambda_t}{\tan\Lambda_\ell(\eta)}\right] + 2\pi\bar{b}\ \bar{G}/\tan\Lambda_\ell(\eta)}{2\pi(\bar{a} + \bar{b}\eta)\ \sec^2\Lambda_\ell(\eta)\ [\beta^2 + 1 + 2\ \tan^2\Lambda_\ell(\eta)]} \tag{A-3}$$

where $\bar{G} \equiv \beta^2 \sec^2 \Lambda_\ell(\eta) + \sin^2 \Lambda_\ell(\eta) \cdot \sec^4 \Lambda_\ell(\eta)$ (A-4)

Equation (A-3) can be integrated from $\eta = 1$ to $\eta = 0$ using a numerical integration scheme such as the Runge-Kutta method. The initial value is given by eq. (A-1).

A problem arises, however, when integrating eq. (A-3) for the case where $c_t = 0$. From eq. (A-1), this gives an initial value of $\Lambda_\ell(\eta = 1) = \frac{\pi}{2}$. For this initial value, eq. (A-3) is singular and the numerical integration scheme can not be started. A solution can be obtained for this case as well as all other cases if eq. (A-3) is multiplied by $-3 \cos^2\Lambda_\ell(\eta) \sin\Lambda_\ell(\eta)$. This leads to the following differential equation

$$\frac{d(\cos^3\Lambda_\ell)}{d\eta} = \frac{-3\ \bar{H}^{3/2}\ [\sin\Lambda_\ell(\eta) - \cos\Lambda_\ell(\eta)\ \tan\Lambda_t] - 6\pi\bar{b}\ \bar{H}\ \cos^3\Lambda_\ell(\eta)}{2\pi(\bar{a} + \bar{b}\eta)(1 + \bar{H})} \tag{A-5}$$

where $\bar{H} \equiv 1 - M^2 \cos^2\Lambda_\ell(\eta)$ (A-6)

Eq. (A-5) is finite for the initial values $0 \leq \Lambda_\ell(\eta = 1) \leq \frac{\pi}{2}$ and thus can be integrated numerically.

APPENDIX B

Analytical Solution to the Basic Strake Design Equation

Starting with equation A-2

$$c_r - \frac{2\pi(\bar{a} + \bar{b}\eta)(b/2)}{\sqrt{\beta^2 \sec^2\Lambda_\ell(\eta) + \sin^2\Lambda_\ell(\eta)\sec^4\Lambda_\ell(\eta)}}$$

$$\left(\frac{b}{2}\right) \int_0^\eta (\tan\Lambda_\ell(\eta) - \tan\Lambda_t)\, d\bar{\eta} \qquad \text{(B-1)}$$

and assuming $M = 0$, i.e. $\beta^2 = 1$, eq. (B-1) can be simplified to

$$c_r - \frac{2\pi(b/2)(\bar{a} + \bar{b}\eta)}{\sec^2\Lambda_\ell(\eta)} = \left(\frac{b}{2}\right) \int_0^\eta (\tan\Lambda_\ell(\bar{\eta}) - \tan\Lambda_t)\, d\bar{\eta} \qquad \text{(B-2)}$$

Defining $z(\eta) \equiv \tan\Lambda_\ell(\eta)$ and $K_1 \equiv \tan\Lambda_t$, a constant, equation (B-2) can be written as

$$c_r - \frac{2\pi(b/2)(\bar{a} + \bar{b}\eta)}{1 + z^2(\eta)} = \left(\frac{b}{2}\right) \int_0^\eta (z(\bar{\eta}) - K_1)\, d\bar{\eta} \qquad \text{(B-3)}$$

Next, differentiate eq. (B-3) with respect to η to get

$$\frac{dz}{d\eta} - \frac{(z - K_1)(1 + z^2)^2 + 2\pi\bar{b}(1 + z^2)}{4\pi z(\bar{a} + \bar{b}\eta)} = 0 \qquad \text{(B-4)}$$

where $z = z(\eta)$.

An exact differential equation is formed from eq. (B-4) by separation of variables

$$-\frac{zdz}{(1 + z^2)\left[(1 + z^2)(z - K_1) + 2\pi\bar{b}\right]} = -\frac{d\eta}{4\pi(\bar{a} + \bar{b}\eta)} \qquad \text{(B-5)}$$

Integrating (B-5) yields

$$\int \frac{zdz}{(1 + z^2)\left[(1 + z^2)(z - K_1) + 2\pi\bar{b}\right]} = \frac{1}{4\pi\bar{b}} \ln(\bar{a} + \bar{b}\eta) + C_2 \qquad \text{(B-6)}$$

Additional consideration must be given to solving the integral to the left of the equality in eq. (B-6).

A solution to this integral can be obtained through integration by partial fractions if the second term of the denominator has the form

$$(1 + z^2)(z - K_1) + 2\pi\bar{b} = (z - A)(z - B)(z - C) \tag{B-7}$$

Letting

$$f = \frac{1}{3}(3 - K_1^{\,2}) \tag{B-8}$$

$$g = \frac{1}{27}[27\,(2\pi\bar{b} - K_1) + 9K_1 - 2K_1^3] \tag{B-9}$$

and

$$F = \sqrt[3]{-\frac{g}{2} + \sqrt{\frac{g^2}{4} + \frac{f^3}{27}}} \tag{B-10}$$

$$G = \sqrt[3]{-\frac{g}{2} - \sqrt{\frac{g^2}{4} + \frac{f^3}{27}}} \tag{B-11}$$

and further

$$R = \frac{K_1}{3} - \frac{F + G}{2} \tag{B-12}$$

$$Q = \frac{F - G}{2}\sqrt{3} \tag{B-13}$$

then the roots to eq. (B-7) are

$$A = F + G + \frac{K_1}{3} \tag{B-14}$$

$$B = R + iQ \tag{B-15}$$

$$C = R - iQ \tag{B-16}$$

By using the relation

$$B = \bar{C} \tag{B-17}$$

and making the assumption that z is real, eq. (B-7) can be rewritten as

$$(1 + z^2)(z - K_1) + 2\pi\bar{b} = [(z - R)^2 + Q^2](z - A) \tag{B-18}$$

Substituting eq. (B-18) into eq. (B-6) and integrating by partial fractions, an implicit solution results

$$\eta = \frac{1}{\bar{b}} \left\{ C_3 \left[\frac{z^2 + 1}{(z - R)^2 + Q^2} \right] \cdot \left[\frac{(z - R)^2 + Q^2}{(z - A)^2} \right]^{P_1} \cdot e^{P_2 \tan^{-1}\left(\frac{z-R}{Q}\right)} - \bar{a} \right\} \tag{B-19}$$

$$P_1 = \frac{A(A - K_1)}{(R - A)^2 + Q^2} \tag{B-20}$$

$$P_2 = \frac{2[(1 - 3RA)(K_1 - R) - Q^2 A]}{Q[(R - A)^2 + Q^2]} \tag{B-21}$$

For the common case where $c_t = 0$, eq. (A-1) yields a tip sweep of $\Lambda_\ell(\eta = 1) = \pi/2$. The limit of eq. (B-19) as $\Lambda_\ell(\eta = 1) \to \frac{\pi}{2}$ (i.e. $z \to \infty$) is

$$1 = \frac{1}{\bar{b}} \left[C_3 \cdot e^{\frac{\pi}{2} P_2} - \bar{a} \right]$$

Thus, the constant can be evaluated for the case where $c_t = 0$ by the relation

$$C_3 = (\bar{a} + \bar{b})\, e^{-\frac{\pi}{2} P_2} \tag{B-22}$$

Some insight into the nature of the solution can be gained by performing an order of magnitude analysis on eq. (B-19). Assuming the order of magnitudes of the two polynomial quotient terms in eq. (B-19)

are both in the range where the z is the dominant term, then

$$\frac{Q(z^2)}{Q_i(z^2)} = O(1) \tag{B-23}$$

So eq. (B-19) can be rewritten as

$$\frac{1}{C_3}(\bar{a} + \bar{b}\eta) = O(1)\ e^{P_2 \tan^{-1}\left(\frac{z-R}{Q}\right)} \tag{B-24}$$

Taking the logarithm of both sides, and simplifying yields

$$z = Q\tan\left[\frac{1}{P_2}\ \ell n\left(\frac{\bar{a} + \bar{b}\eta}{C_3\ O(1)}\right)\right] + R \tag{B-25}$$

Since $z \equiv \tan \Lambda_\ell(\eta)$, then

$$\Lambda_\ell(\eta) = \tan^{-1}\left\{Q\ \tan\left[\frac{1}{P_2}\ \ell n\left(\frac{\bar{a} + \bar{b}\eta}{C_3\ O(1)}\right)\right] + R\right\} \tag{B-26}$$

Considering the η dependent term within the braces, it could be said that the tangent-arctangent functions tend to cancel each other leaving a logarithmic expression containing η. Physically, this means that if $\bar{a} + \bar{b}\eta$ is positive and linearly increasing in value with η, (i.e. $\bar{a} > 0$, $\bar{b} > 0$), then the leading edge sweep, $\Lambda_\ell(\eta)$, will tend to increase logarithmically in the spanwise direction producing a gothic shape. Conversely, if $\bar{a} + \bar{b}\eta$ is positive but linearly decreasing in value with η, (i.e. $\bar{a} > 0$, $\bar{b} < 0$), then $\Lambda_\ell(\eta)$ will tend to decrease logarithmically in the spanwise direction yielding an unsweeping strake shape. Therefore, those suction distributions which meet the design criterion of being triangular and reaching a peak near the tip will most likely produce a gothic shaped strake.

REFERENCES

1. Lamar, J. E.: Strake Wing Analysis and Design. AIAA Paper No. 78-1201, July 1978.

2. Wentz, W. H., Jr., and Kohlman, David L.: Wind Tunnel Investigations of Vortex Breakdown on Slender Sharp-Edged Wings. NASA CR-98737, 1968.

3. Lamar, J. E.: Some Recent Applications of the Suction Analogy to Vortex-Lift Estimates - in Aerodynamic Analysis Requiring Advanced Computers. NASA SP-347, March 1975.

4. Lamar, J. E.: Recent Studies of Subsonic Vortex Lift Including Parameters Affecting Stable Leading-Edge Vortex Flow. Journal of Aircraft, Vol. 14, No. 12, pp. 1205-1211, December 1977.

5. Margason, R. J. and Lamar, J. E.: Vortex-Lattice FORTRAN Program for Estimating Subsonic Aerodynamic Characteristics of Complex Planforms. NASA TN D-6142, 1971.

6. Lamar, J. E. and Gloss, B. B.: Subsonic Aerodynamic Characteristics of Interacting Lifting Surfaces with Separated Flow Around Sharp Edges Predicted by a Vortex-Lattice Method. NASA TN D-7921, September 1975.

7. Luckring, J. M.: Theoretical and Experimental Aerodynamics of Strake-Wing Interactions Up to High Angles-of-Attack. AIAA Paper No. 78-1202, July 1978.

8. Wagner, S.: On the Singularity Method of Subsonic Lifting-Surface Theory. AIAA Paper No. 69-37, 1969. Presented at the AIAA 7th Aerospace Sciences Meeting, New York.

Table I. - Pertinent Geometric Properties of Basic Strake Series

Strake Designation	$\Lambda_\ell(\eta=0)$ (deg.)	$\left(\ell/(b/2)\right)$	$\left[\frac{(b/2)_s}{(b/2)_w}\right]_{exp}$	$R_a = \frac{S_s}{S_{ref}}$
SA-1/SX-10	60.65	7.00	0.297	0.325
SA-2	60.65	7.00	0.212	0.166
SA-3	60.65	7.00	0.144	0.077
SX-7	56.89	5.18	0.297	0.227
SX-3	50.42	2.78	0.297	0.098
SE-1	50.42	5.63	0.297	0.325
SE-2	50.42	4.64	0.297	0.246
SE-3	50.42	3.63	0.297	0.166
SC-A1	60.00	6.10	0.297	0.305
SC-A2	60.00	5.19	0.297	0.266
SC-A3	60.00	3.98	0.297	0.195
SC-A4	60.00	2.77	0.297	0.114
SC-T1	60.65	5.83	0.262	0.188
SC-T2	60.65	5.22	0.226	0.124
SC-T3	60.65	4.53	0.181	0.065
SC-T4	60.65	3.65	0.119	0.021
SC-S15	73.32	7.79	0.253	0.259
SC-S30	77.57	8.62	0.208	0.192
SC-S45	80.12	9.59	0.163	0.131
Strake III (ref. 7)	80.35	5.18	0.353	0.267

Table II. - Basic Data Presentation and Pertinent Suction Characteristics

Basic Data		Suction Distribution Descriptions					
Fig. No.	Strake Designation	Initial Value	Initial Slope	Suction Break, Fraction of b/2	Outboard Slope	Tip Value	Fig. No.
20	S3A-C	2	48	0.65	53.7	52	8(a)
20	S3B-C	25	48	0.65	-12	52	8(b)
21	S4A-C	4	9.23	0.65	48	26.8	8(c)
21	S5A-C	4	20	0.90	380	60	8(d)
21	S6A-C	10	48	1.00	---	58	8(e)
22	S8A-C	12	-15	0.65	48	19.05	7(a)
22	S8A-P	12	-15	0.65	48	19.05	7(b)
22	S8B-C	14	-15	0.65	48	21.05	7(c)
22	S8B-P	14	-15	0.65	48	21.05	7(d)
23	S10A-C	4	-5	0.65	-2.1	0.0	9
23	S10B-C	4	-5	0.65	23.6	9	7(e)
23	S10C-C	5	-5	0.65	23.6	10	7(f)
23	S10D-C	9	-5	0.65	23.6	14	8(f)
24	S11A-C	5	-5	0.65	166	60	7(g)
24	S11A-P	5	-5	0.65	166	60	7(h)
25	S12A-C	4	0	0.65	137	52	8(g)
25	S12A-P	4	0	0.65	137	52	7(i)
25	S12B-C	4	101	0.65	-51	52	8(h)
25	S12B-P	4	101	0.65	-51	52	7(j)
26	S13A-C	5	-8	0.50	8	5	7(k)
26	S13B-C	5	6	0.50	-6	5	8(i)

Table III. - Qualitative Evaluation of Strake Performance - By Groups

Strake Designation	Slope of inboard region of suction Dist.	Tip Suction Value	Quality of B.D. Characteristics
S3A-C	high	high	good
S3B-C	high	high	good
S4A-C	low	low	fair
S5A-C	low	high	fair
S6A-C	high	high	good
S8A-C	negative	low	poor
S8A-P	negative	low	poor
S8B-C	negative	low	poor
S8B-P	negative	low	poor
S10A-C	negative	zero	very poor
S10B-C	negative	low	poor
S10C-C	negative	low	poor
S10D-C	negative	low	poor
S11A-C	negative	high	poor
S11A-P	negative	high	poor
S12A-C	low	high	poor
S12A-P	low	high	poor
S12B-C	high	high	good
S12B-P	high	high	good
S13A-C	negative	low	poor
S13B-C	low	low	poor

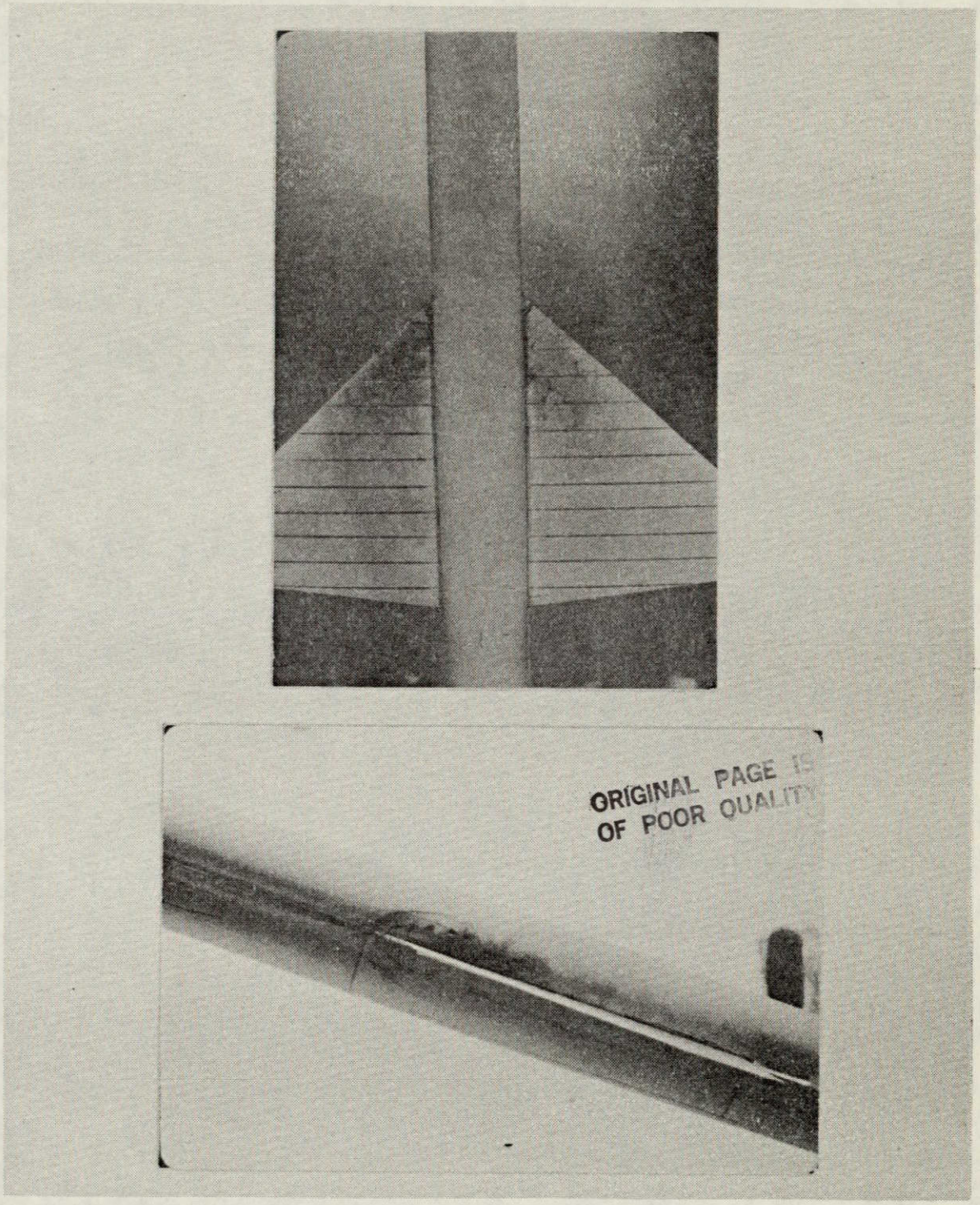

44° wing alone, forward position

Figure 1.- Water tunnel photograph of wing flow-field at $\alpha = 20^{\circ}$.

ORIGINAL PAGE IS
OF POOR QUALITY

ORIGINAL PAGE IS
OF POOR QUALITY

Figure 2.- Photograph of vortex flow generated by highly swept maneuver strakes on the General Dynamics YF-16 lightweight fighter, from Aviation Week and Space Technology, June 16, 1975, p. 23.

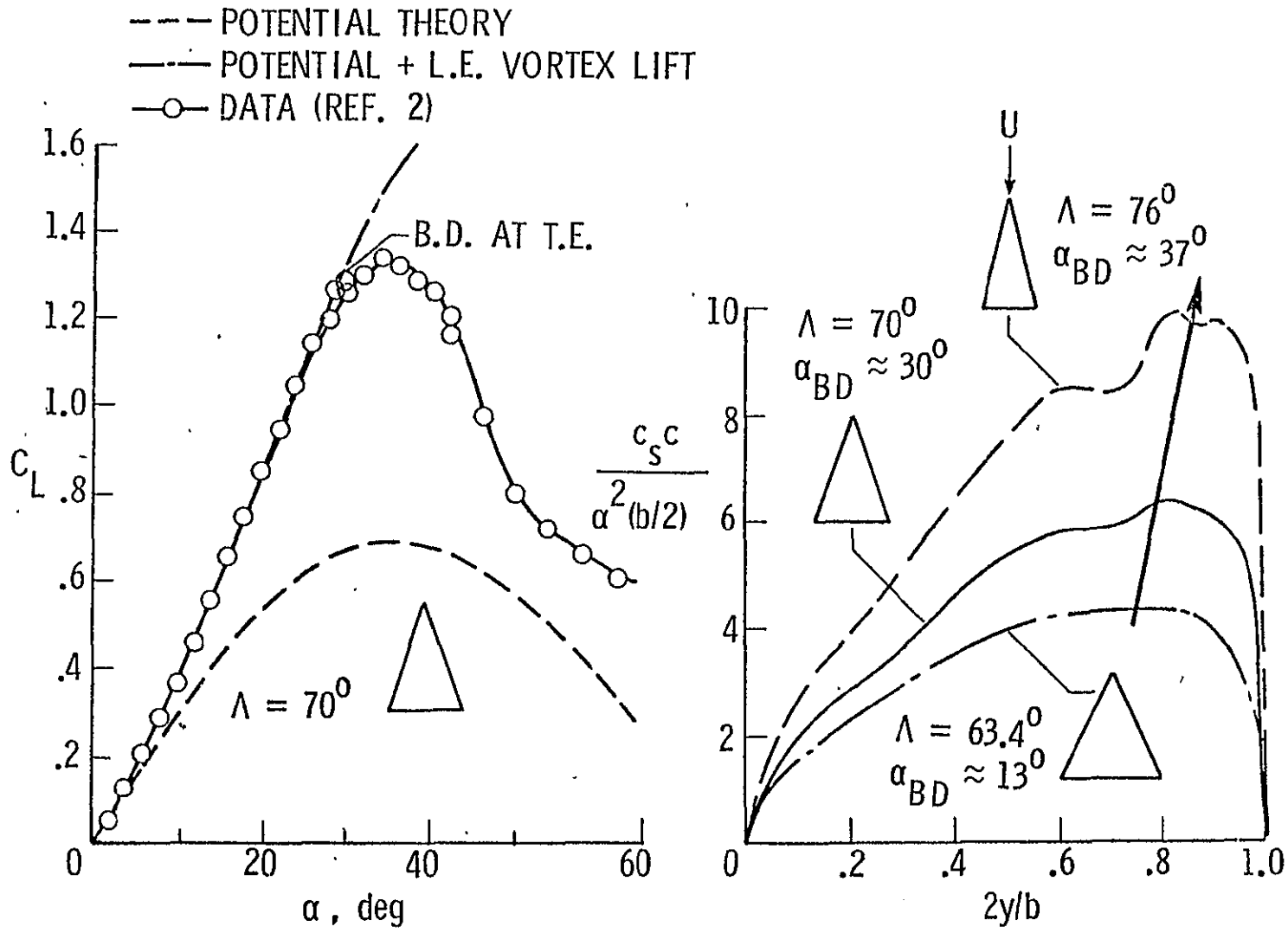

Figure 3.- Delta wing vortex breakdown angle correlation with leading-edge suction distribution.

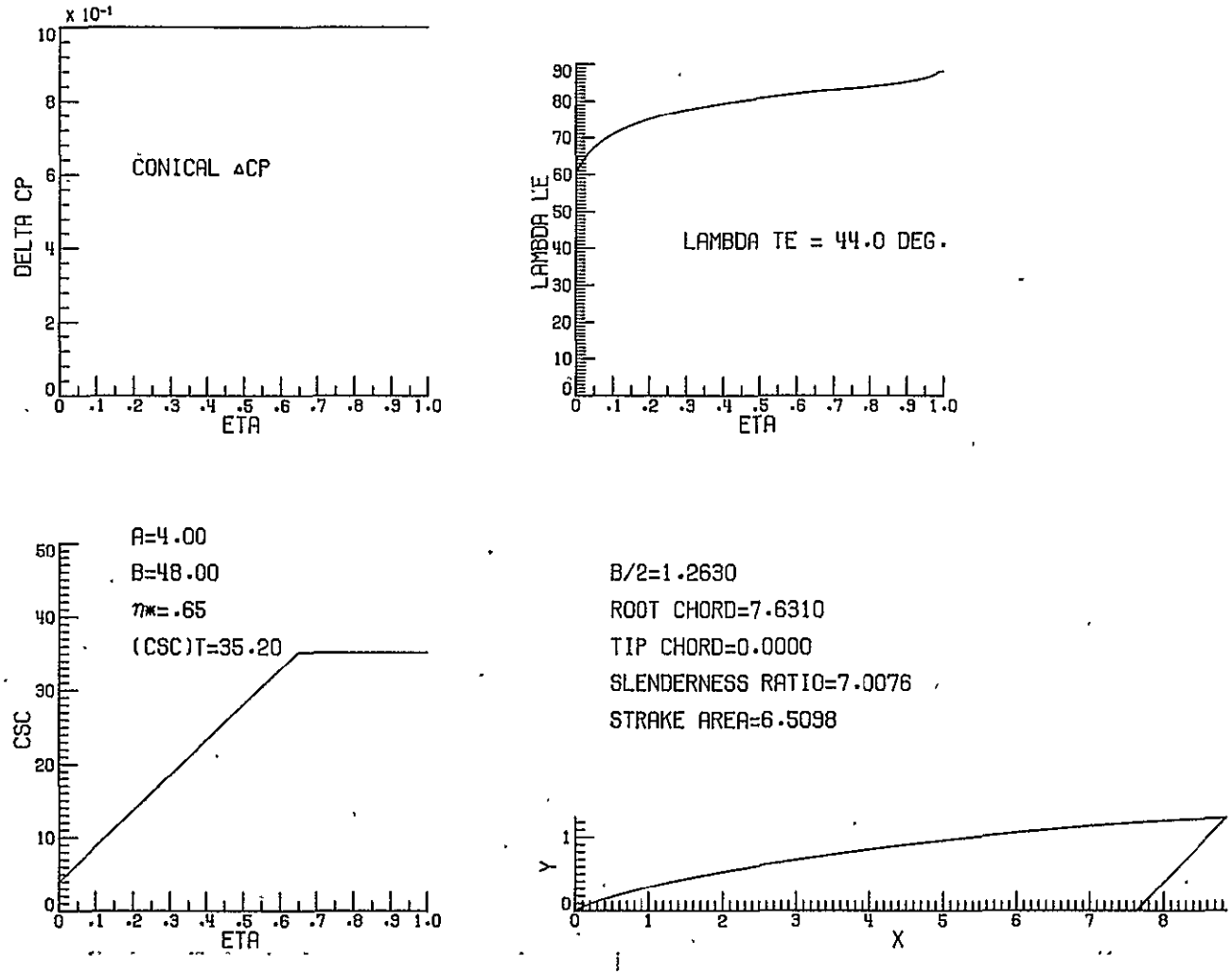

Figure 4.- Design parameters and resulting strake shape - Original gothic shape of ref. 1.

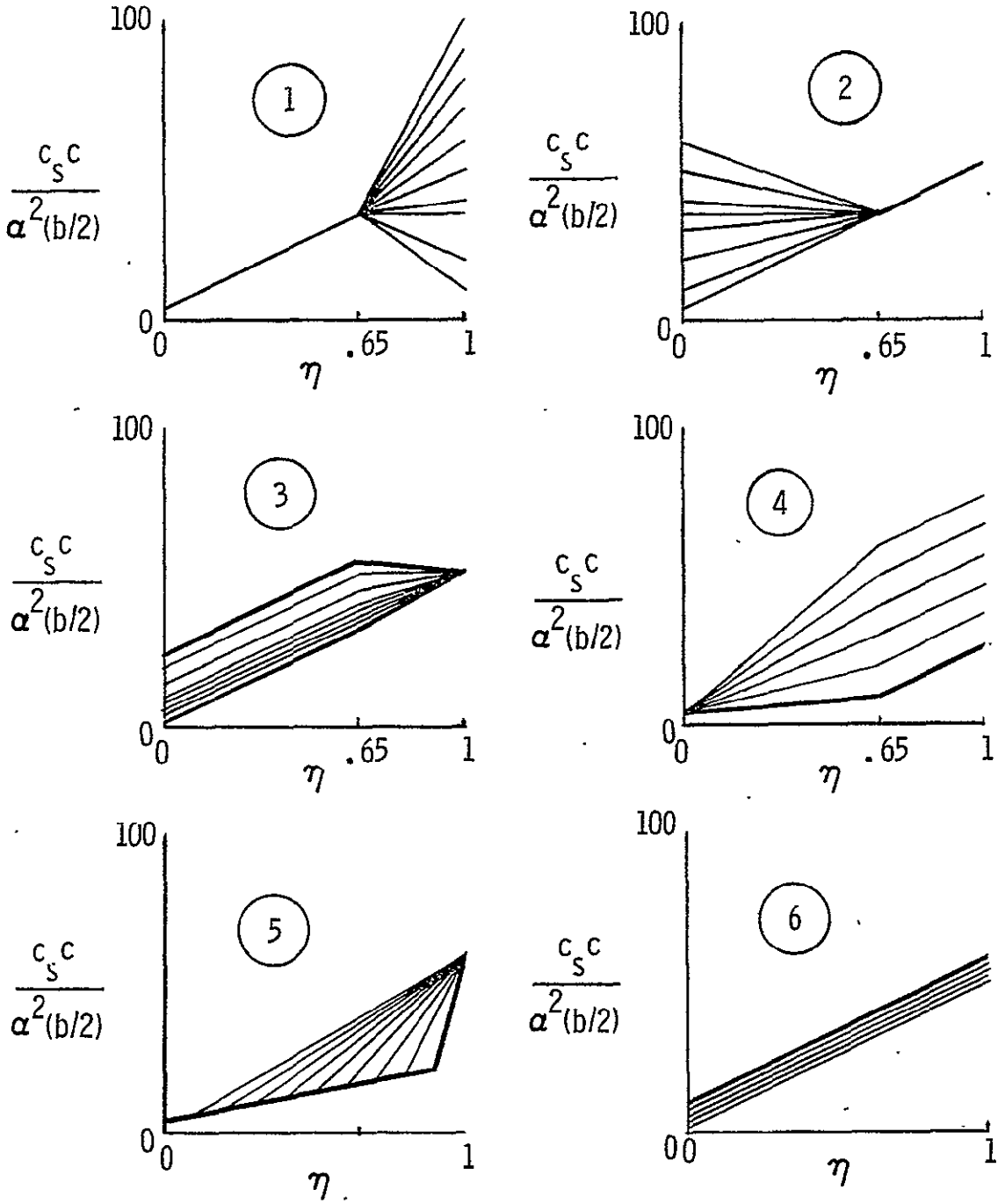

Note: Heavy lines indicate selected strake design distributions.

Figure 5.- Leading-edge suction distributions studied.

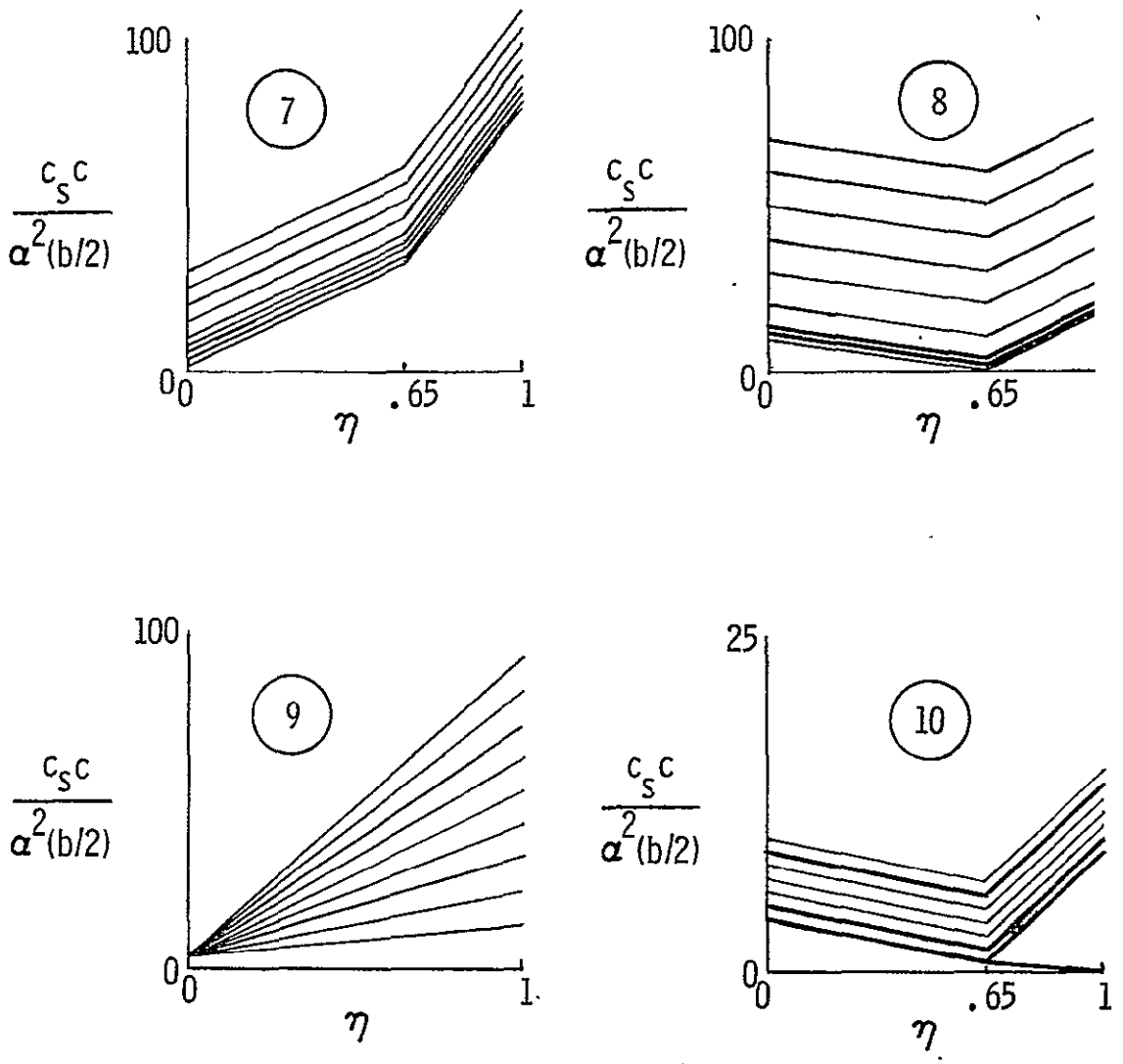

Note: Heavy lines indicate selected strake design distributions.

Figure 5.- Continued.

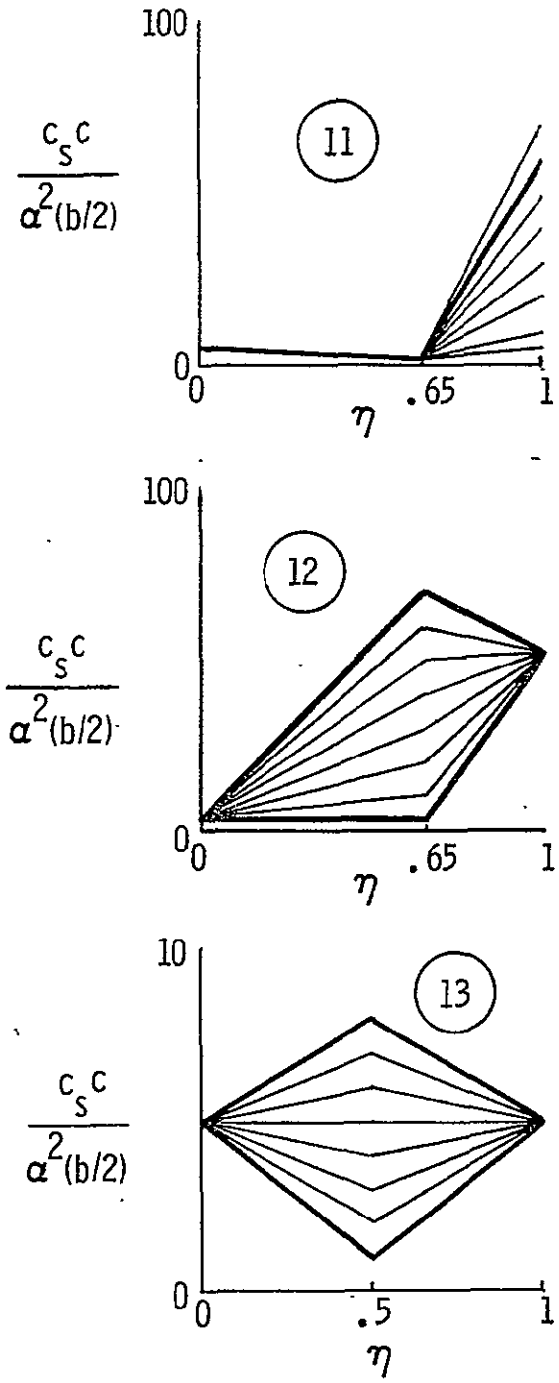

Note: Heavy lines indicate selected strake design distributions.

Figure 5.- Continued.

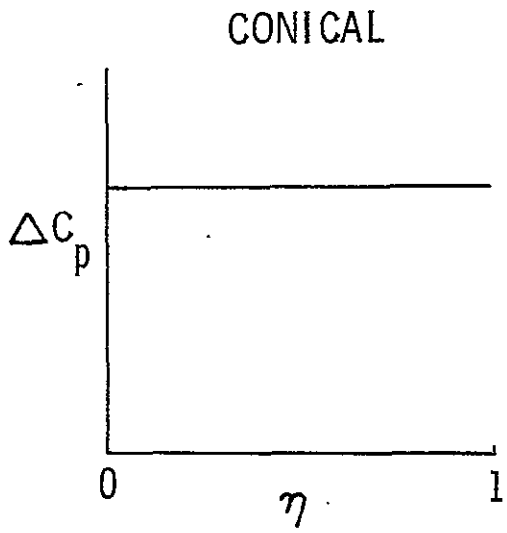

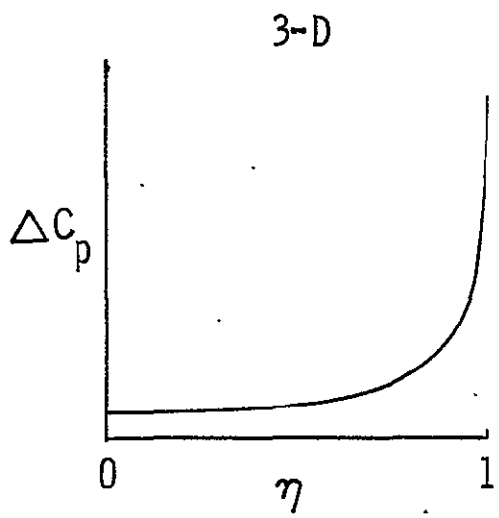

Figure 6.- Lifting pressure distributions studied.

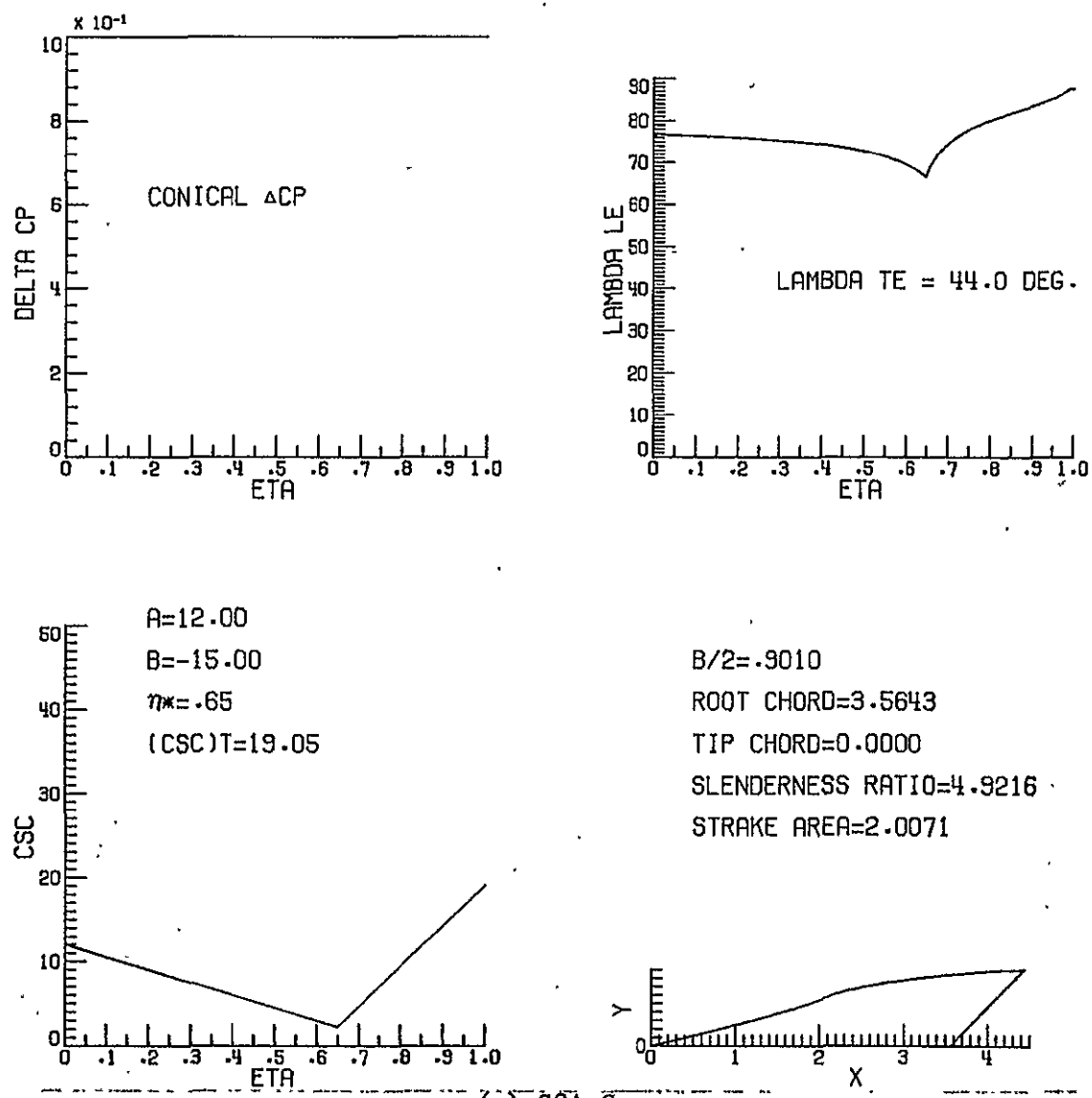

(a) S8A-C

Figure 7.- Design parameters and resulting strake shape - Reflexive group.

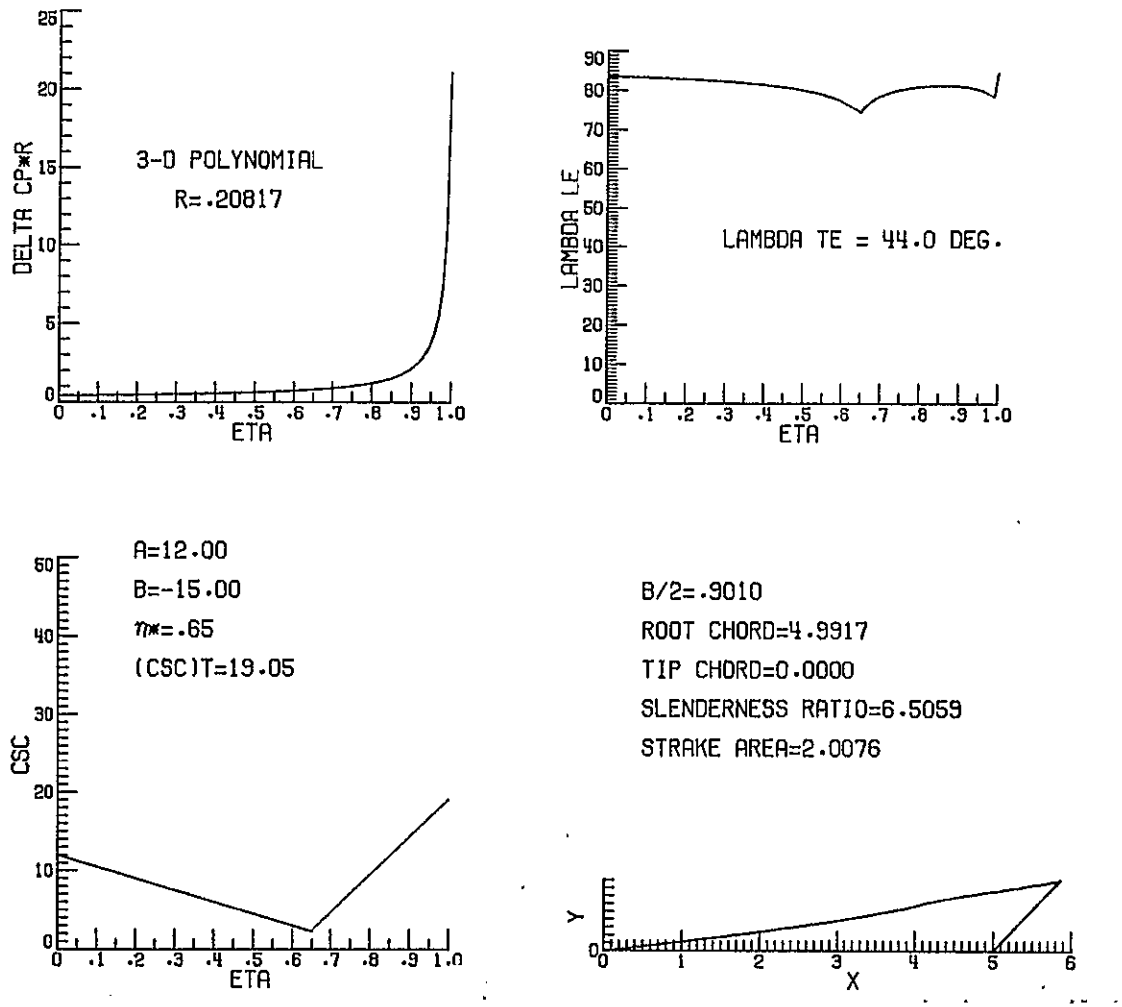

(b) S8A-P

Figure 7.- Continued.

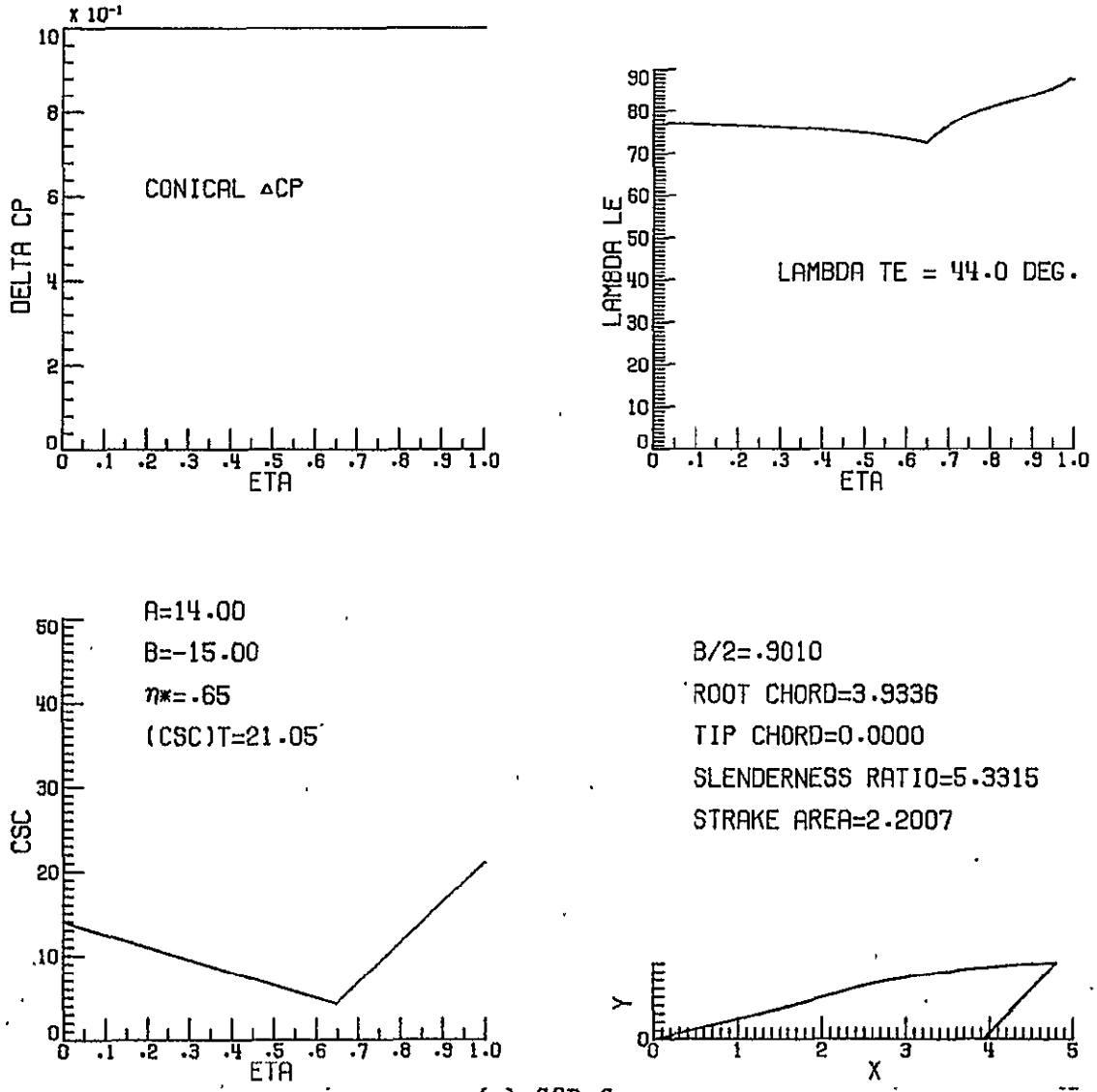

(c) S8B-C

Figure 7.- Continued.

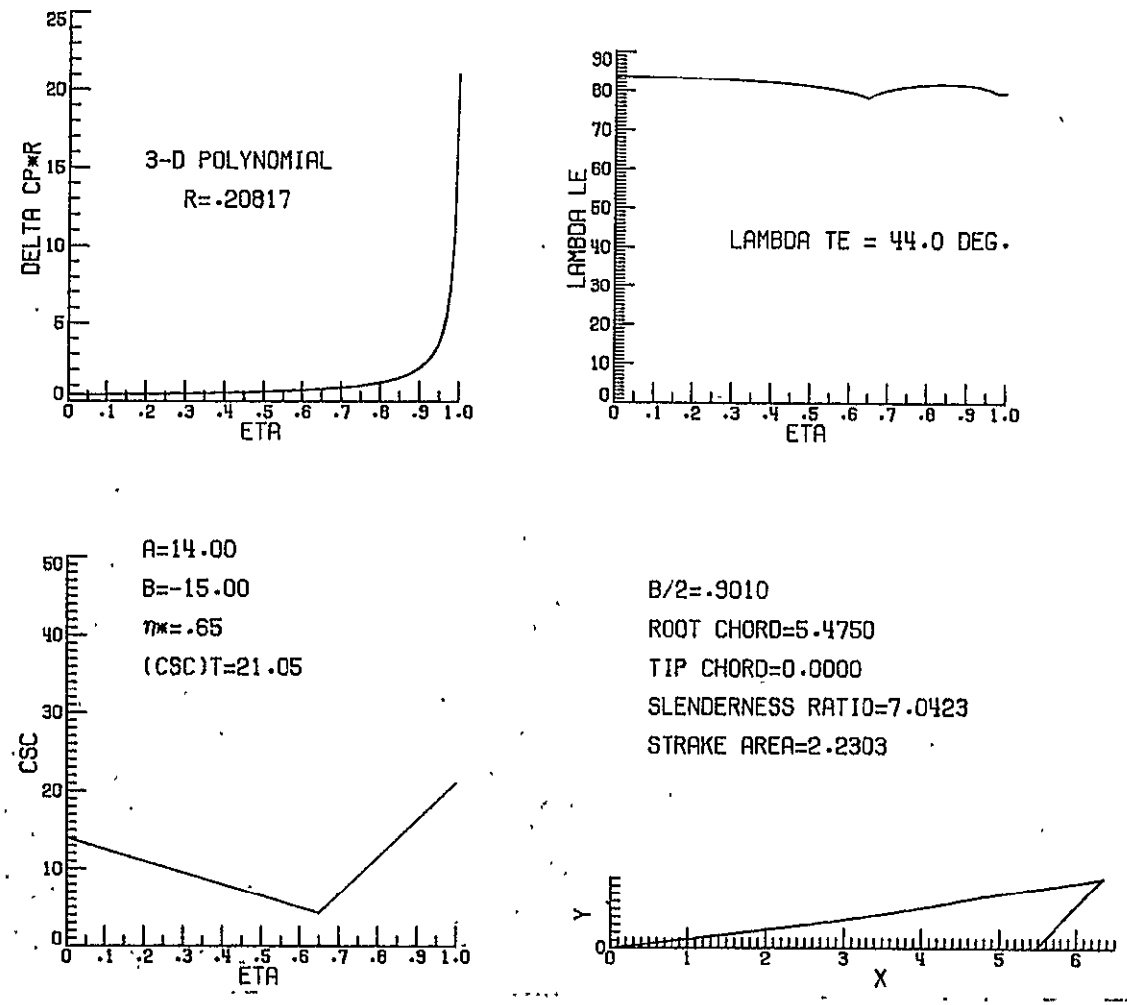

(d) S8B-P

Figure 7.- Continued.

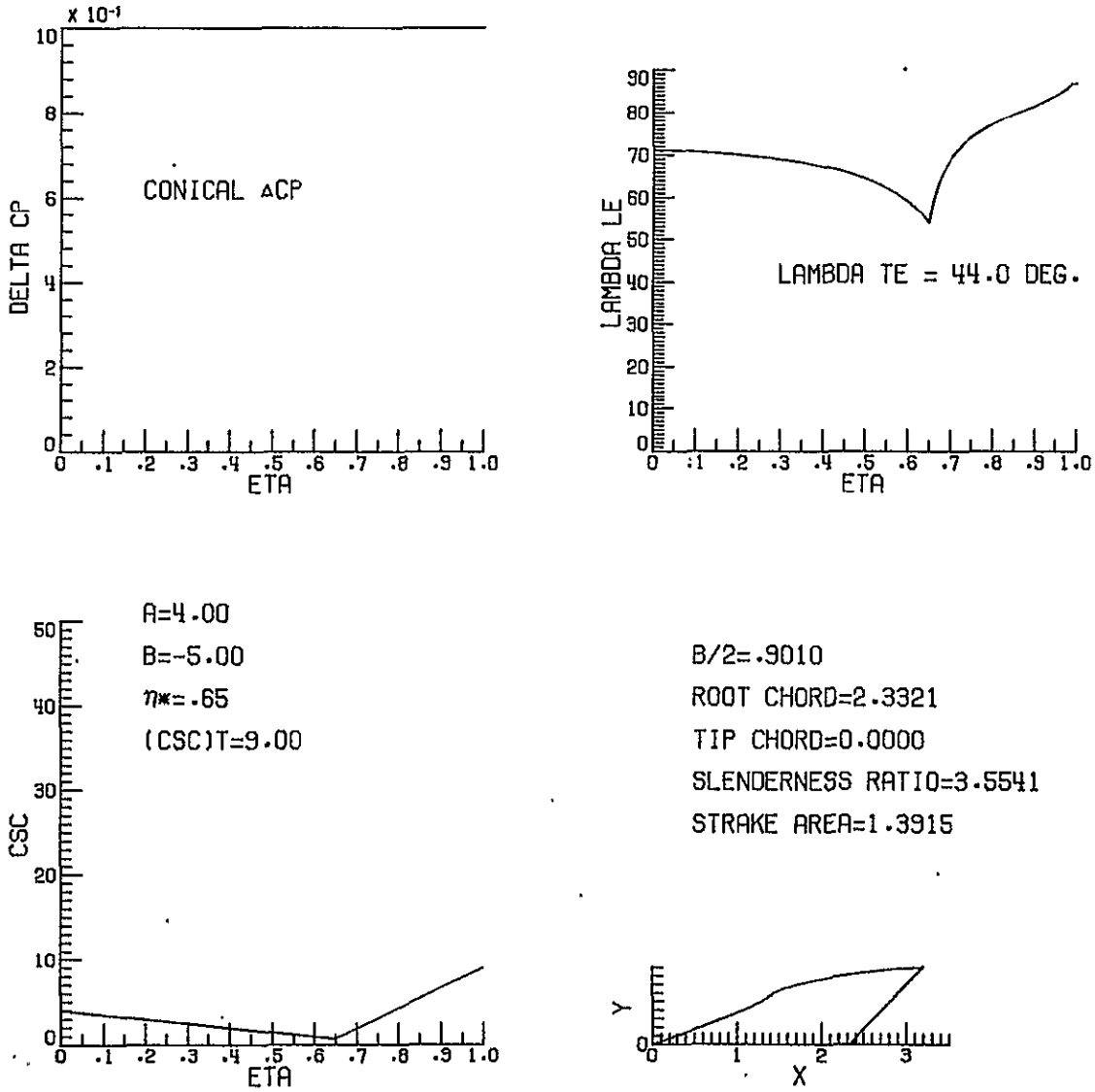

(e) S10B-C

Figure 7.- Continued.

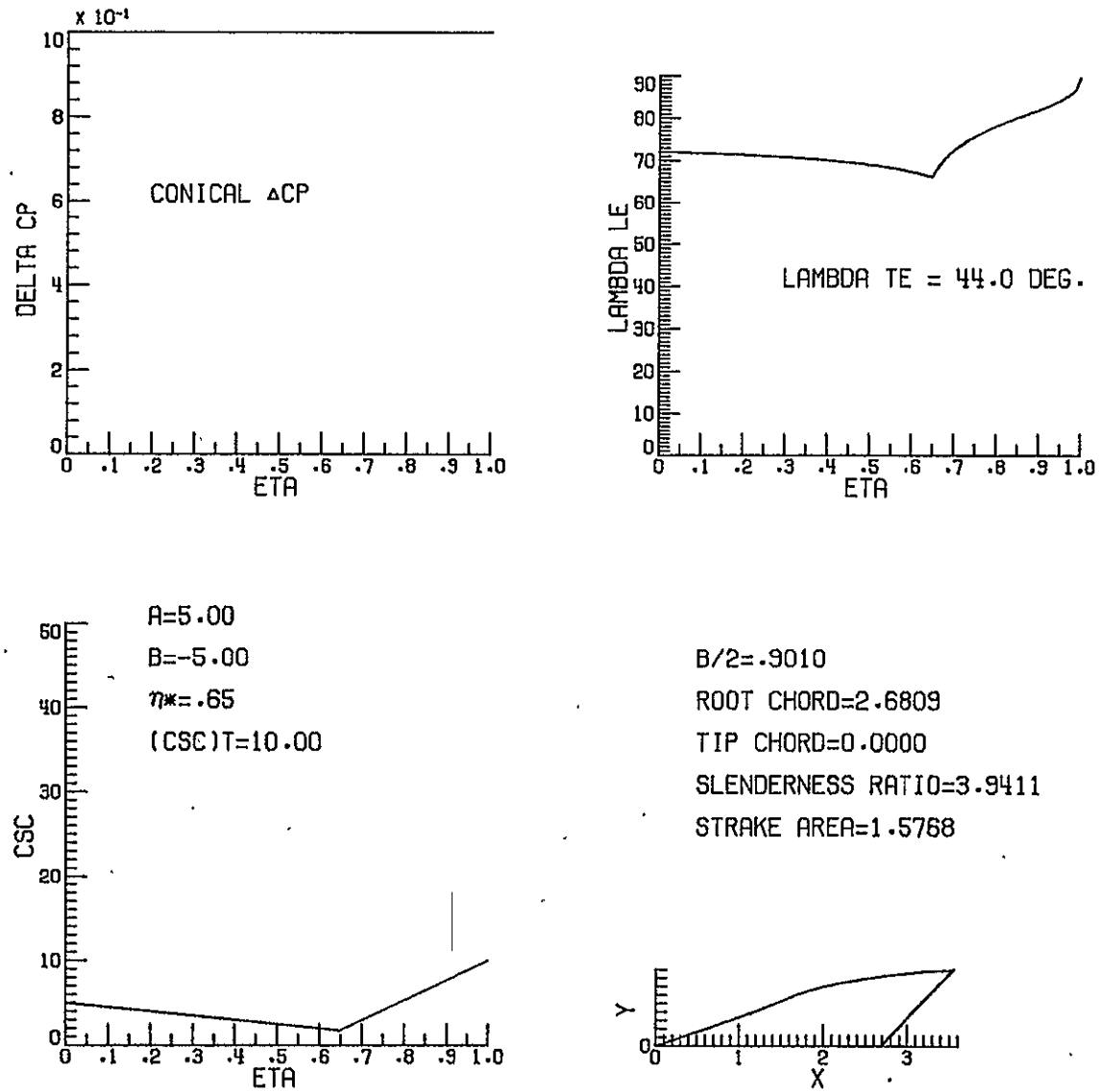

(f) S10C-C

Figure 7.- Continued.

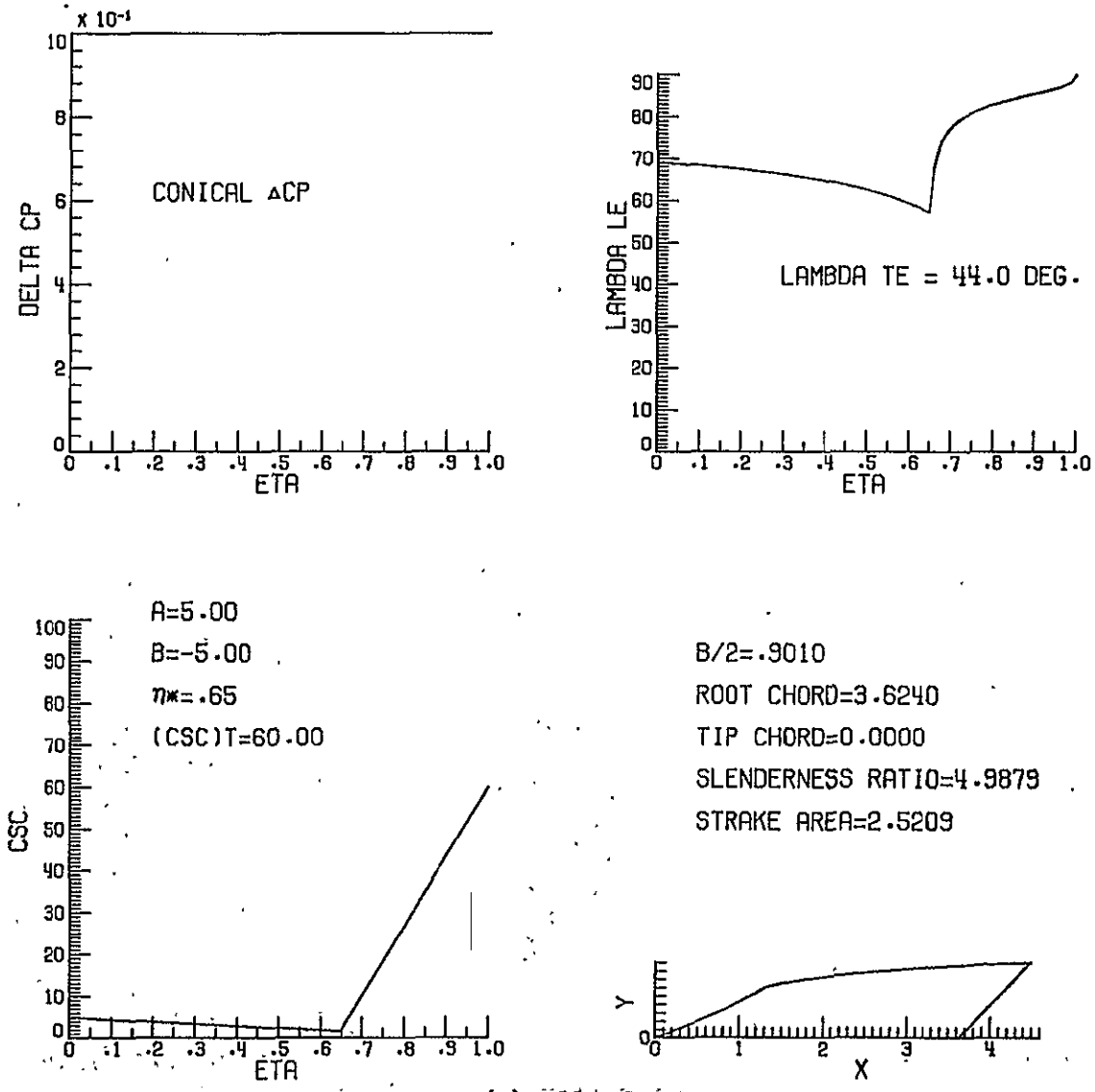

(g) S11A-C

Figure 7.- Continued.

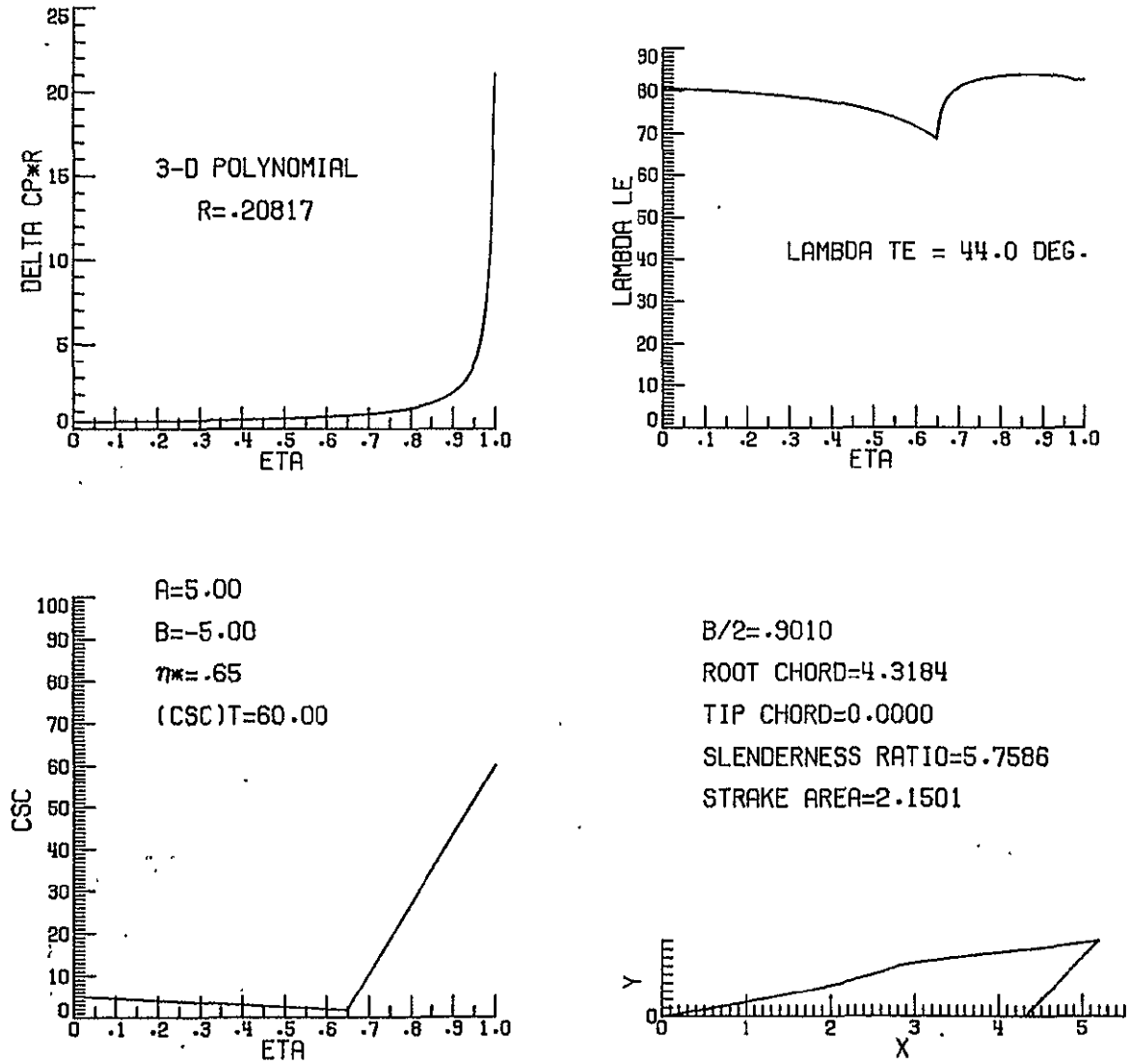

(h) S11A-P

Figure 7.- Continued.

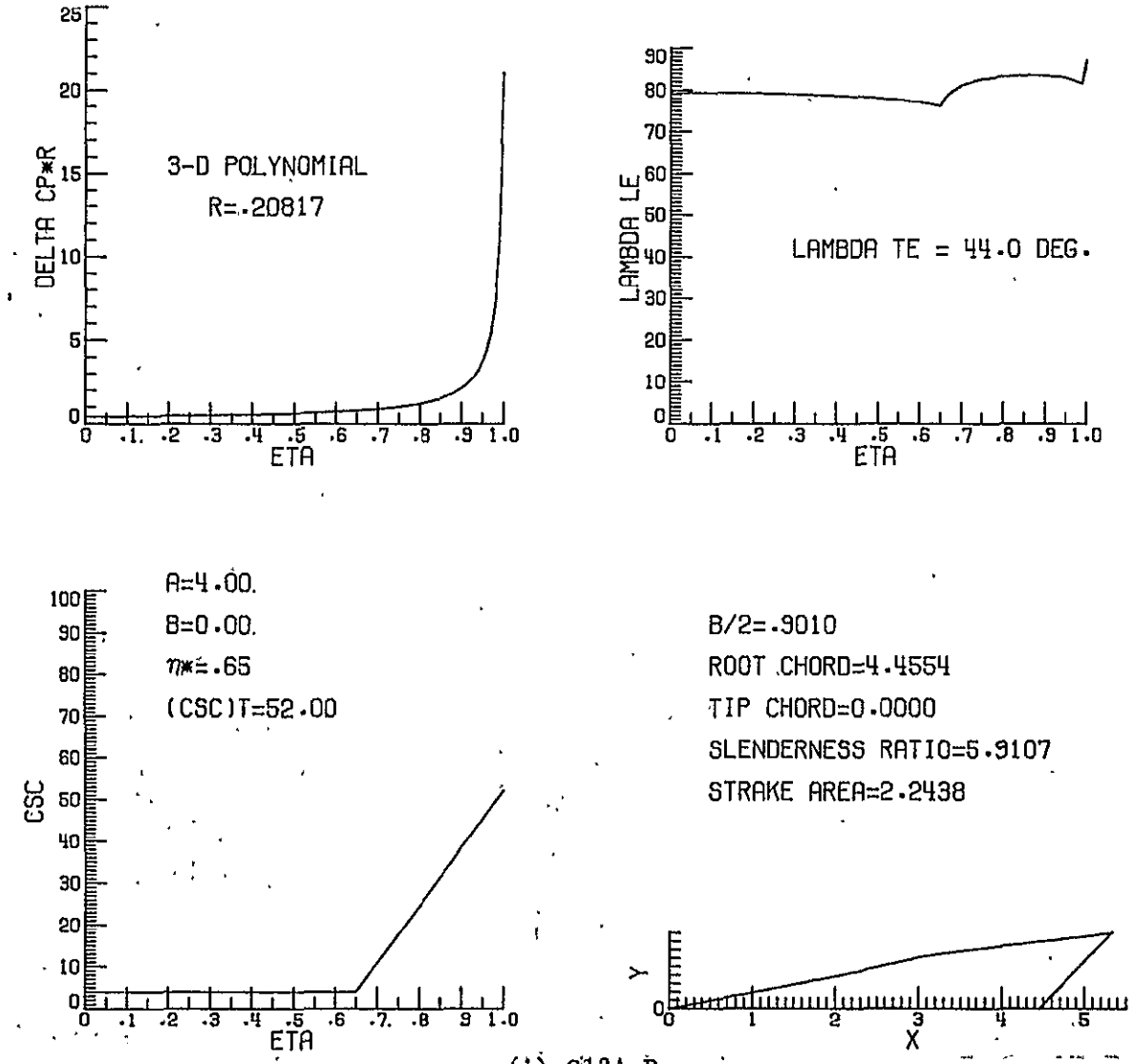

(i) S12A-P

Figure 7.- Continued.

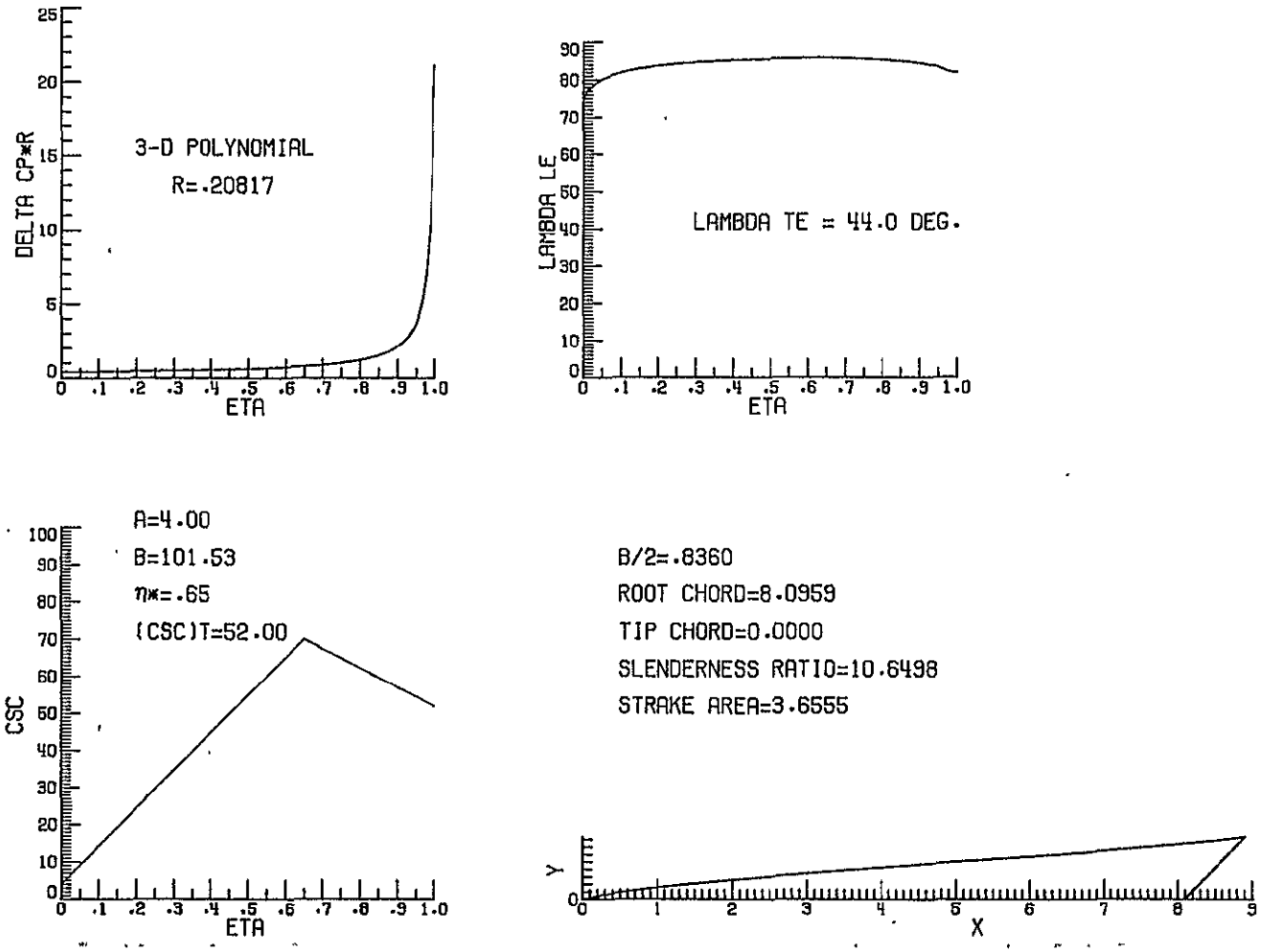

(j) S12B-P

Figure 7.- Continued.

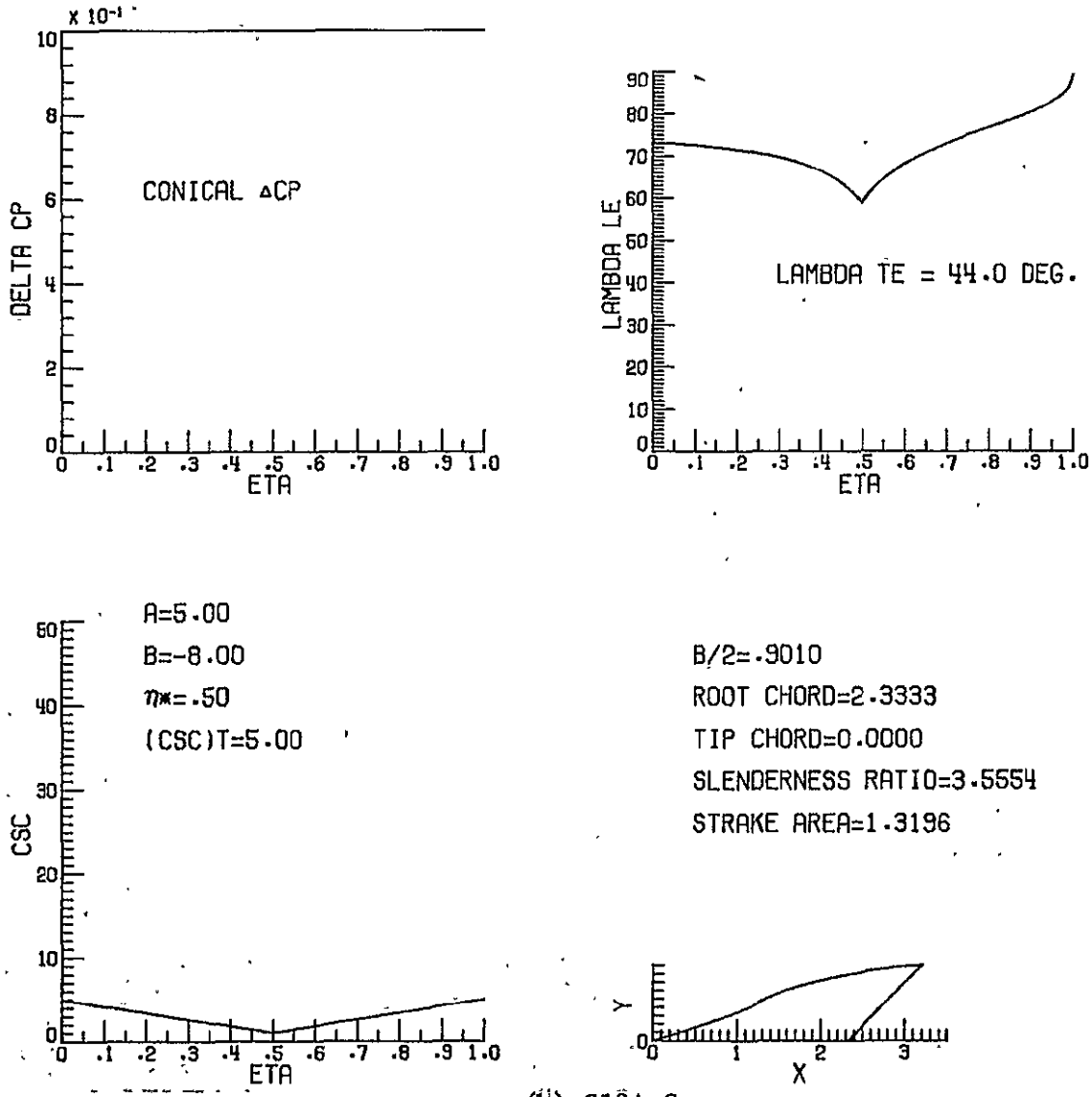

(k) S13A-C

Figure 7.- Continued.

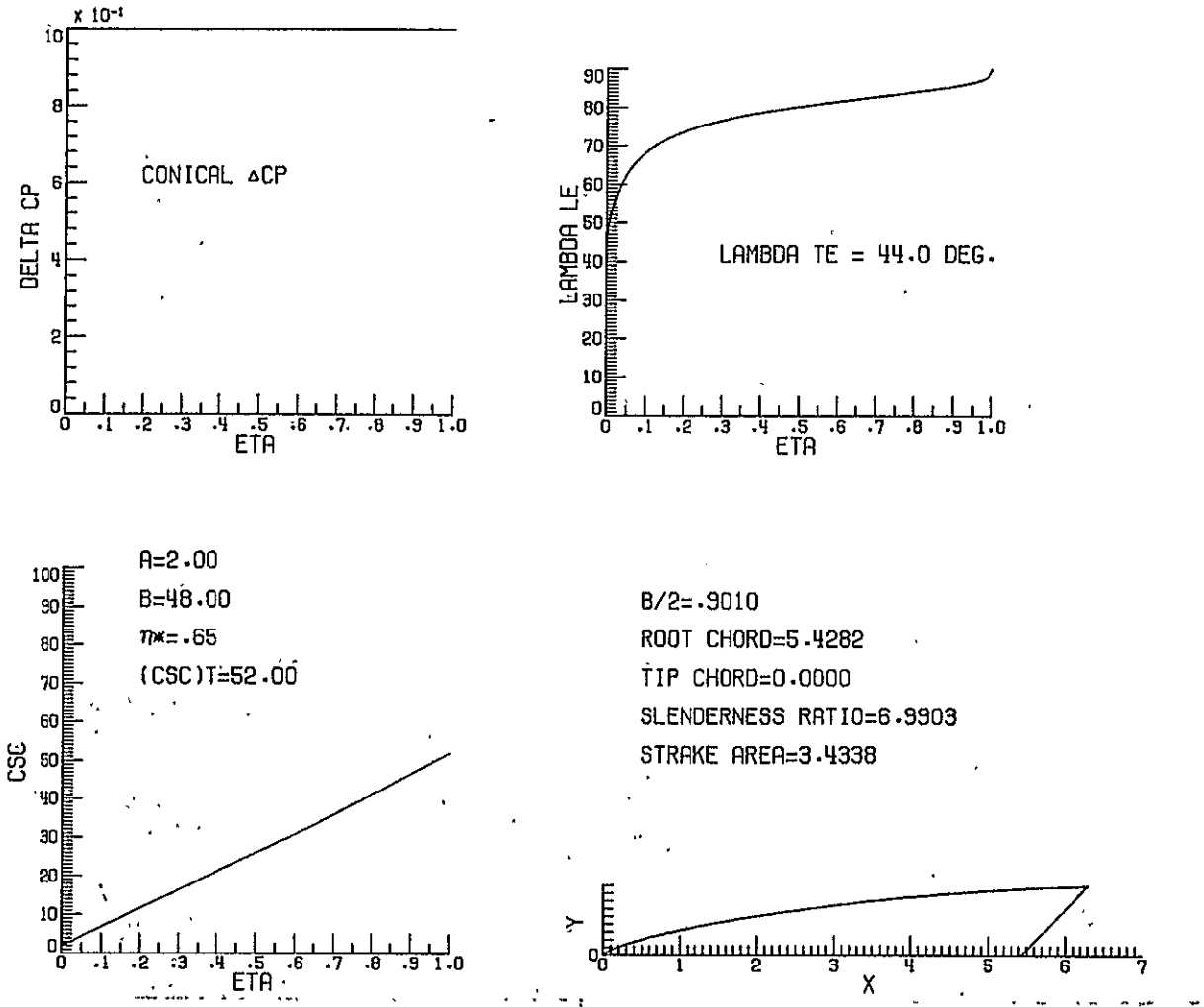

(a) S3A-C

Figure 8. Design parameters and resulting strake shape - Gothic group

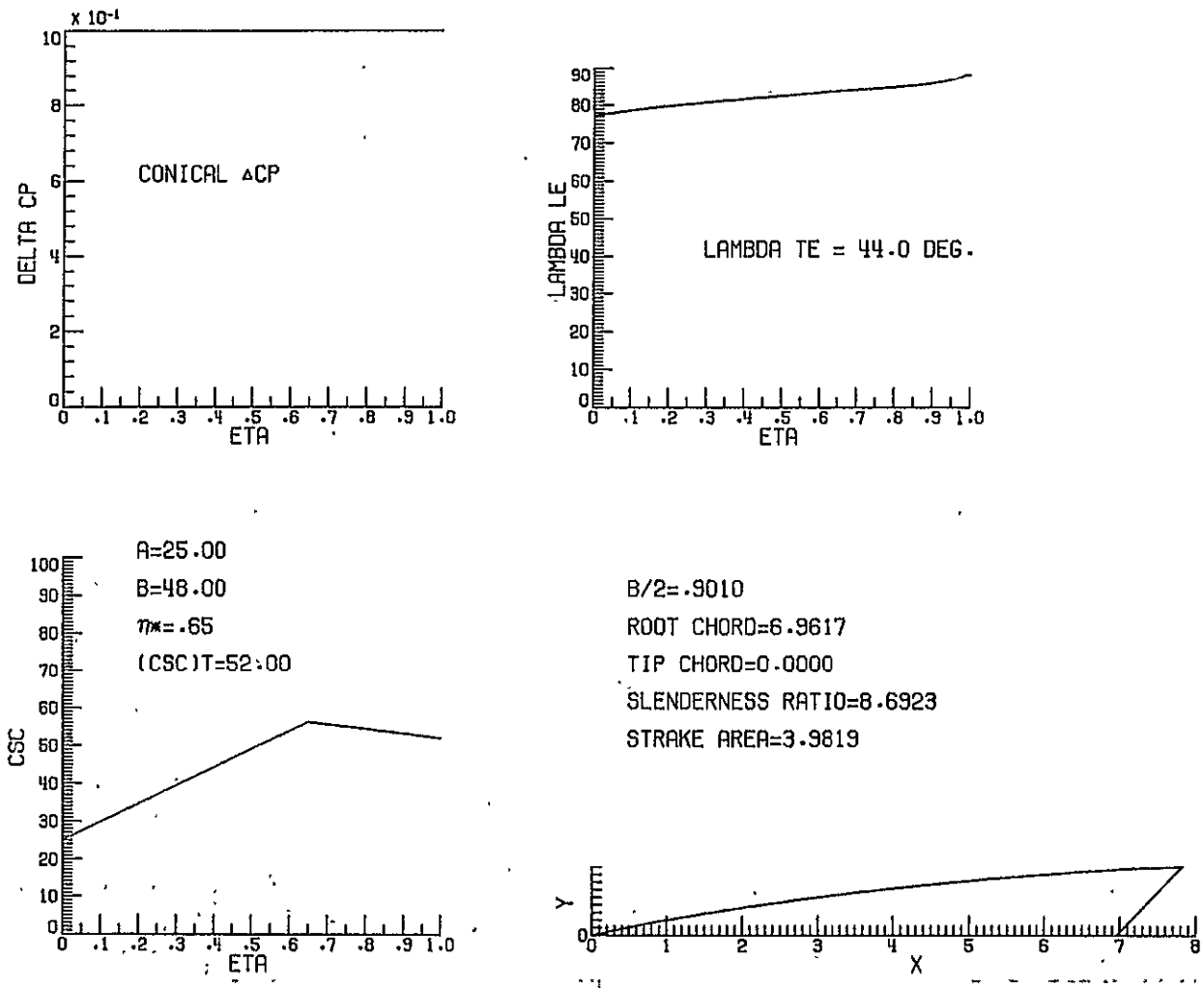

(b) S3B-C

Figure 8.- Continued.

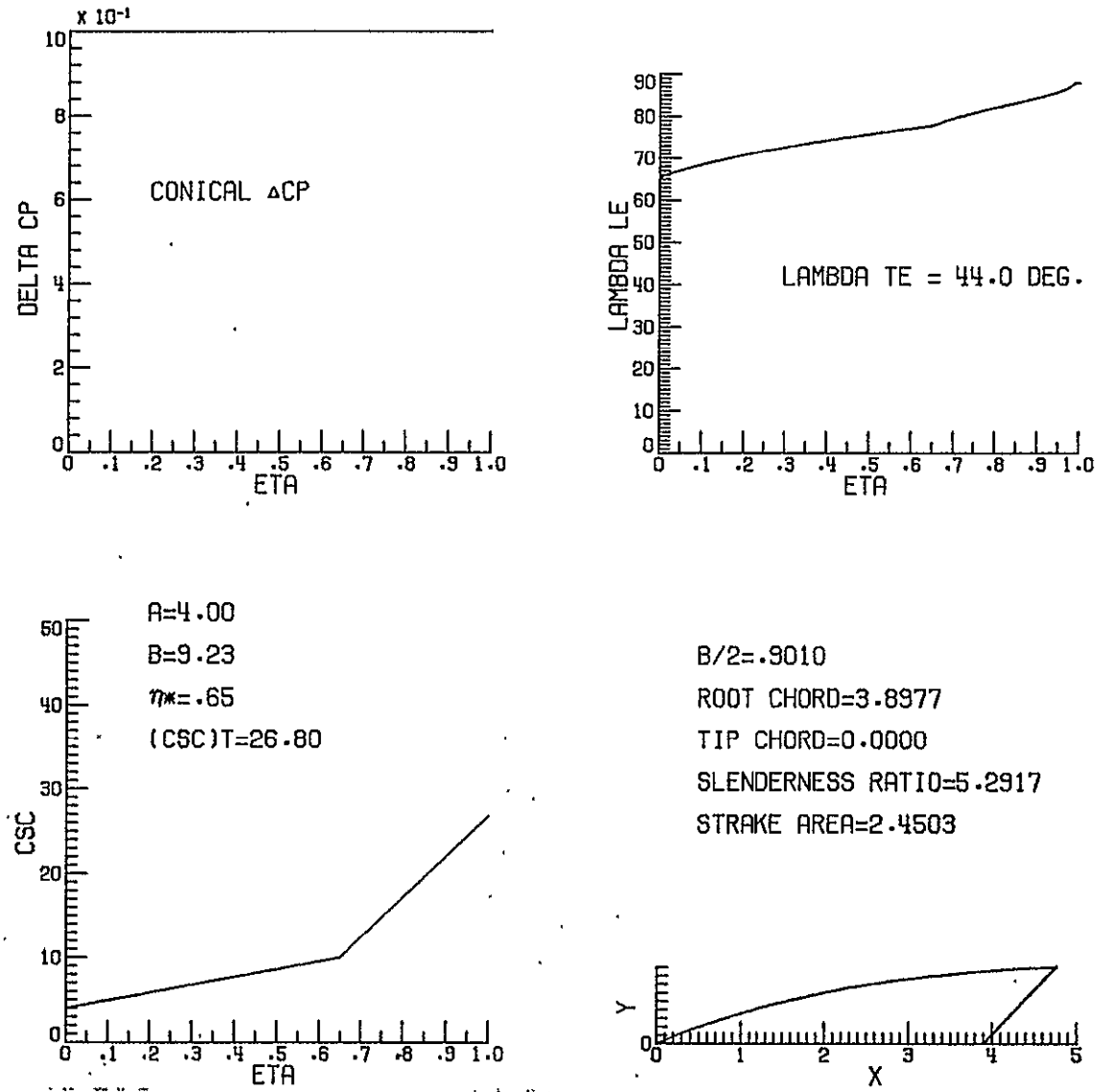

(c) S4A-C

Figure 8.- Continued.

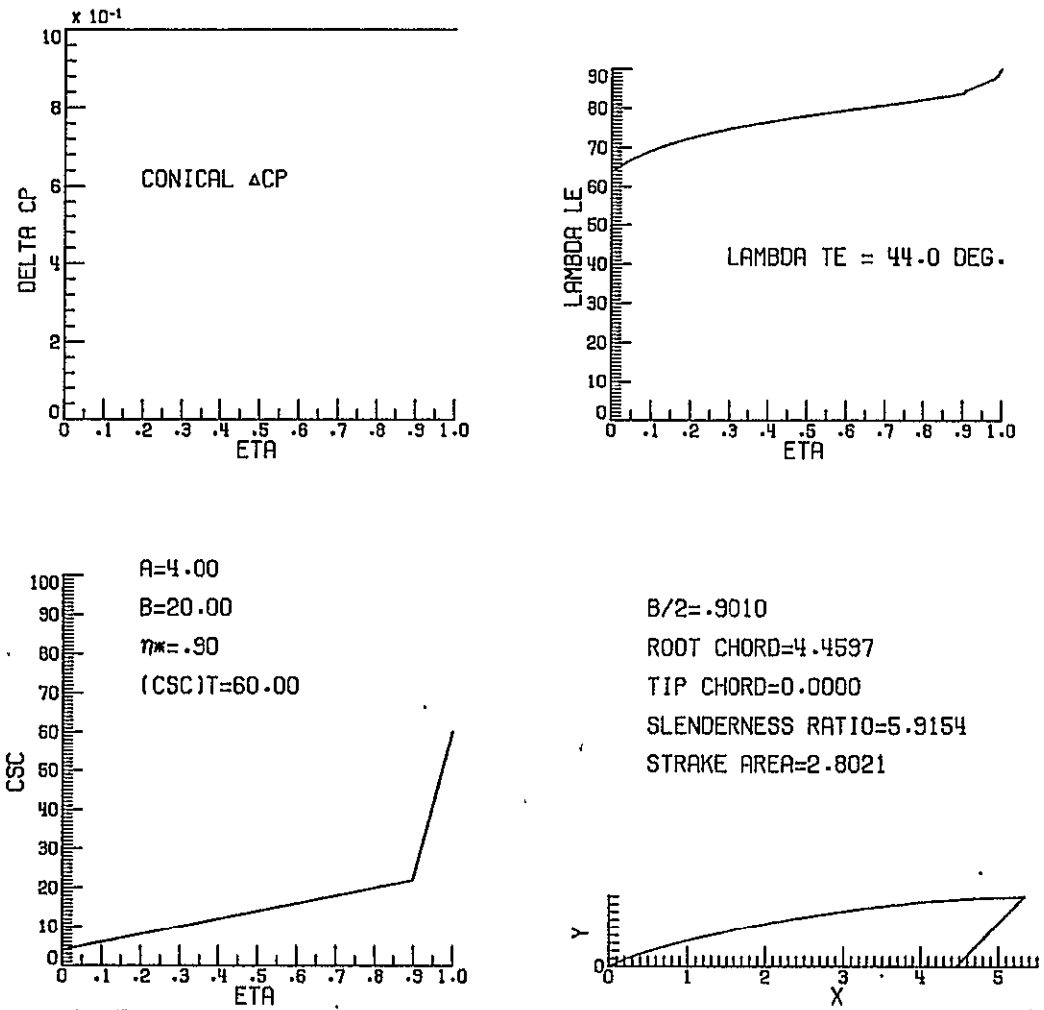

(d) S5A-C

Figure 8.- Continued.

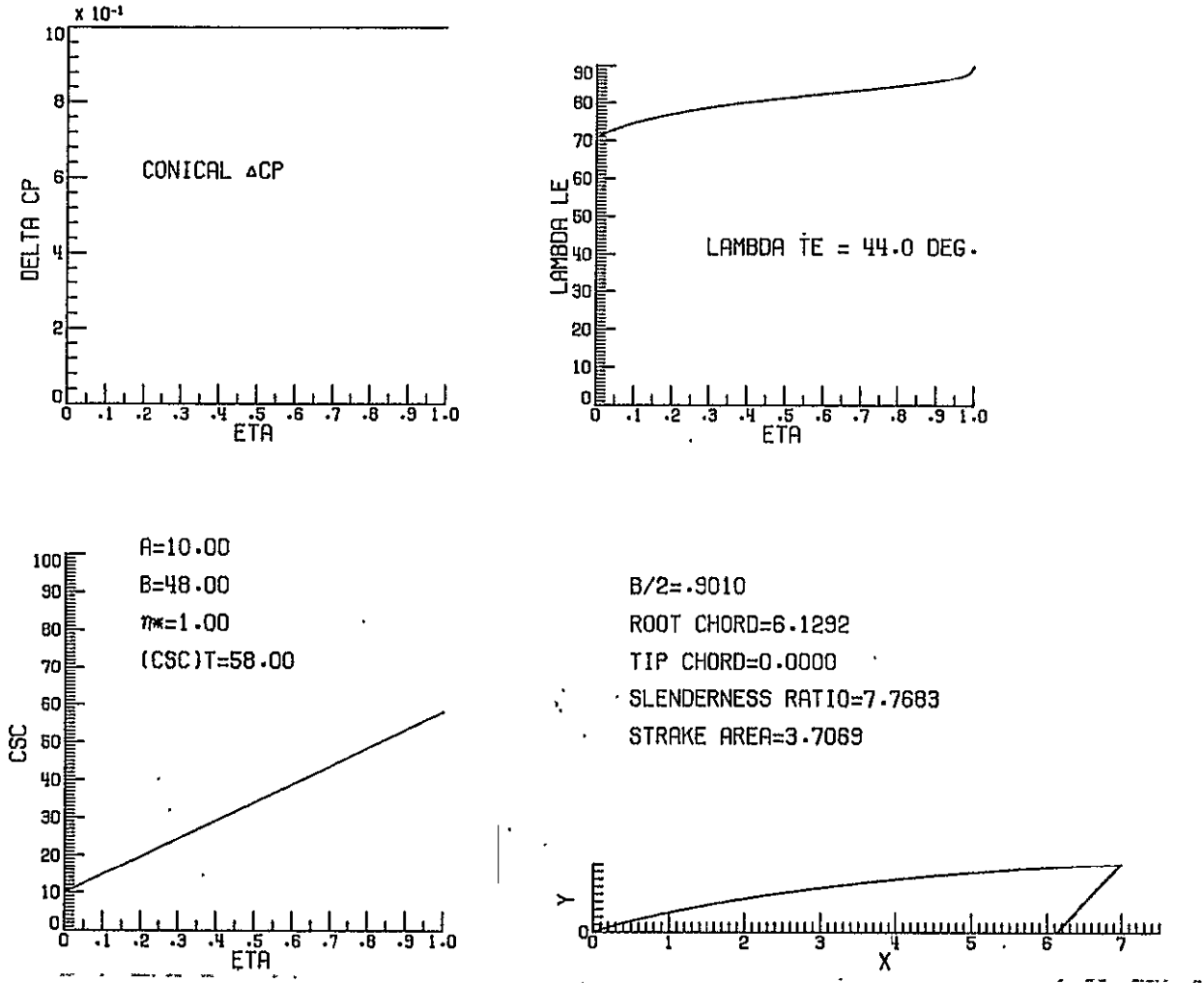

(e) S6A-C

Figure 8.- Continued.

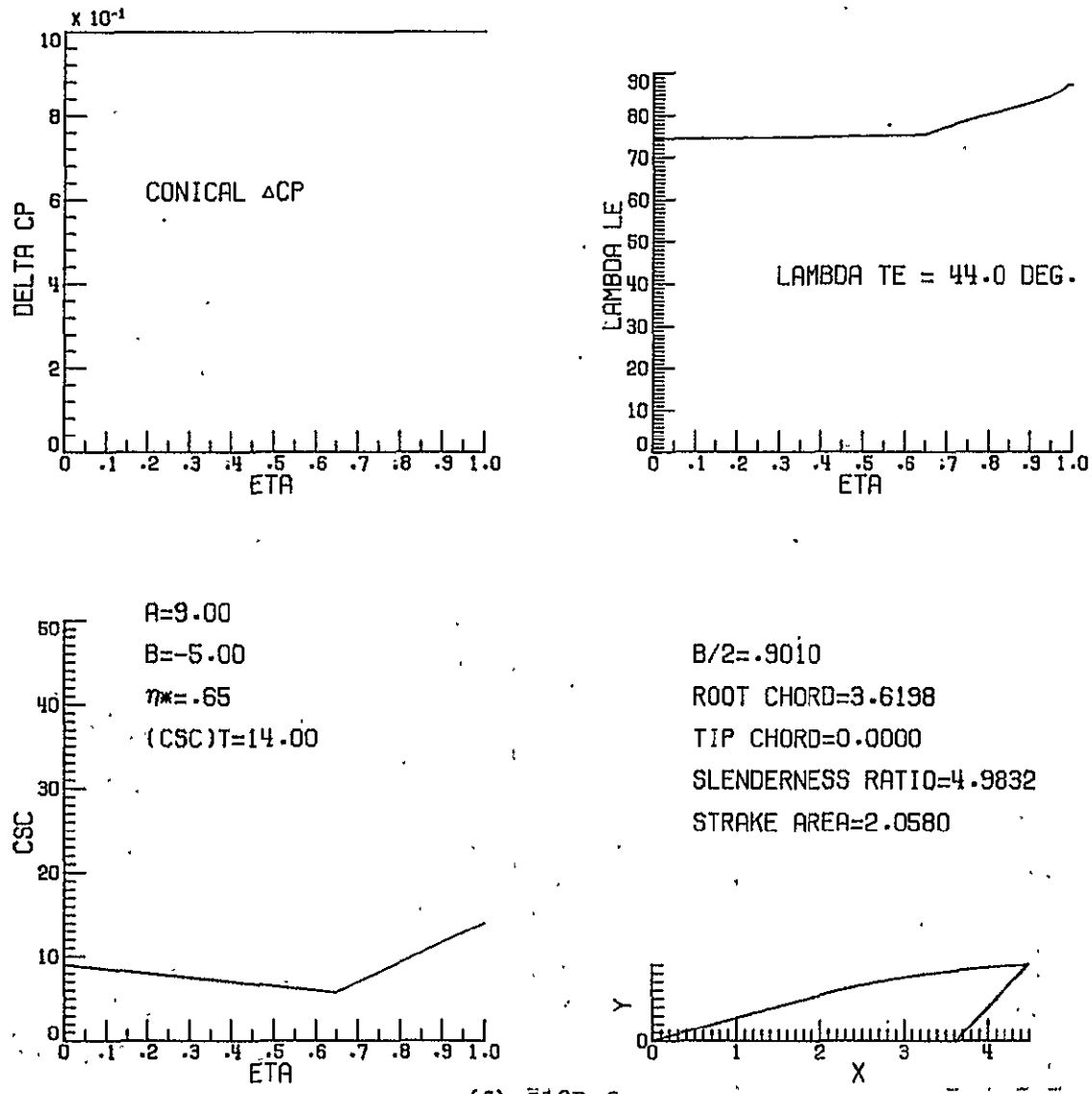

(f) S10D-C

Figure 8.- Continued.

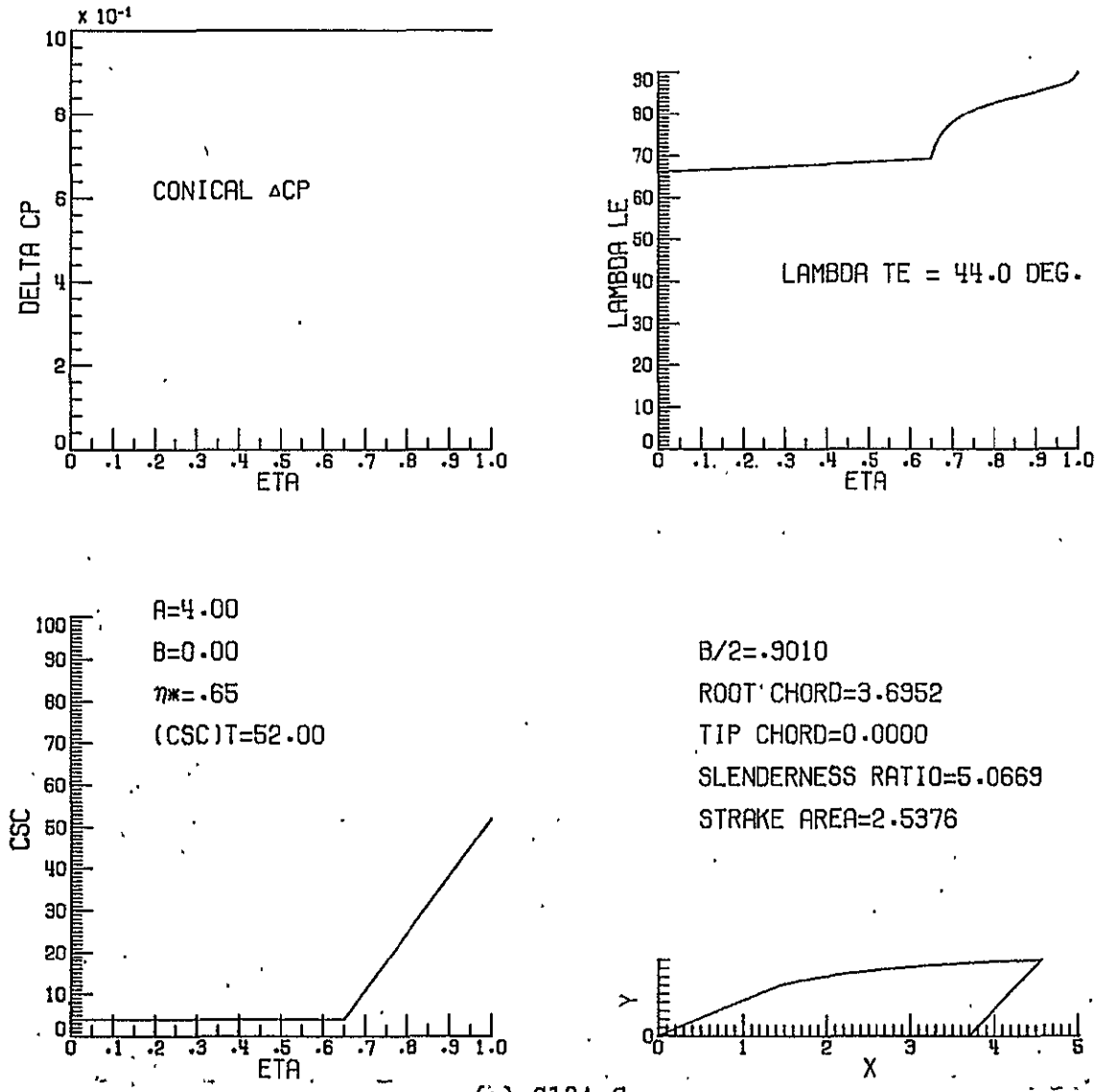

(g) S12A-C

Figure 8.- Continued.

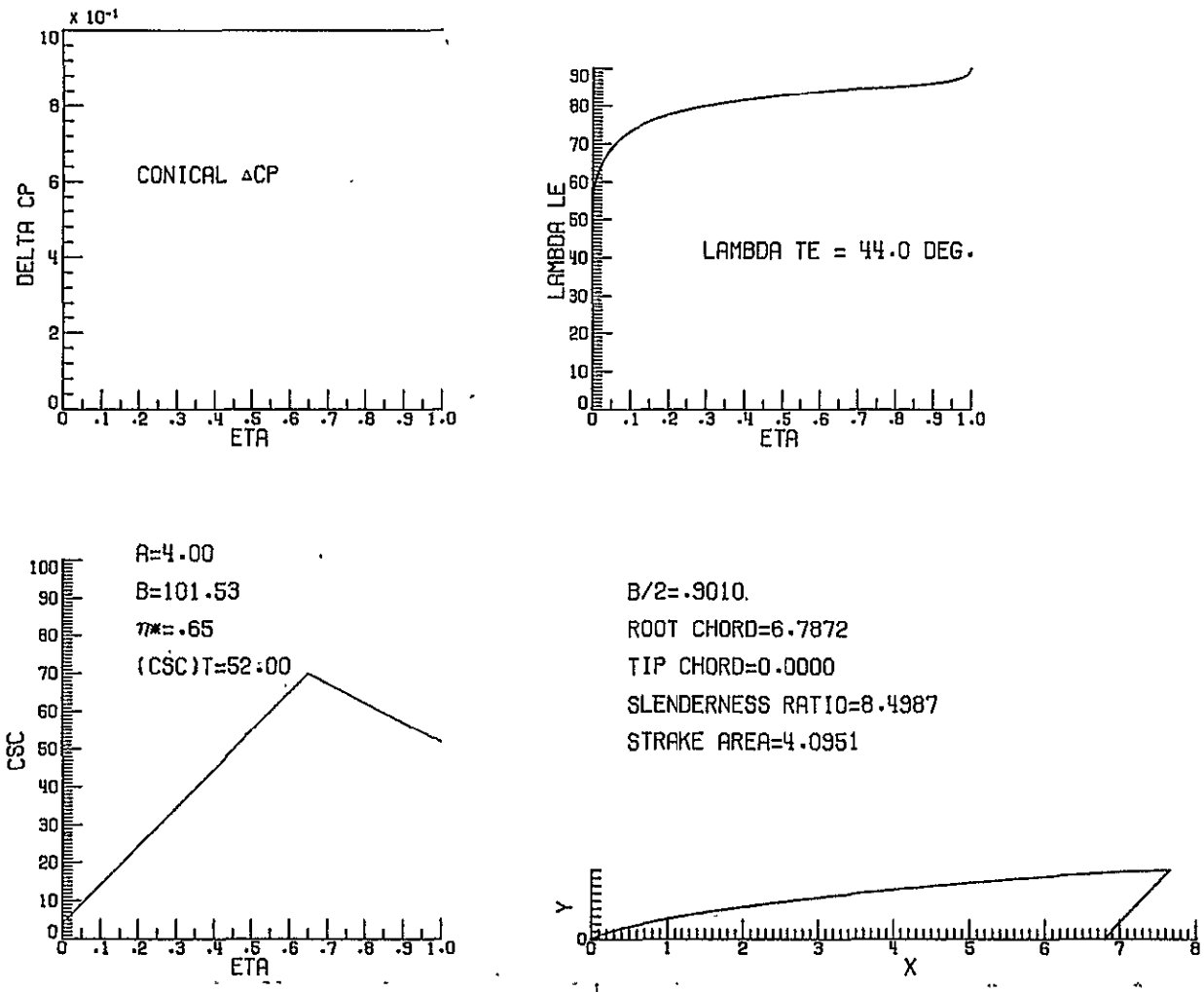

(h) S12B-C

Figure 8.– Continued.

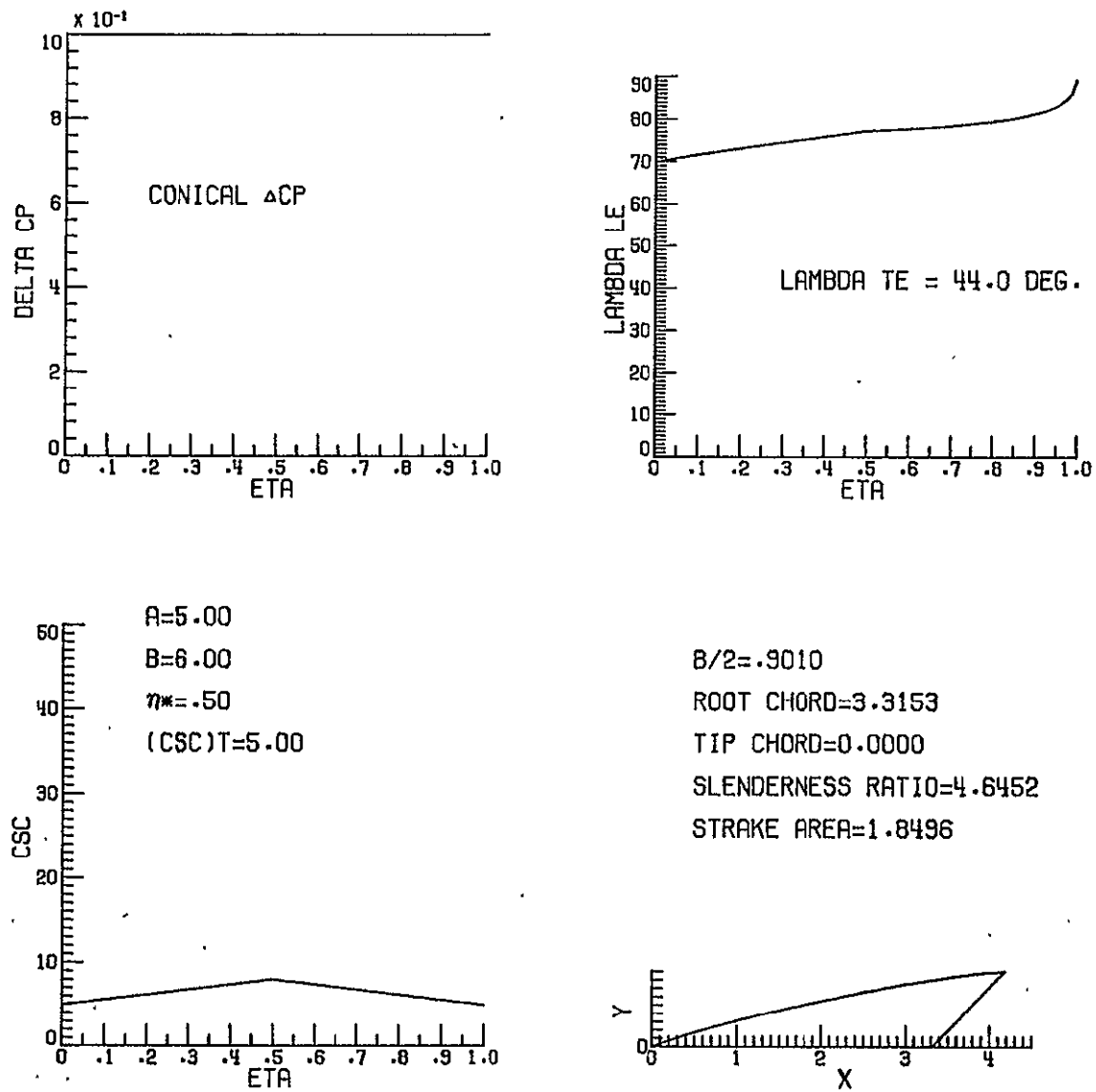

(i) S13B-C

Figure 8.- Continued.

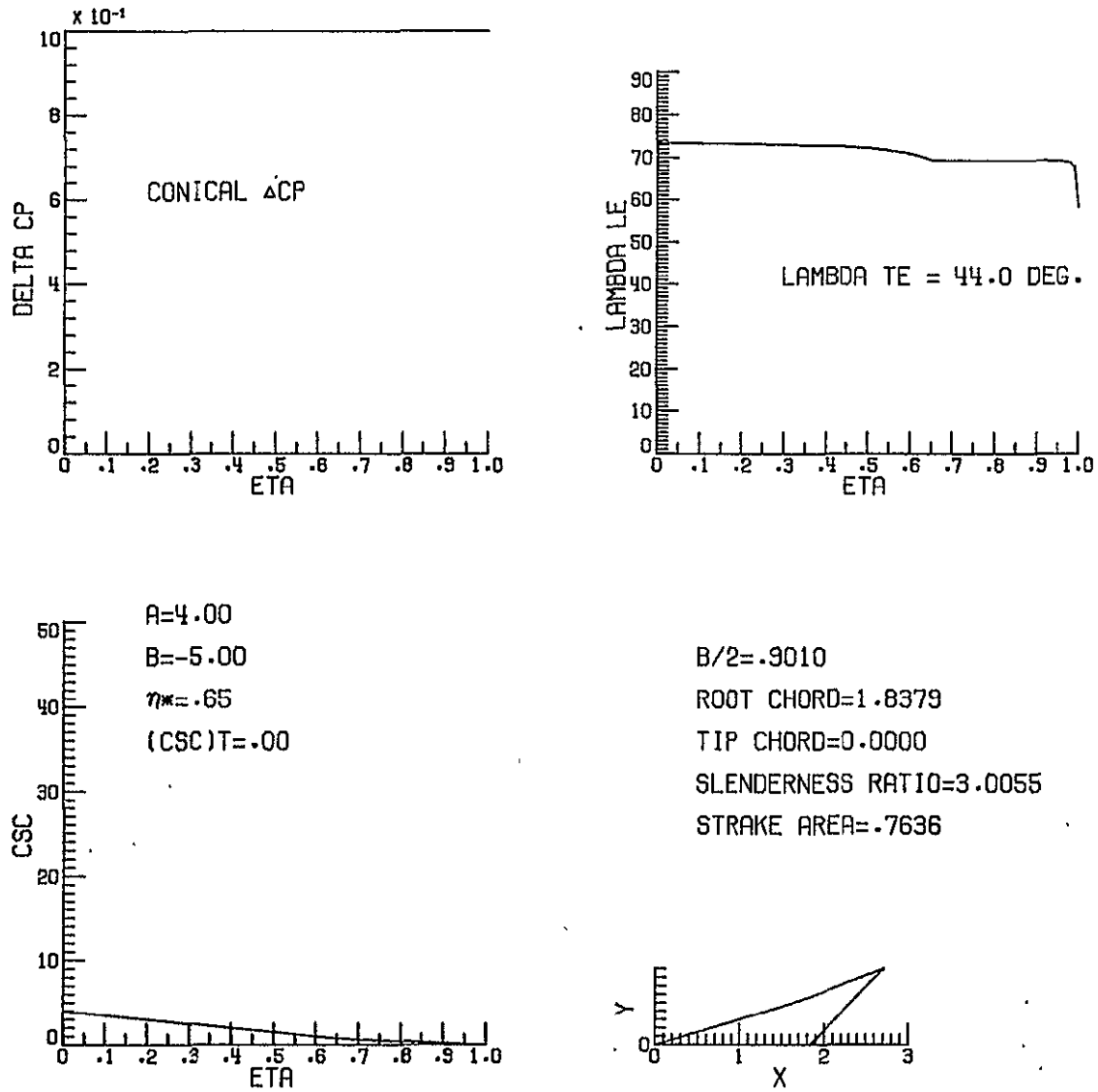

S10A-C

Figure 9.- Design parameters and resulting strake shape - Limiting case.

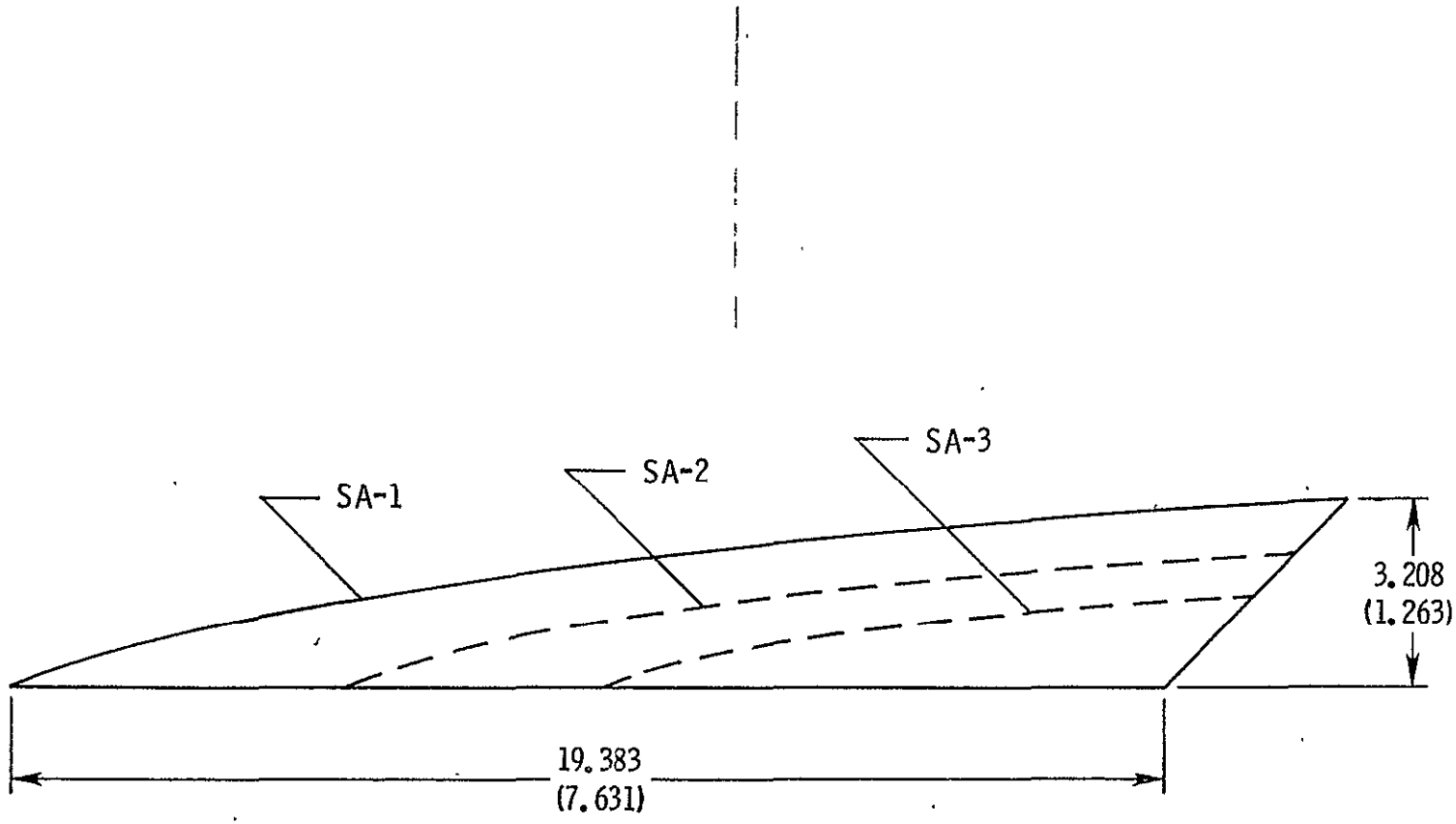

Figure 10.- Area scaling of original strake/SA-1: SA Series.

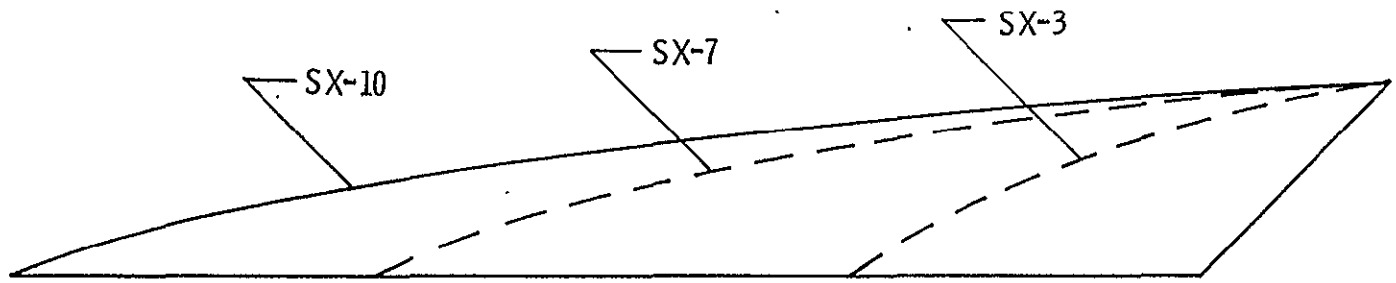

Figure 11.- Chordwise scaling of original strake/SX-10: SX Series.

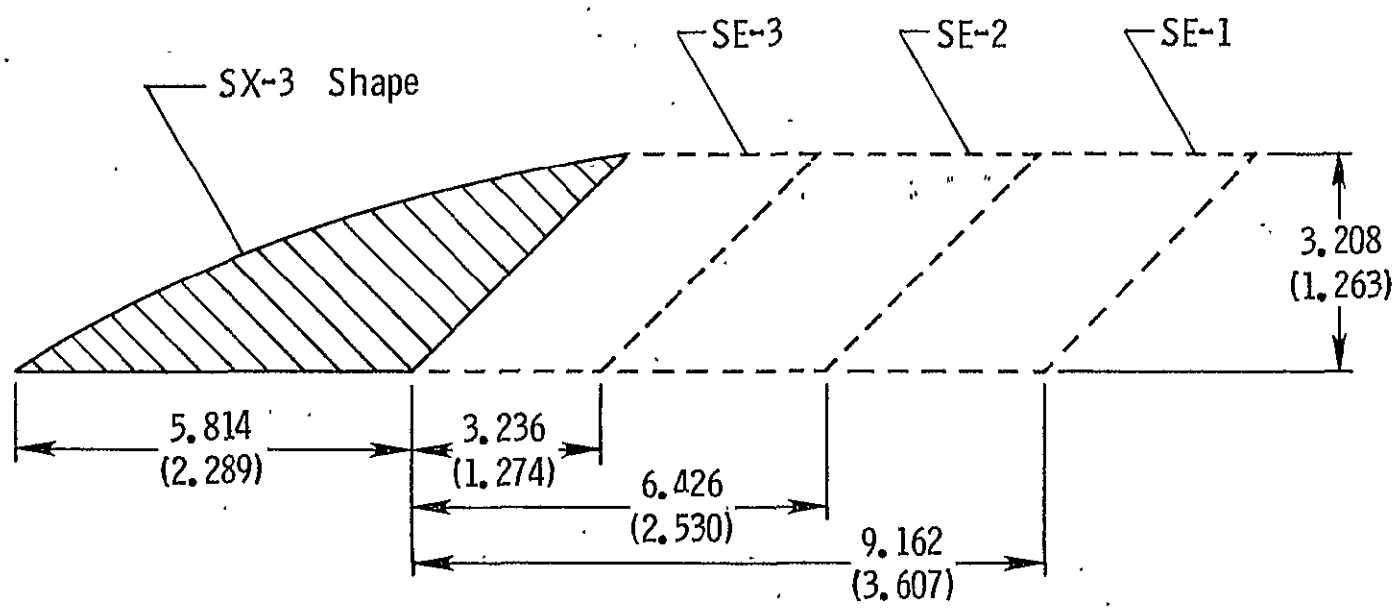

Figure 12.- Addition of trailing edge area/side edge length to the SX-3 strake: SE Series.

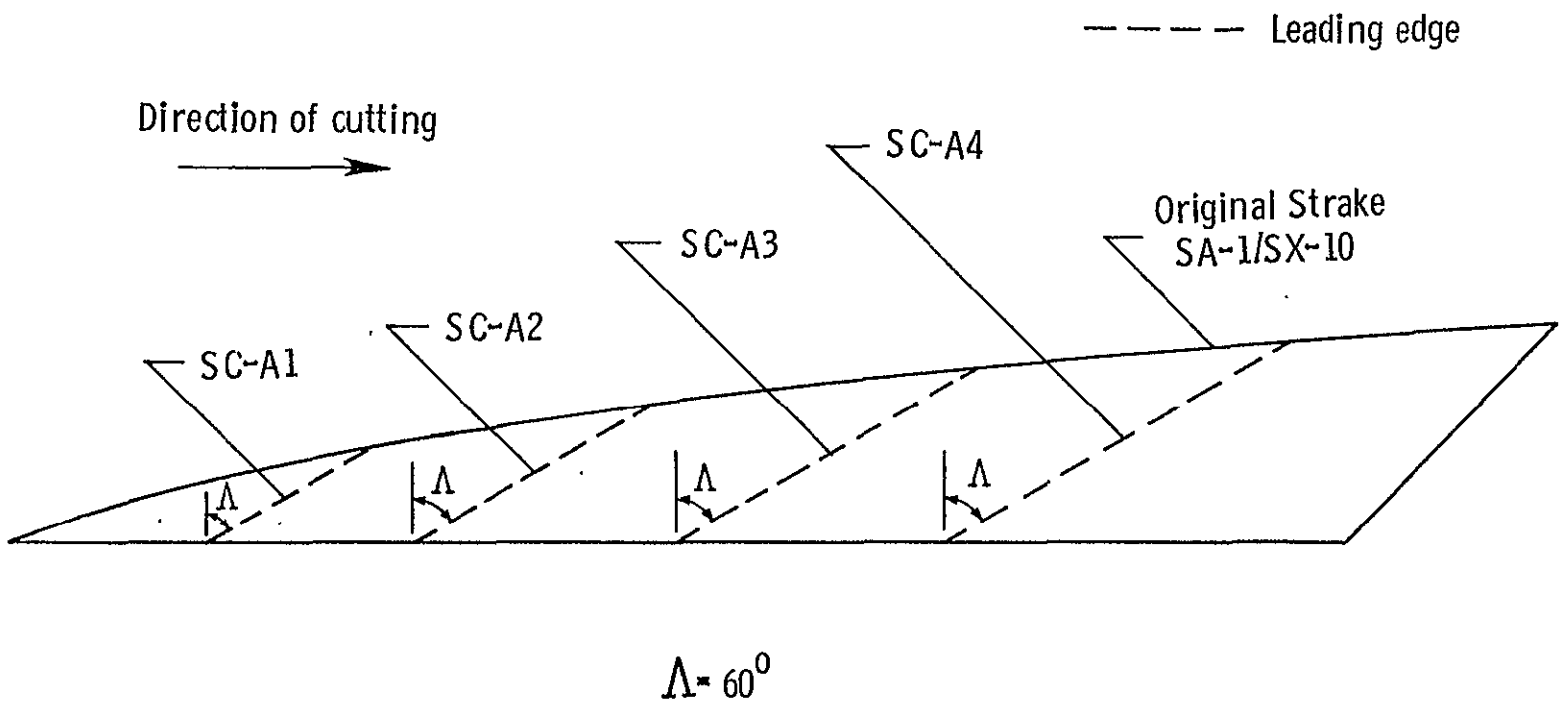

Figure 13.- Generation of apex cut strakes from the original strake: SC-A Series.

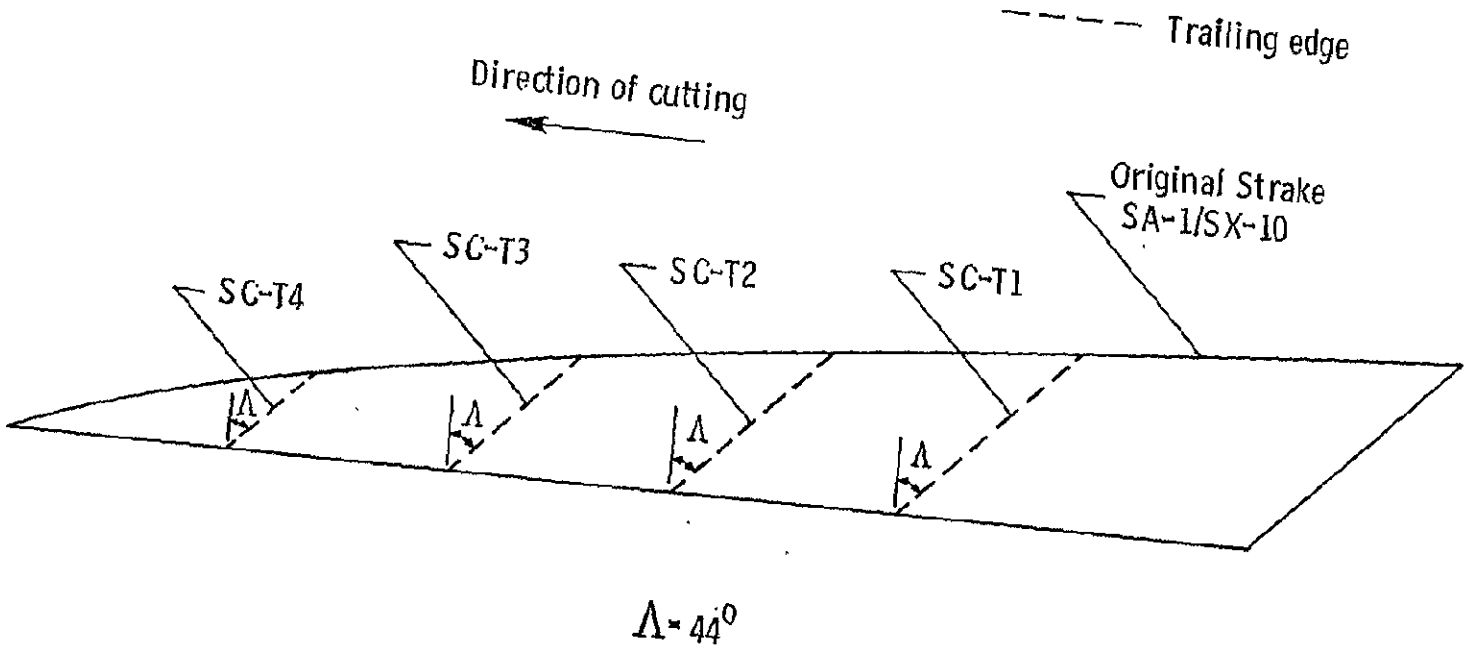

Figure 14.- Generation of trailing edge cut strakes from the original strake: SC-T Series.

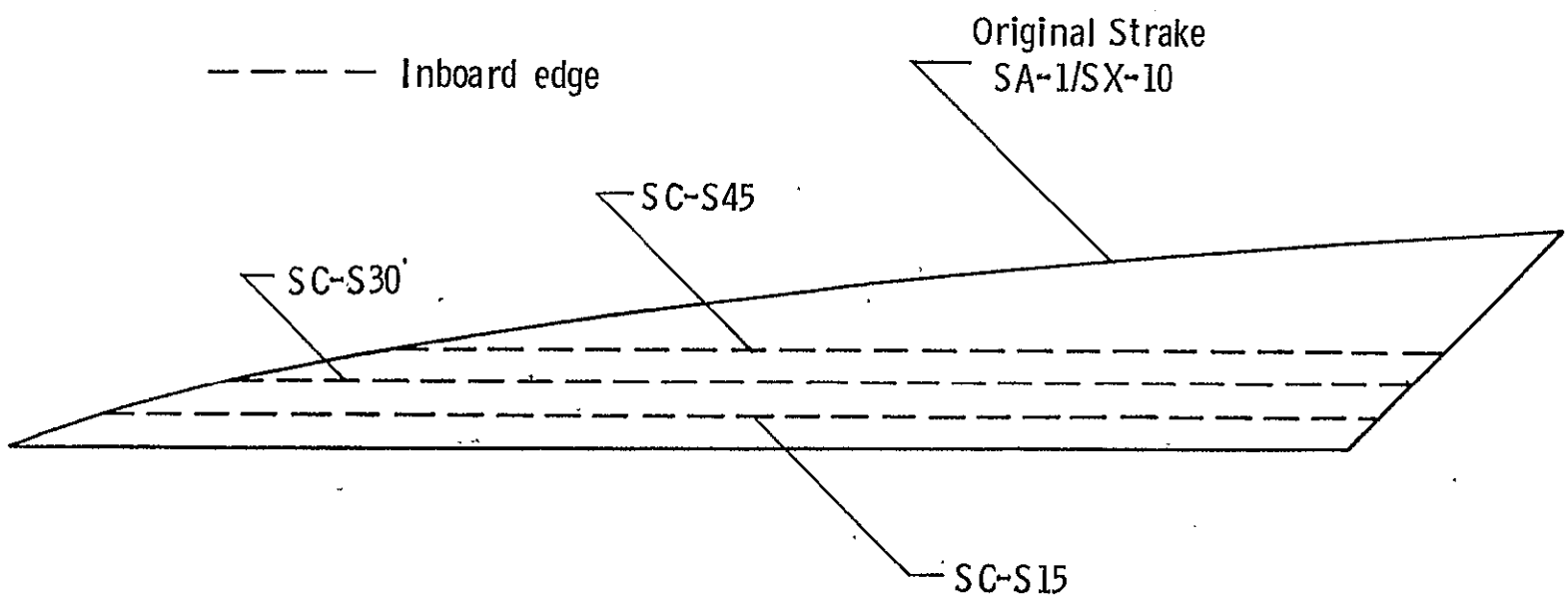

Figure 15.- Generation of spanwise cut strakes from the original strake: SC-S Series.

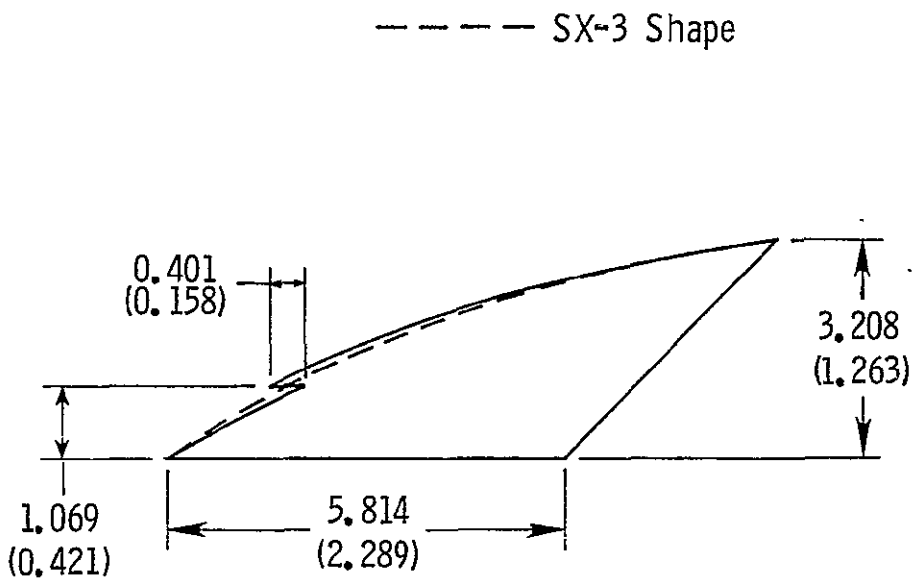

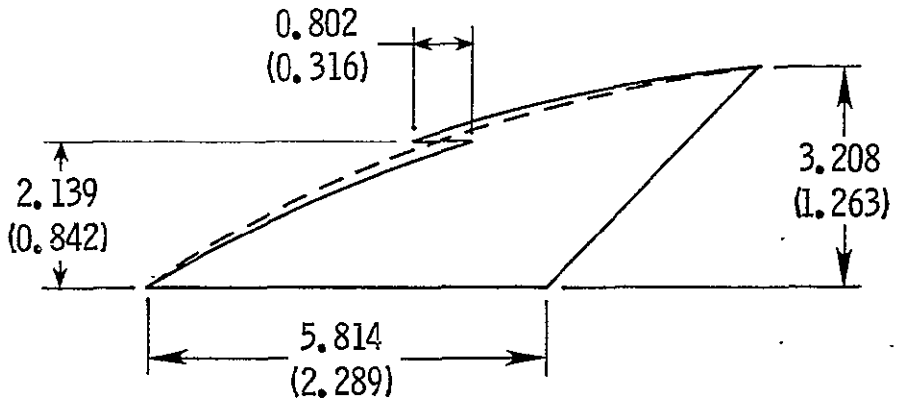

Figure 16.- Snagged variations of the SX-3 strake.

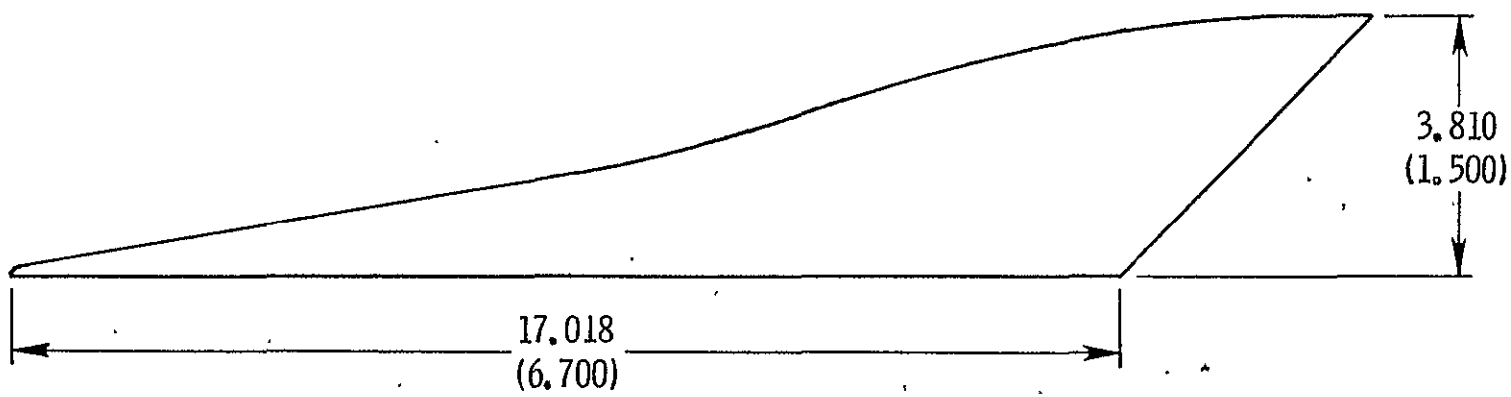

Figure 17.- Strake III of reference 7.

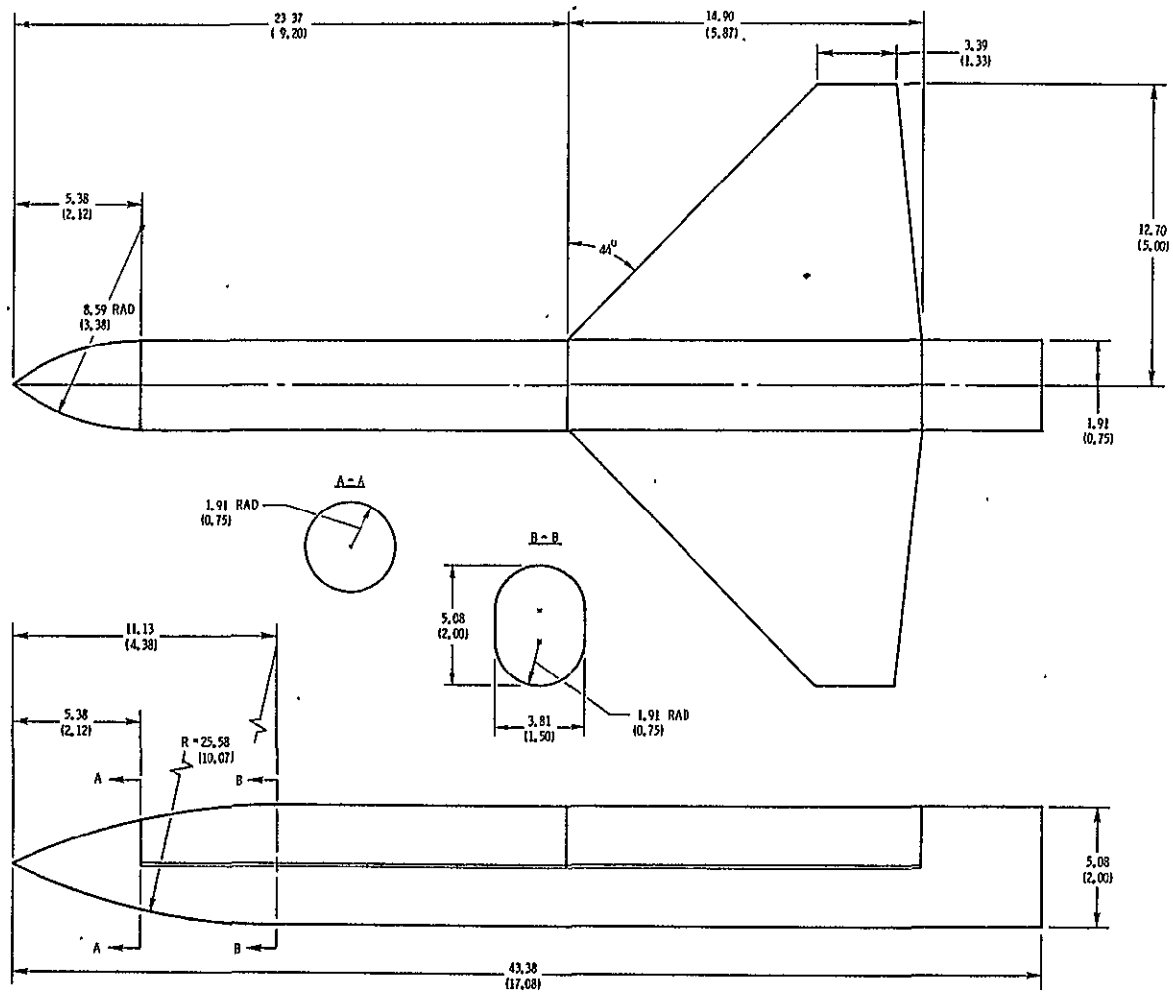

Figure 18.- Drawing of water tunnel wing-fuselage model with wing in forward position. Aft wing position is 2.21 cm (0.87 in.) rearward.

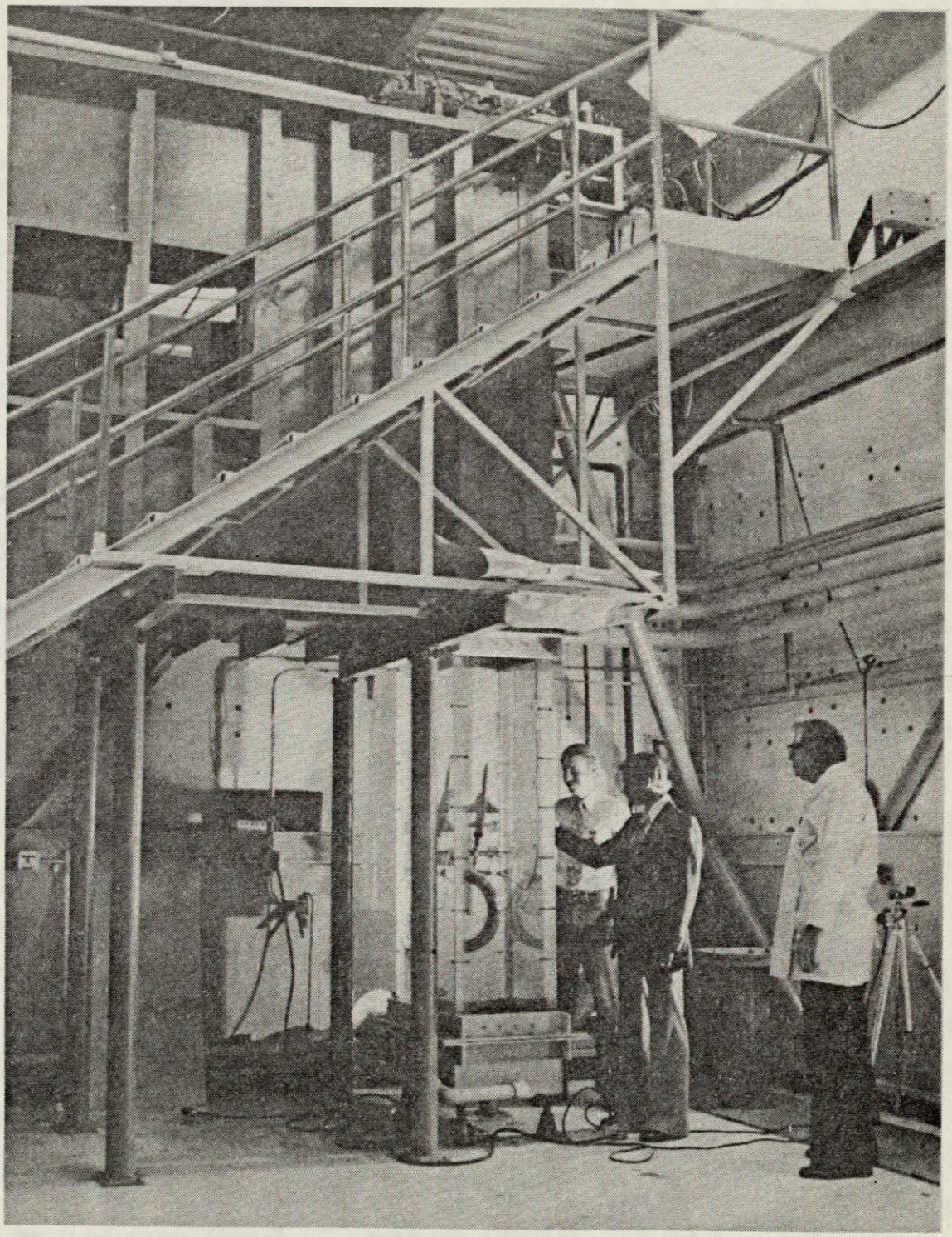

Figure 19.- Northrop 16 x 24 inch diagnostic water tunnel.

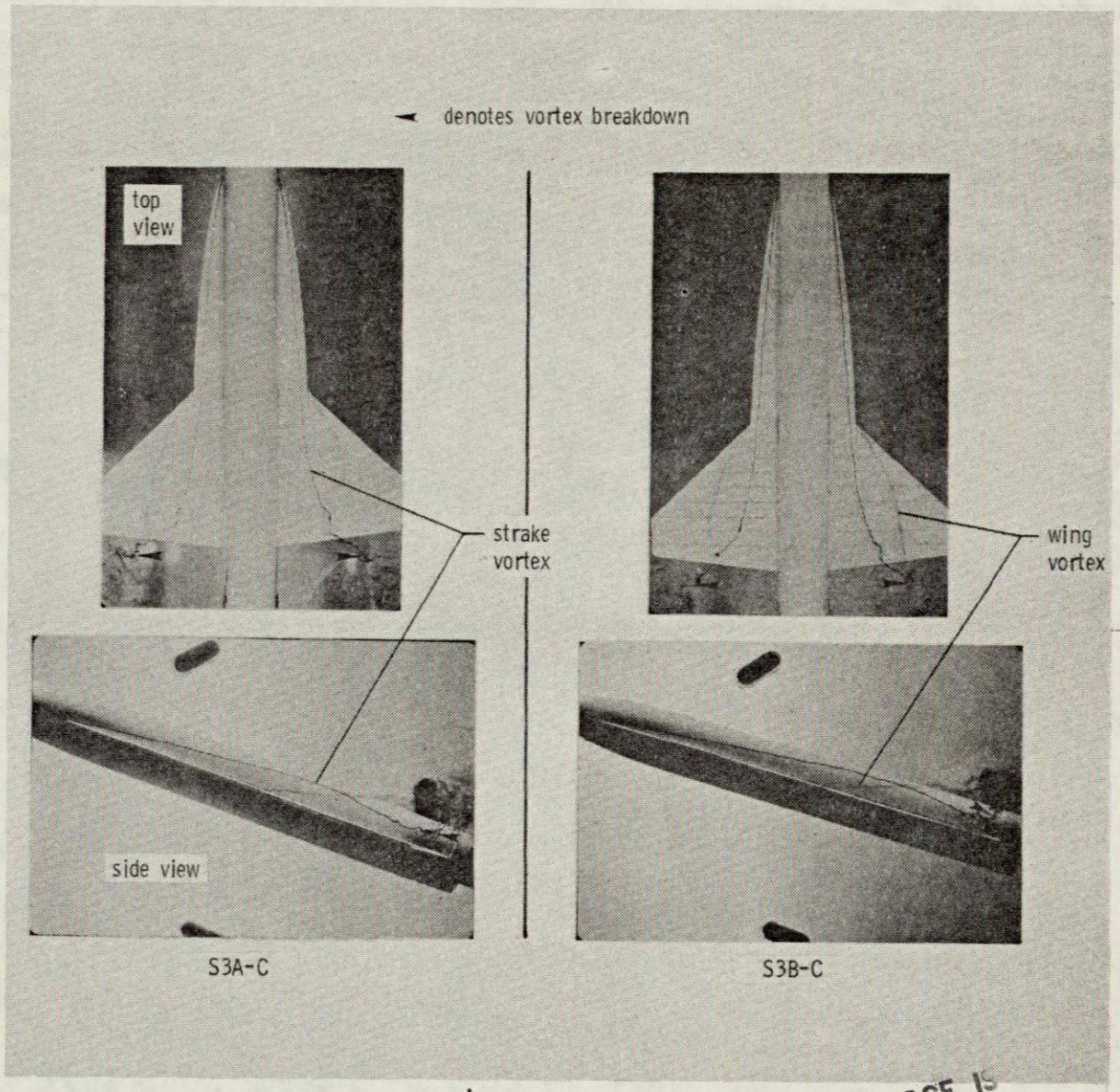

ORIGINAL PAGE IS OF POOR QUALITY

(a) Strake and wing vortex patterns at $\alpha = 20^{\circ}$.

Figure 20.- Group 3 water tunnel photographs and strake vortex breakdown characteristics.

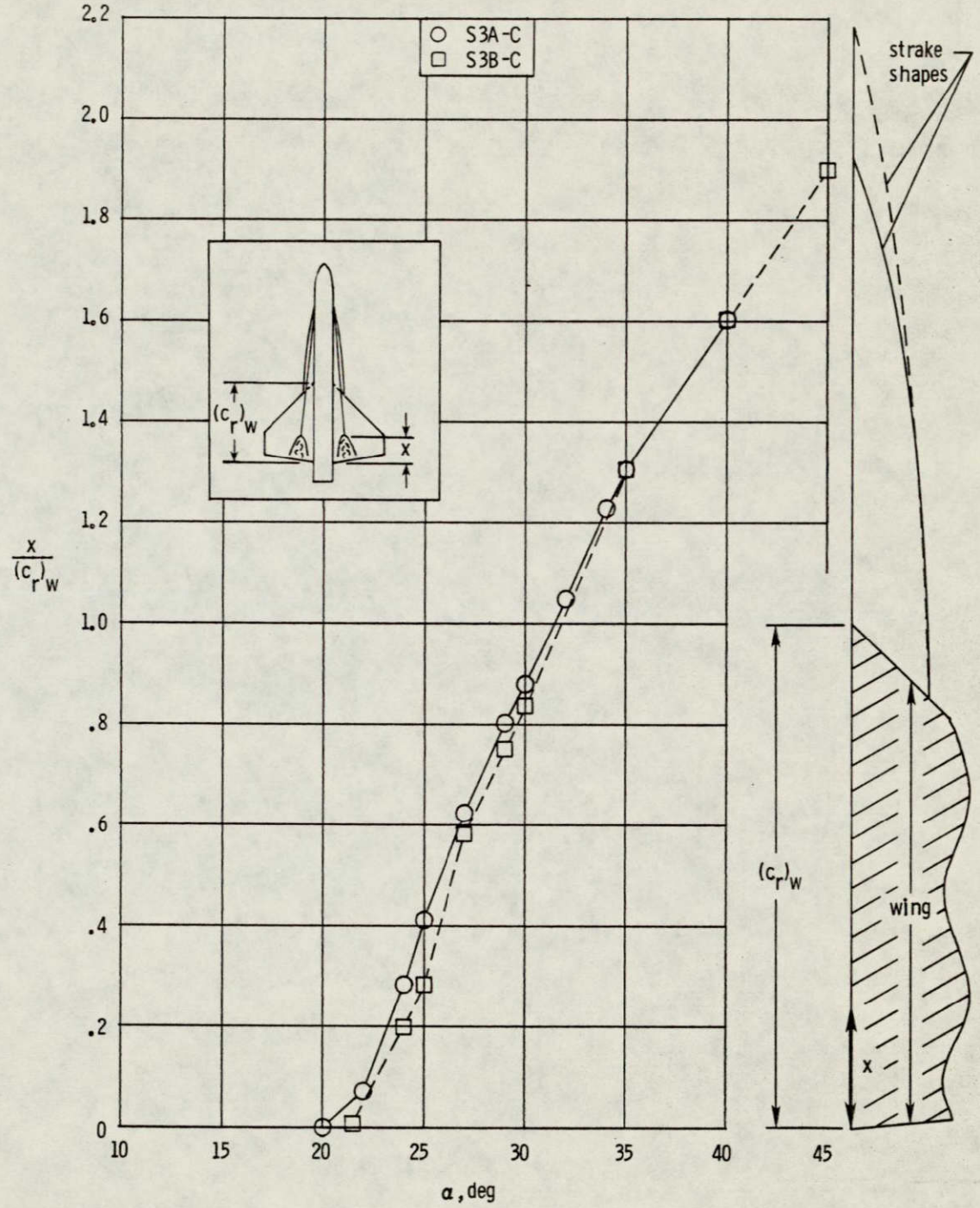

(b) Strake vortex breakdown position.

Figure 20.- Continued.

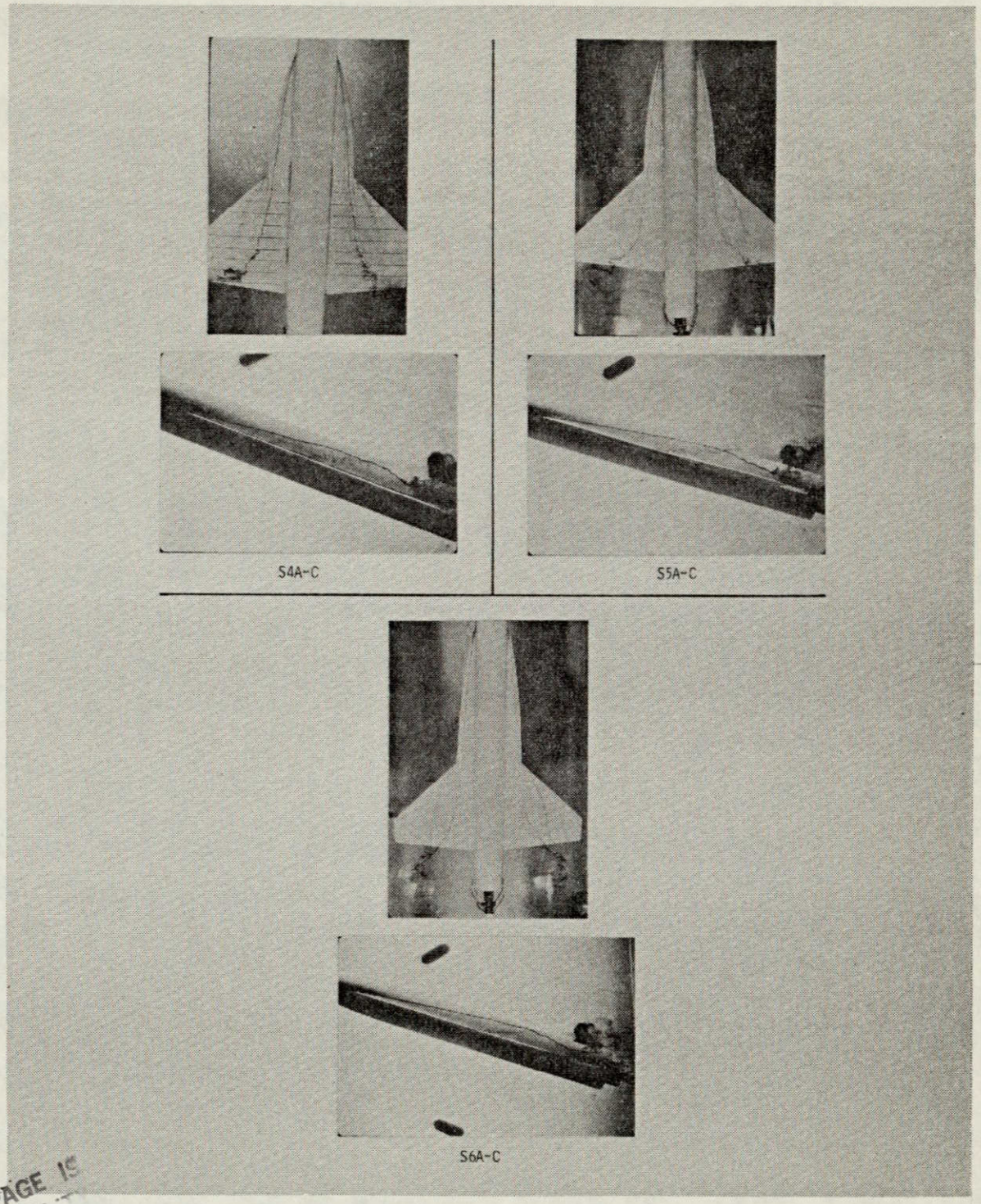

ORIGINAL PAGE IS
OF POOR QUALITY

(a) Strake and wing vortex patterns at $\alpha = 20^{\circ}$.

Figure 21.- Groups 4, 5, and 6 water tunnel photographs and strake vortex breakdown characteristics.

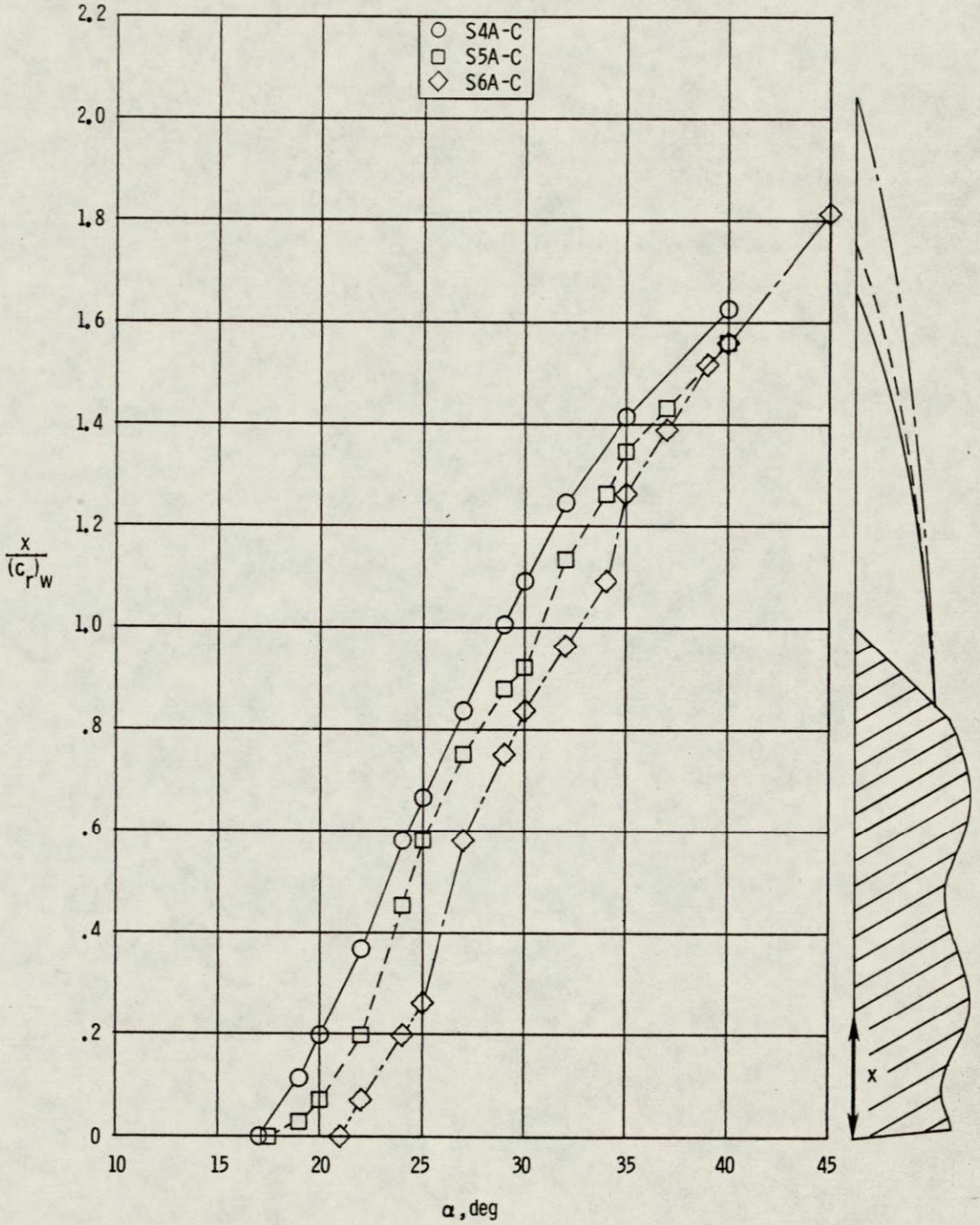

(b) Strake vortex breakdown position.

Figure 21.- Continued.

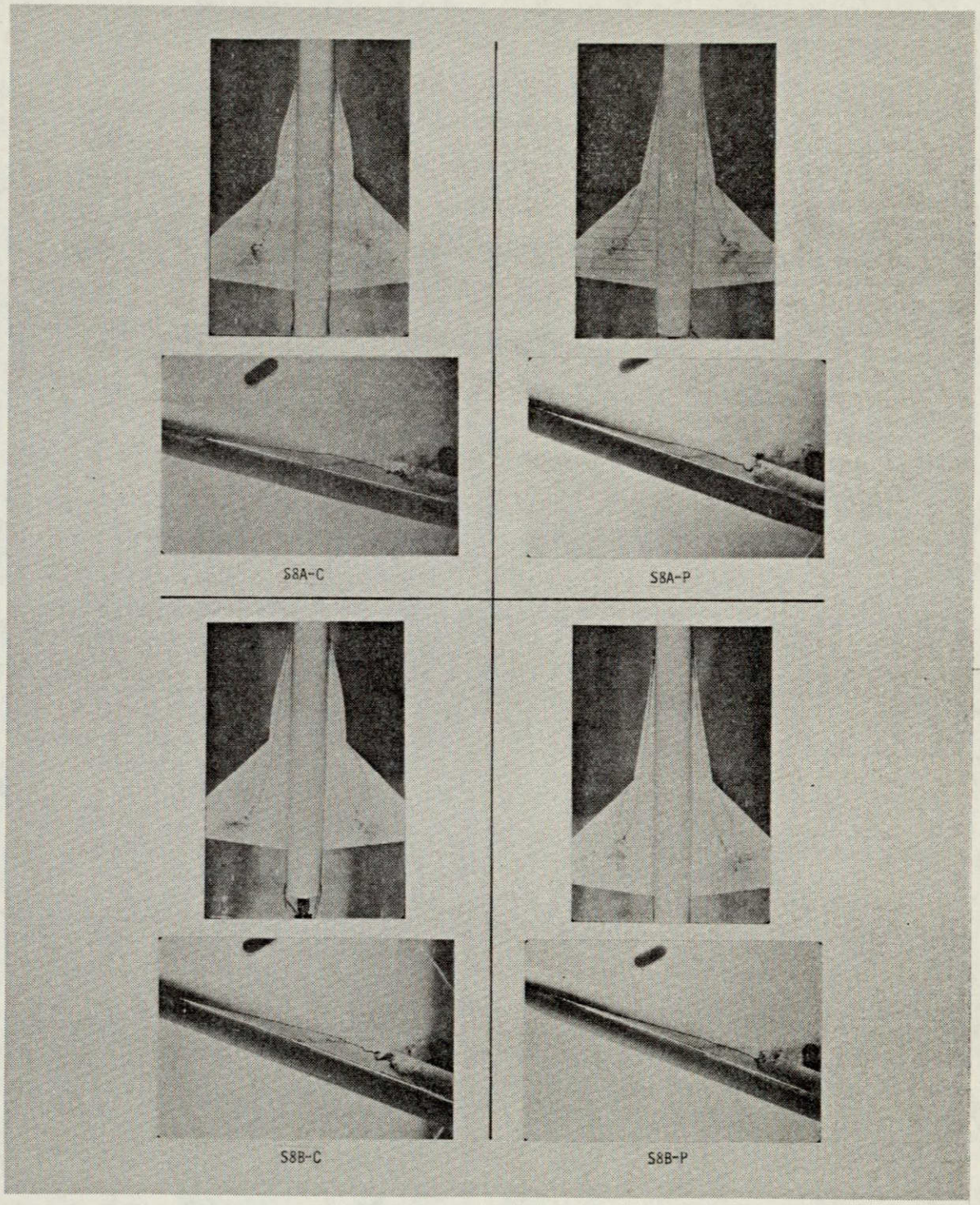

(a) Strake and wing vortex patterns at $\alpha = 20^{\circ}$.

Figure 22.- Group 8 water tunnel photographs and strake vortex breakdown characteristics.

ORIGINAL PAGE IS
OF POOR QUALITY

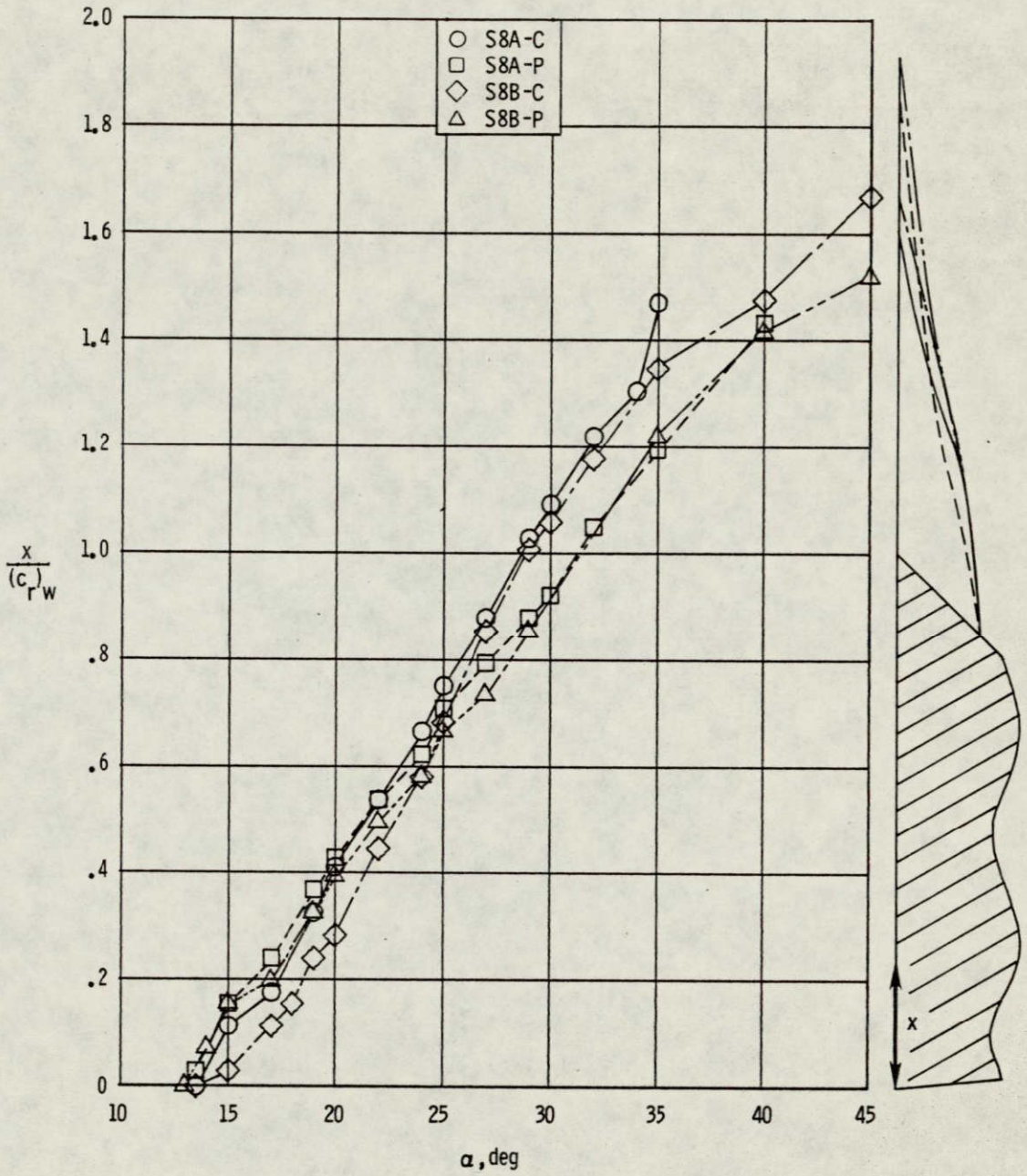

(b) Strake vortex breakdown position.

Figure 22.- Continued.

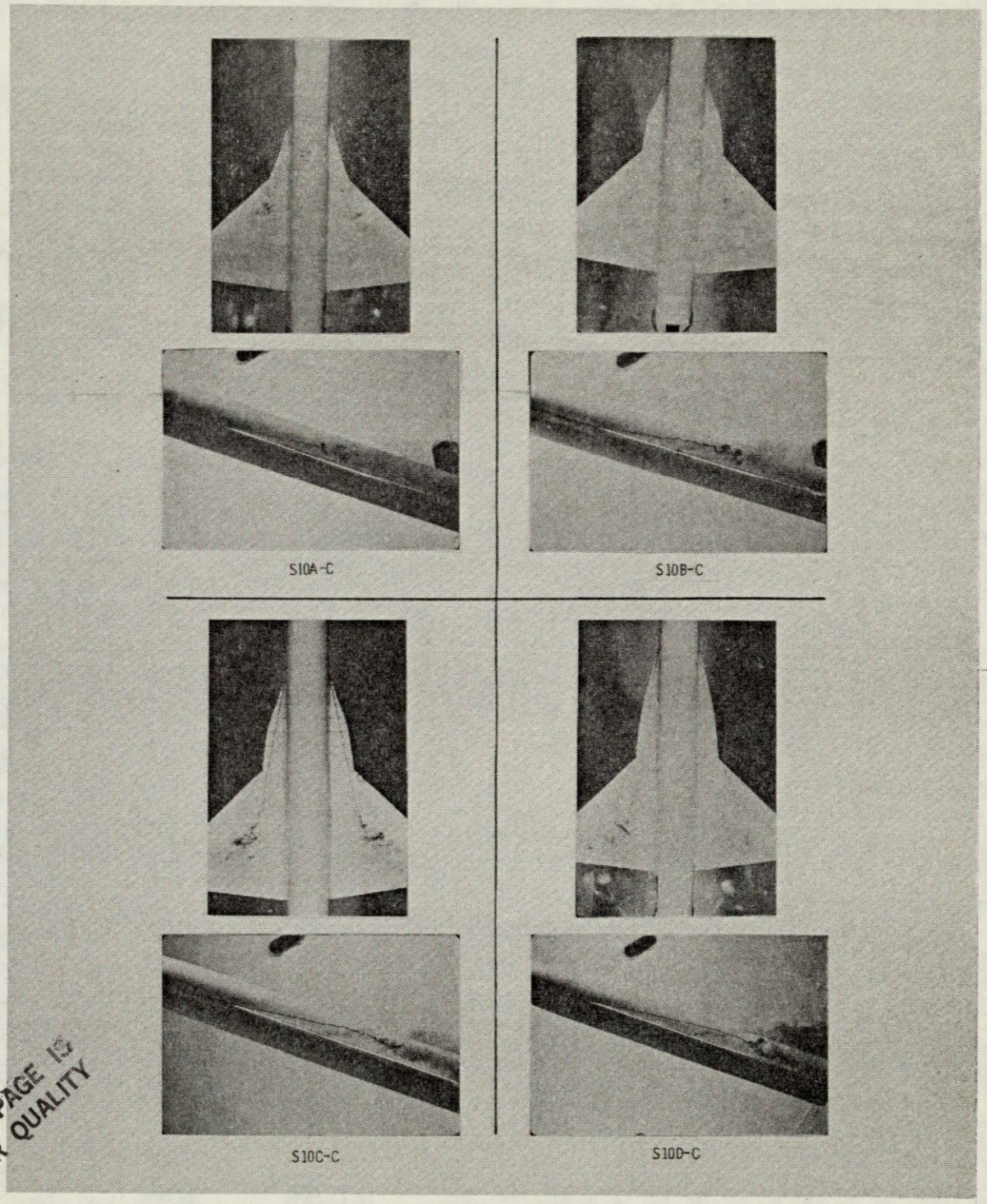

ORIGINAL PAGE IS
OF POOR QUALITY

(a) Strake and wing vortex patterns at $\alpha = 20^{\circ}$.

Figure 23.- Group 10 water tunnel photographs and strake vortex breakdown characteristics.

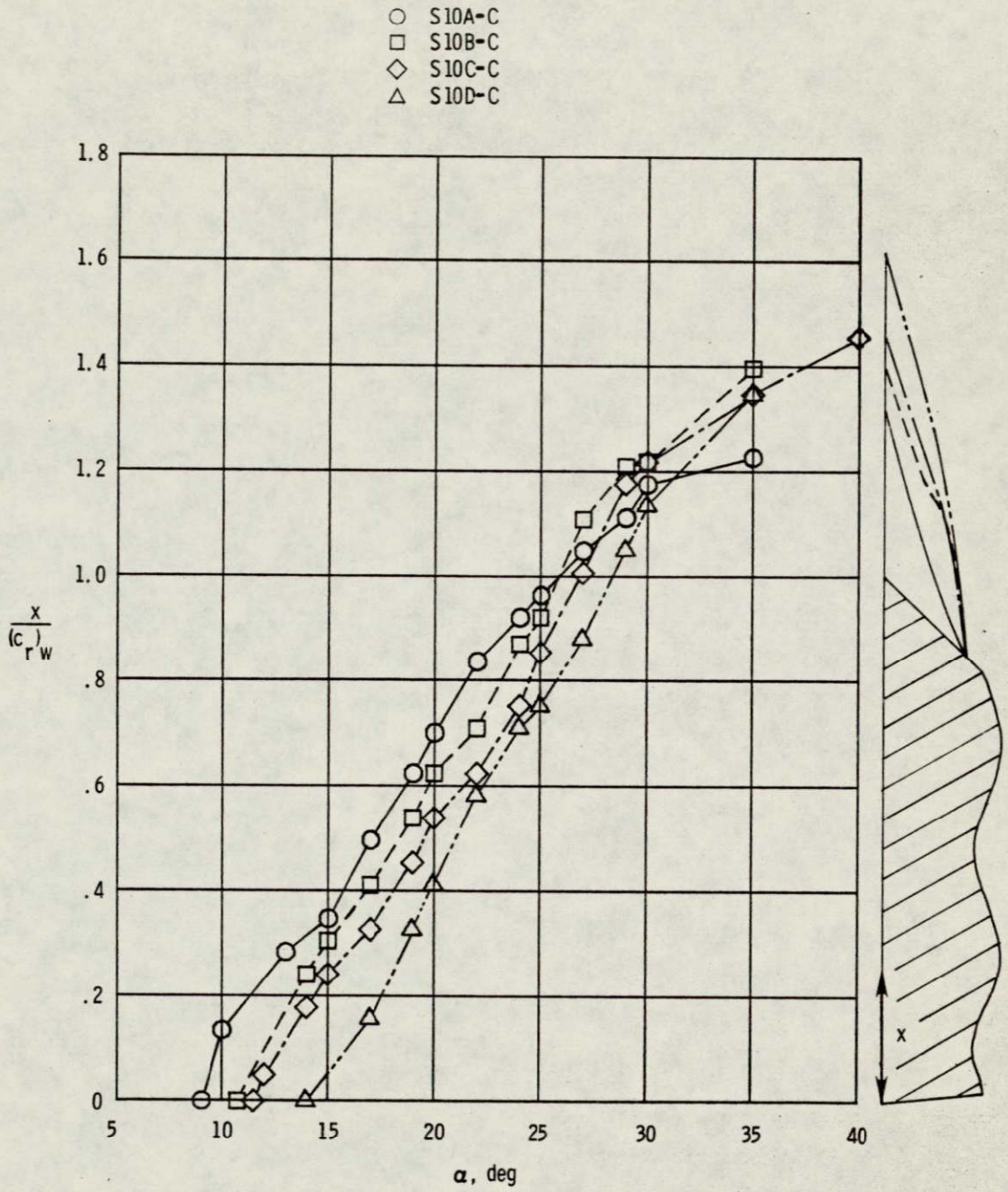

(b) Strake vortex breakdown position.

Figure 23.- Continued.

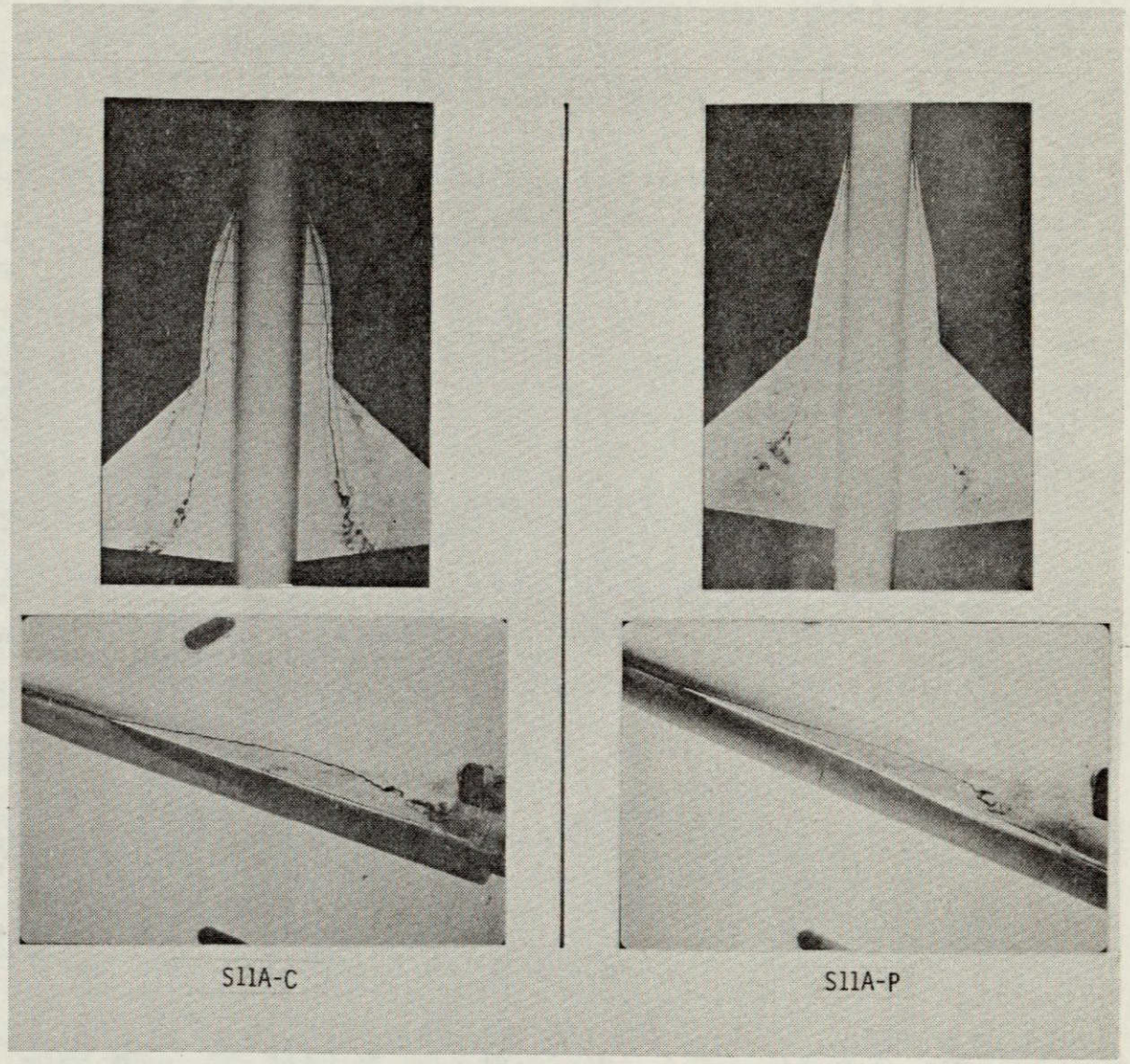

ORIGINAL PAGE IS
OF POOR QUALITY

(a) Strake and wing vortex patterns at $\alpha = 20^{\circ}$.

Figure 24.- Group 11 water tunnel photographs and strake vortex breakdown characteristics.

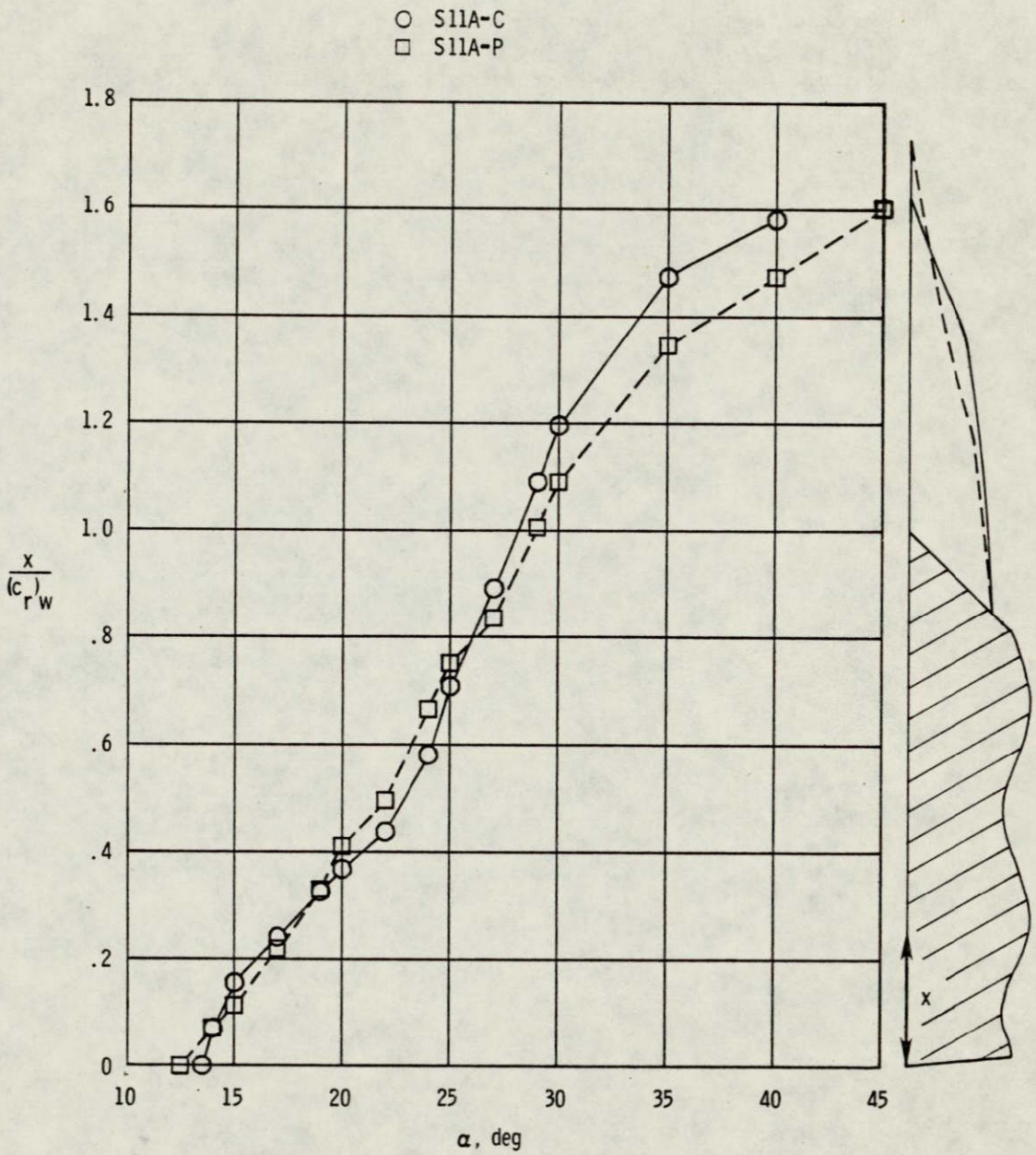

(b) Strake vortex breakdown position.

Figure 24.- Continued.

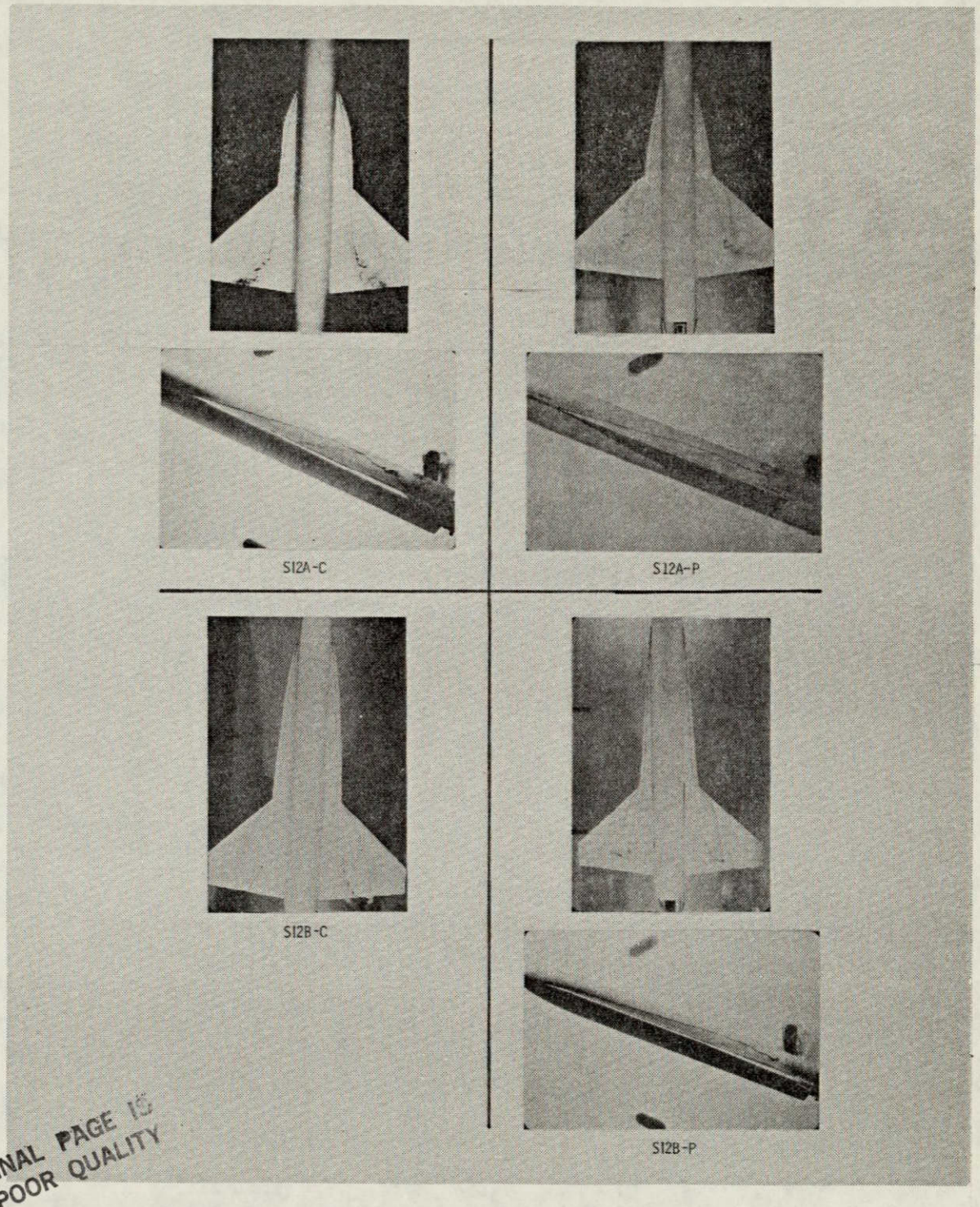

ORIGINAL PAGE IS
OF POOR QUALITY

(a) Strake and wing vortex patterns at $\alpha = 20^{\circ}$.

Figure 25.- Group 12 water tunnel photographs and strake vortex breakdown characteristics.

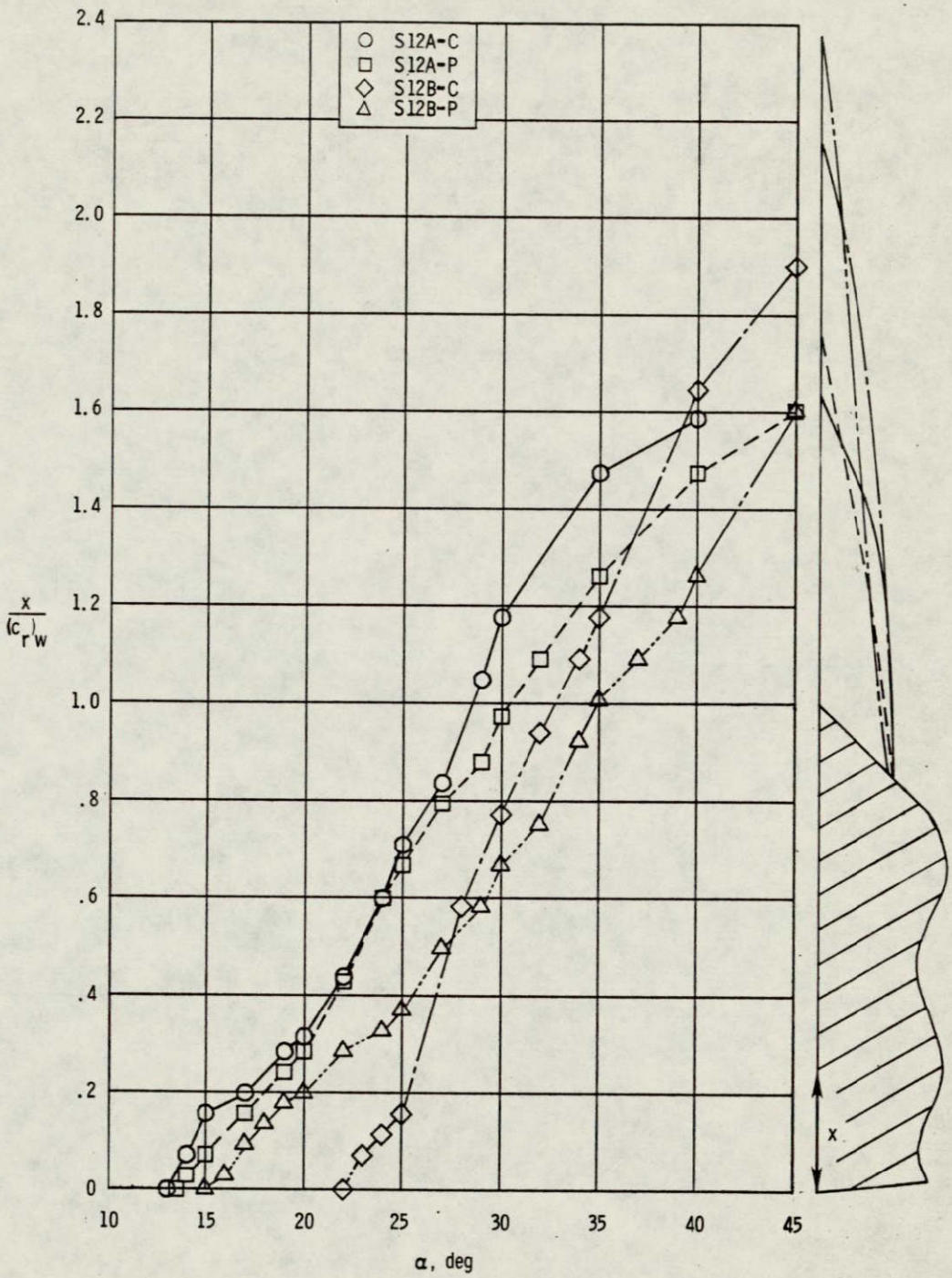

(b) Strake vortex breakdown position.

Figure 25.- Continued.

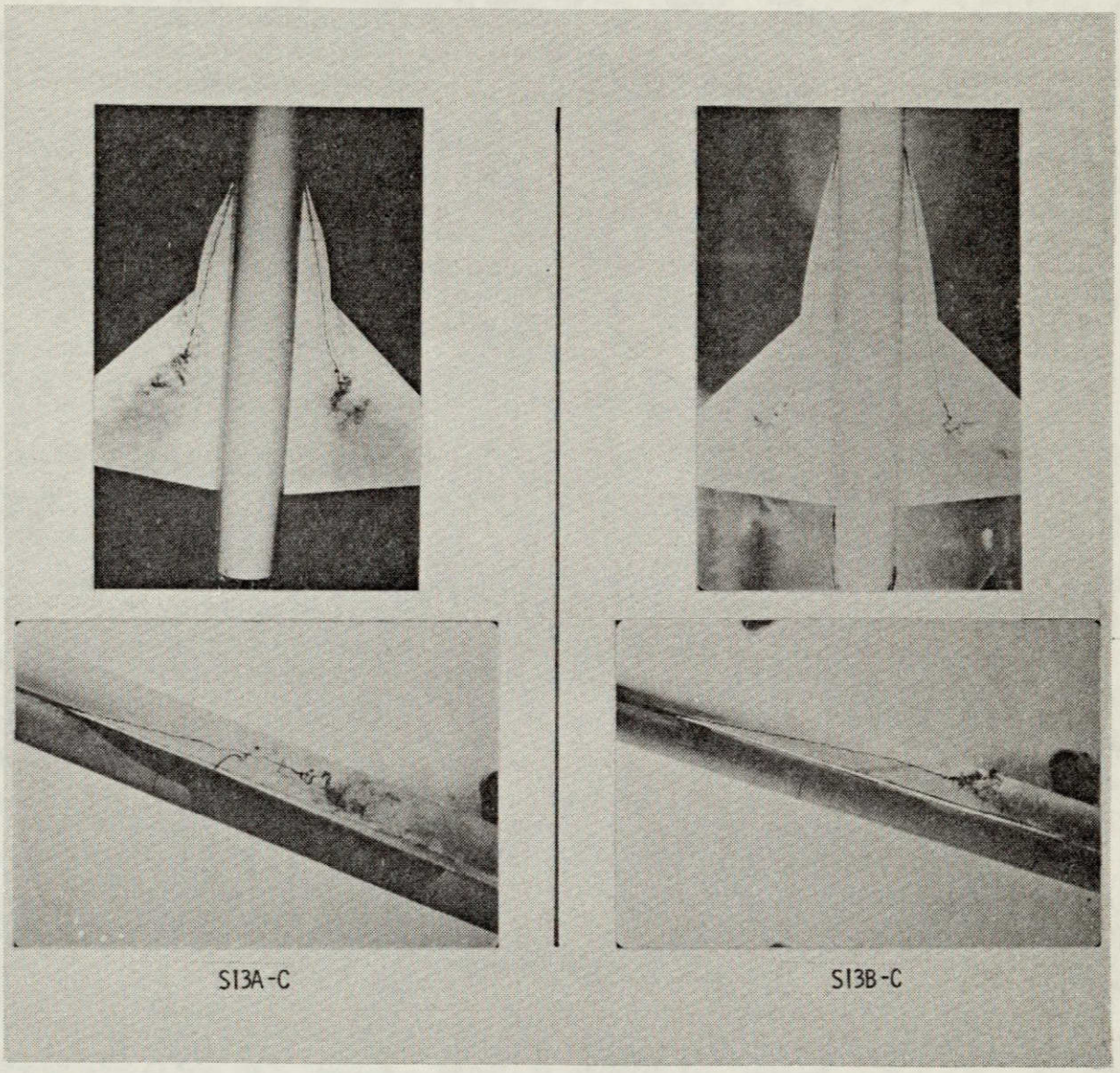

ORIGINAL PAGE IS
OF POOR QUALITY

(a) Strake and wing vortex patterns at $\alpha = 20^{\circ}$.

Figure 26.- Group 13 water tunnel photographs and strake vortex breakdown characteristics.

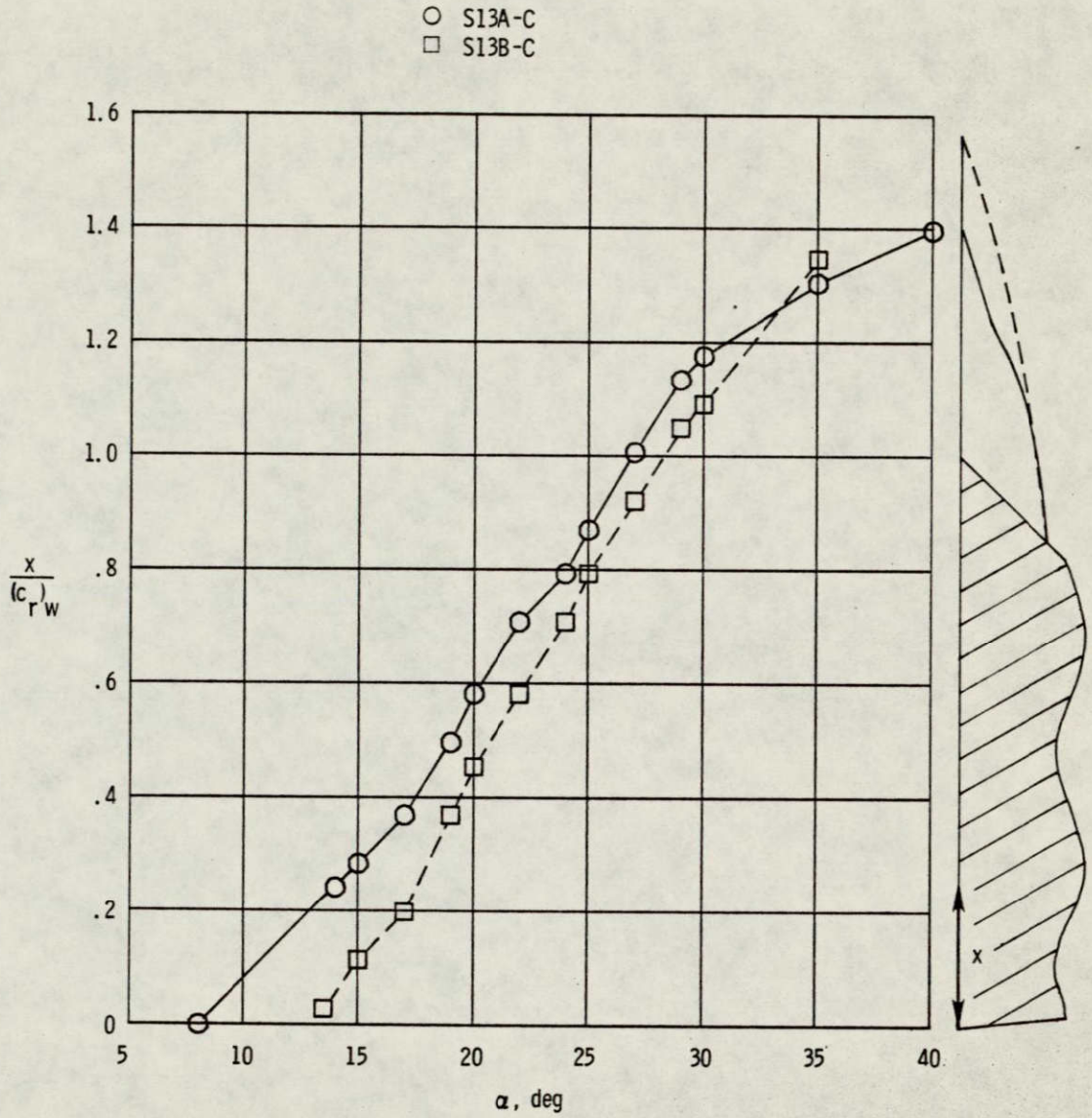

(b) Strake vortex breakdown position.

Figure 26.- Continued.

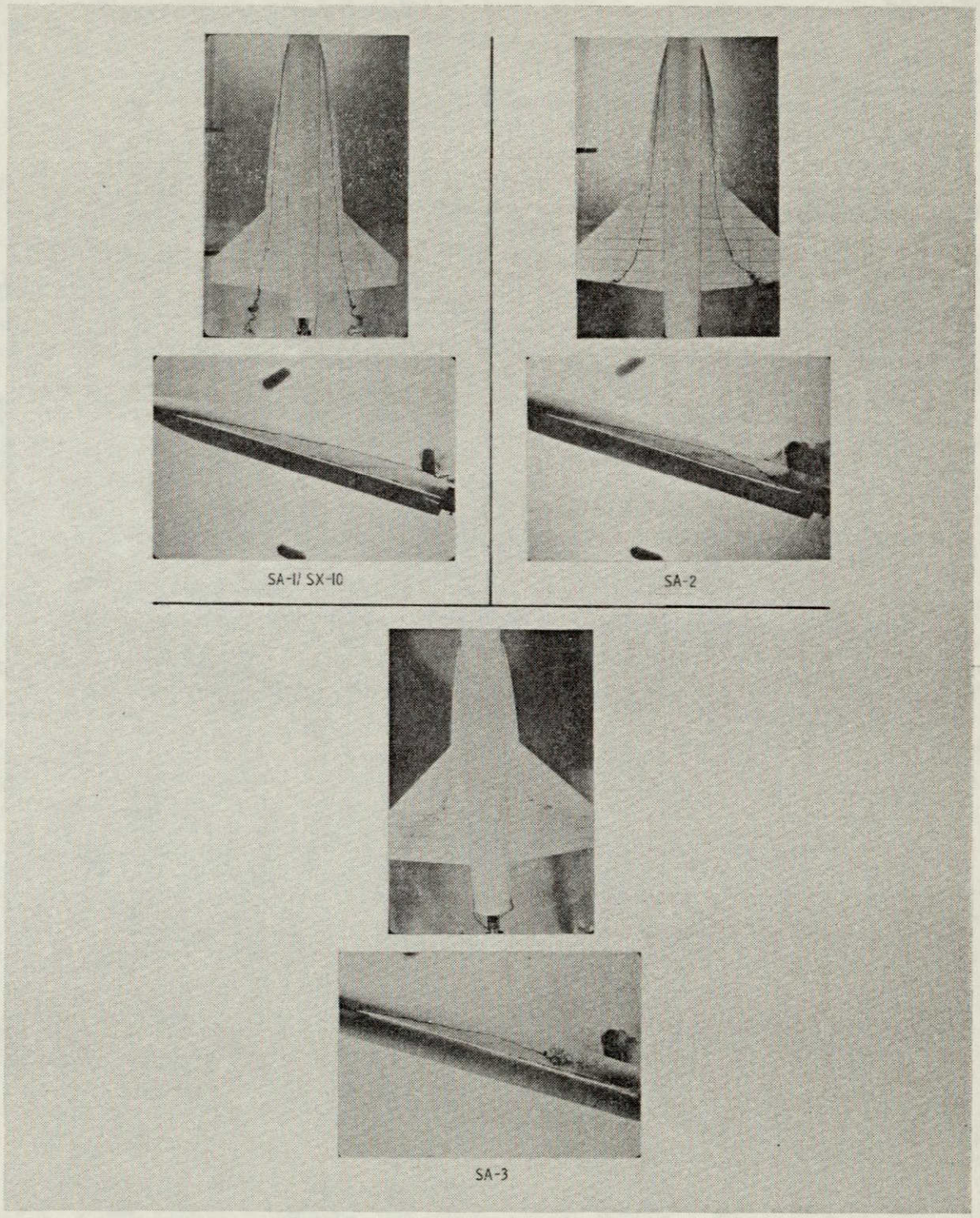

(a) Strake and wing vortex patterns at $\alpha = 20^{\circ}$.

Figure 27.- SA series water tunnel photographs and strake vortex breakdown characteristics.

ORIGINAL PAGE IS
OF POOR QUALITY

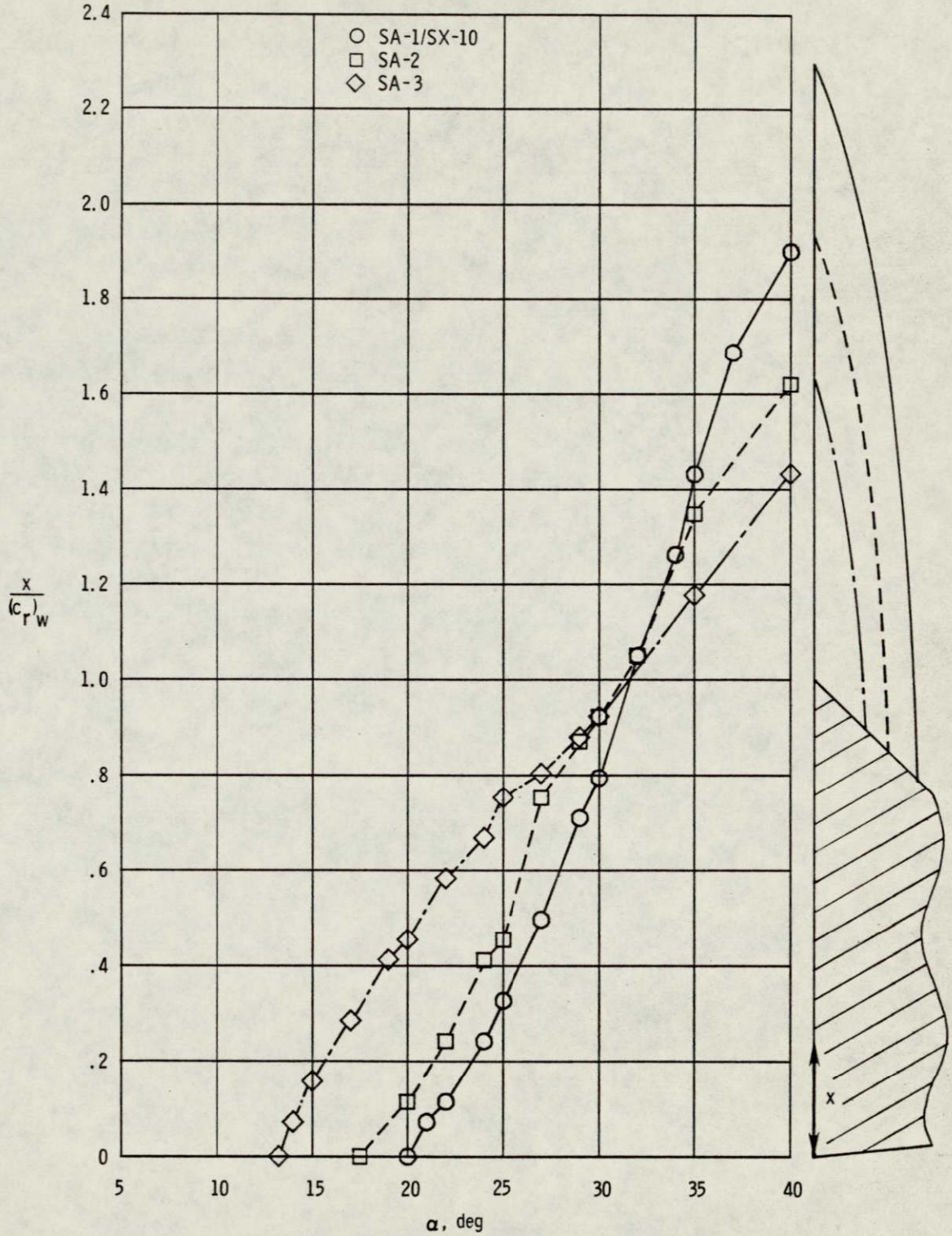

(b) Strake vortex breakdown position.

Figure 27.- Continued.

ORIGINAL PAGE IS
OF POOR QUALITY

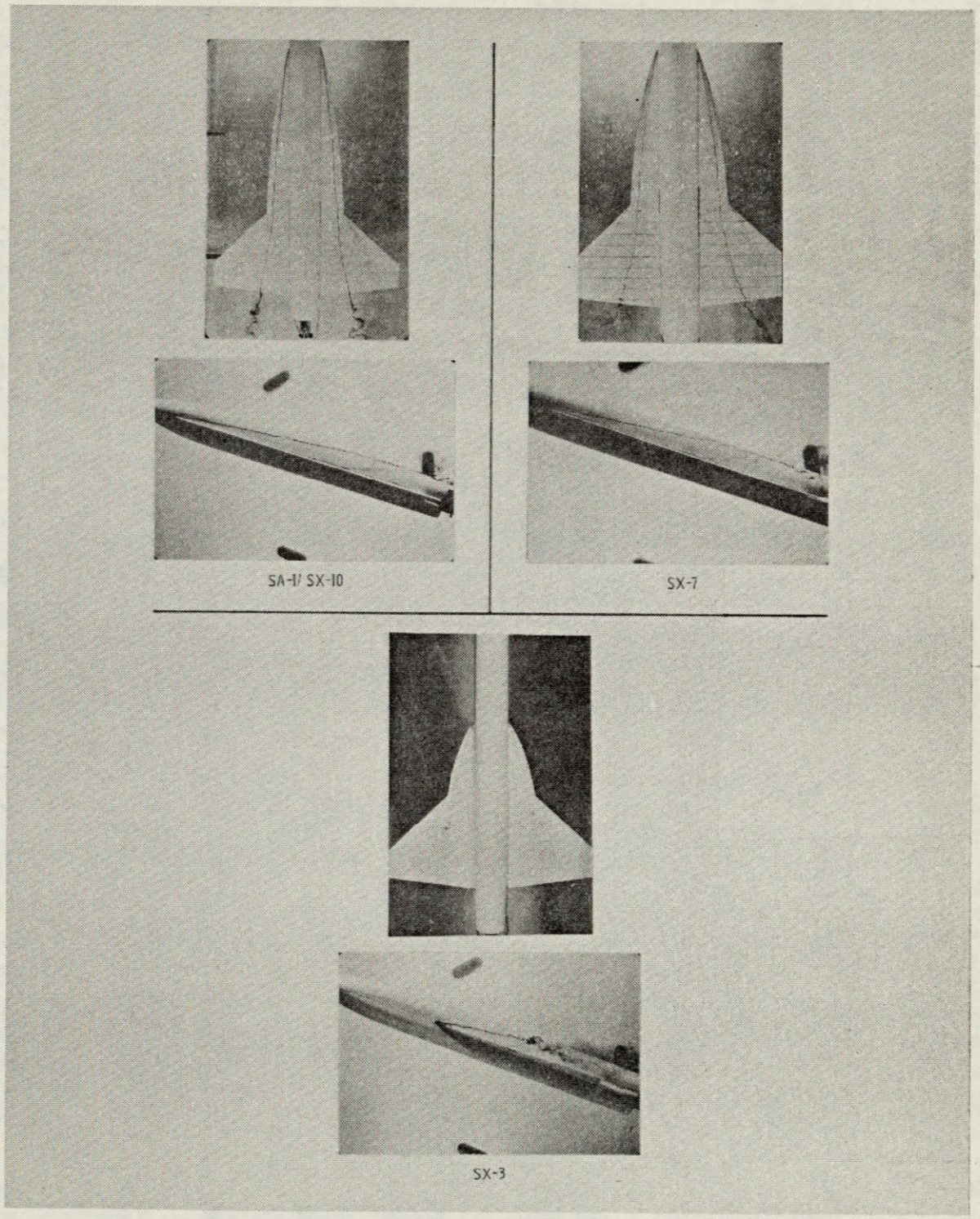

(a) Strake and wing vortex patterns at $\alpha = 20^{\circ}$.

Figure 28.- SX series water tunnel photographs and strake vortex breakdown characteristics.

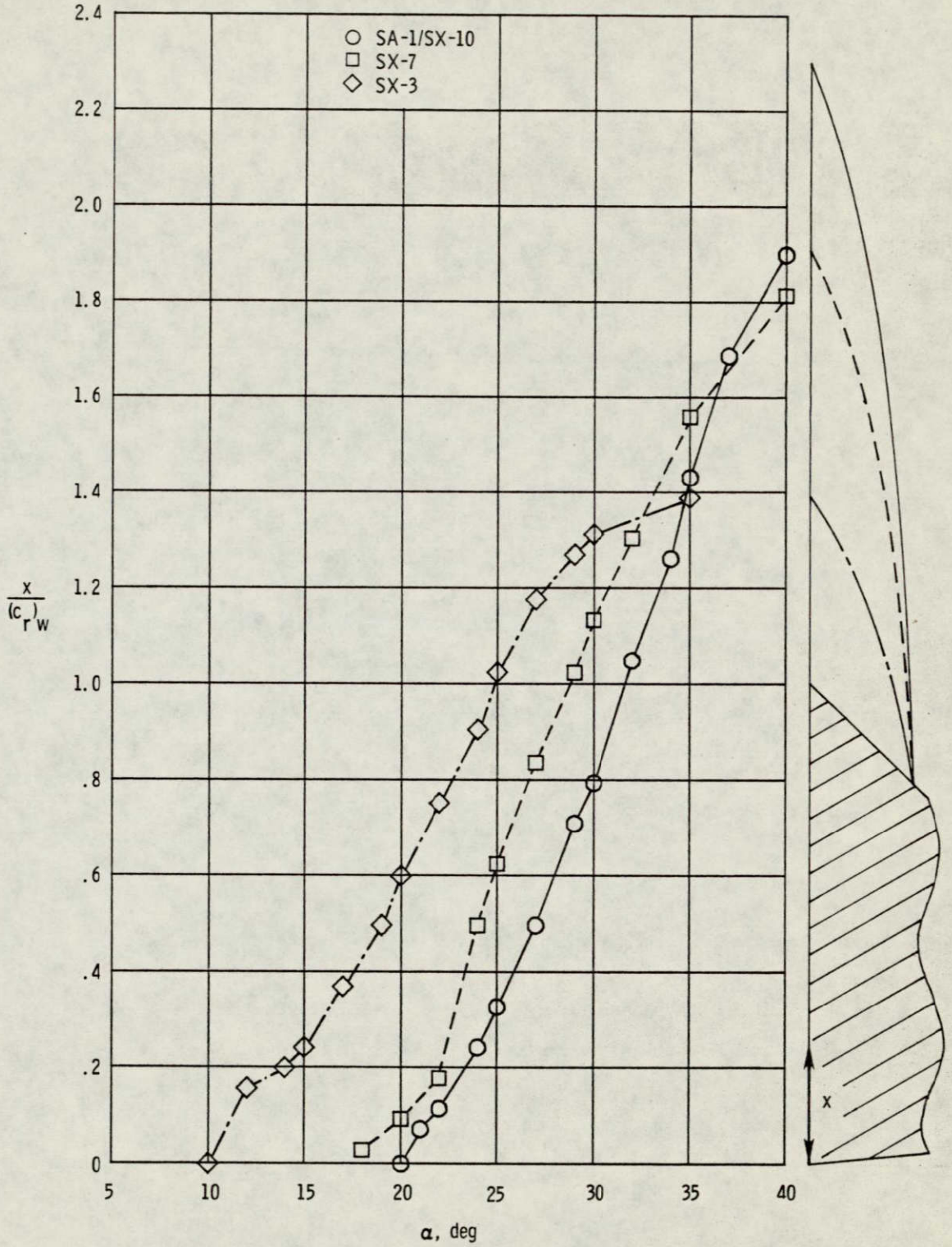

(b) Strake vortex breakdown position.

Figure 28.- Continued.

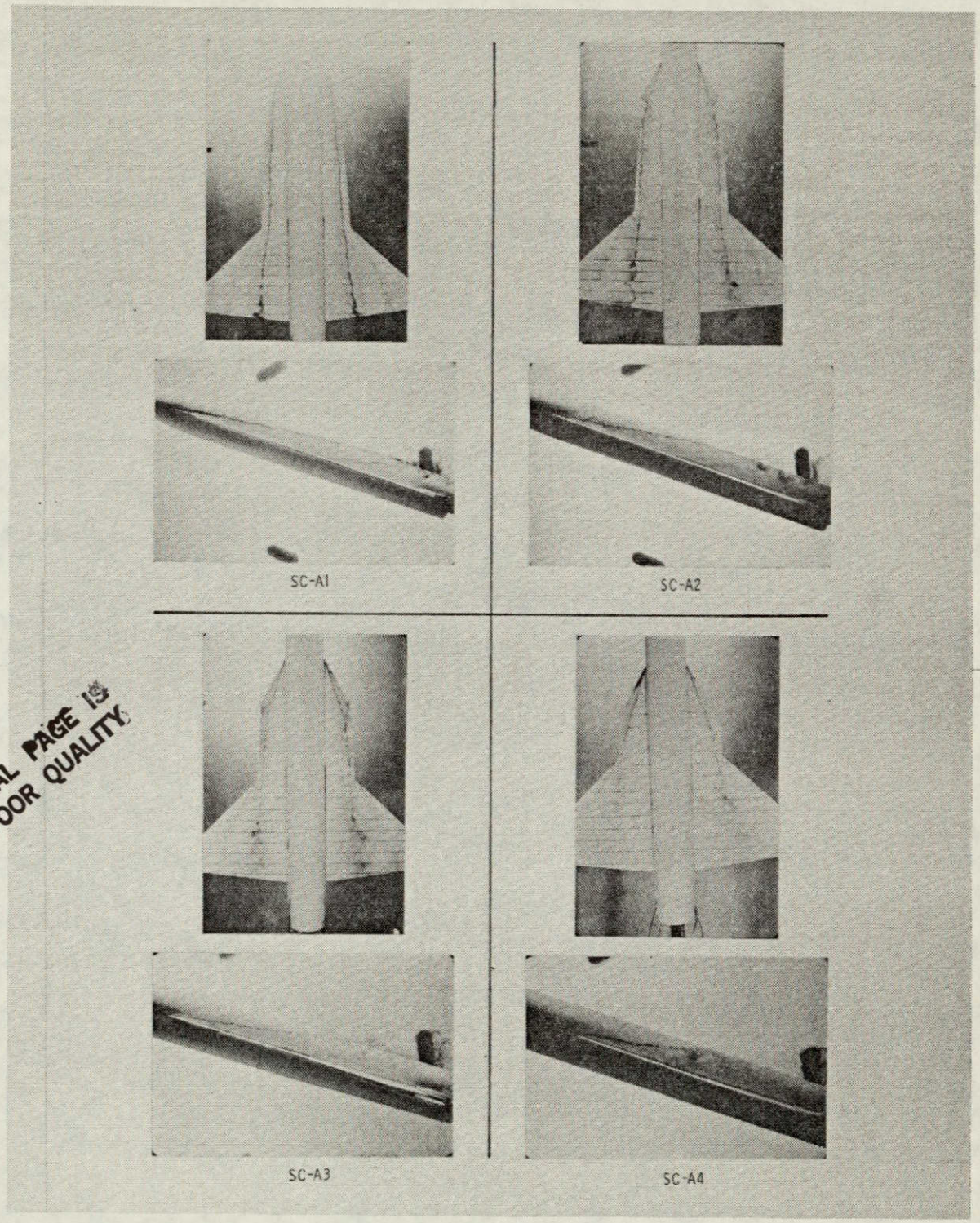

ORIGINAL PAGE IS
OF POOR QUALITY

(a) Strake and wing vortex patterns at $\alpha = 20^{\circ}$.

Figure 29.- Apex cut series water tunnel photographs and strake vortex breakdown characteristics.

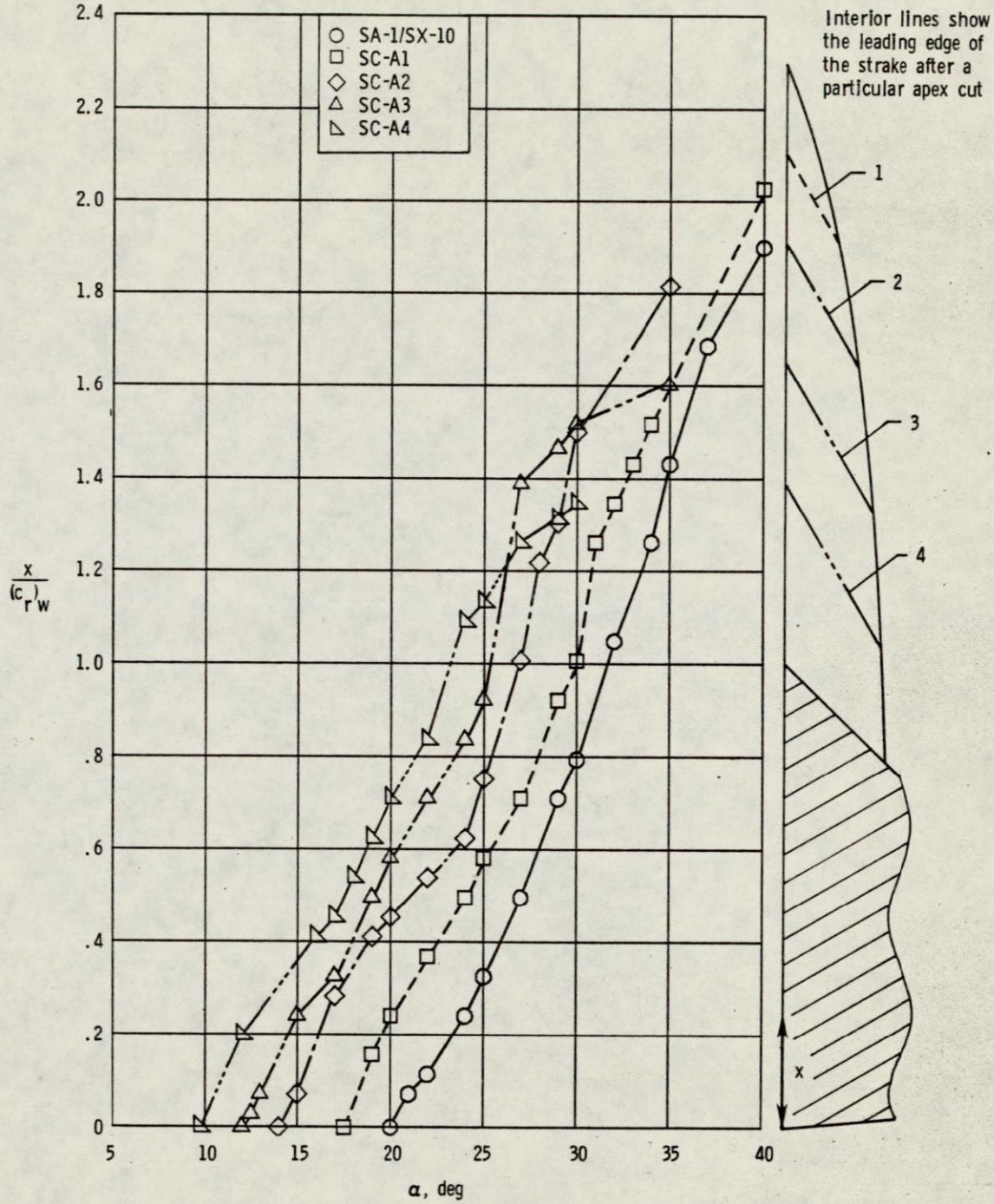

(b) Strake vortex breakdown position.

Figure 29.- Continued.

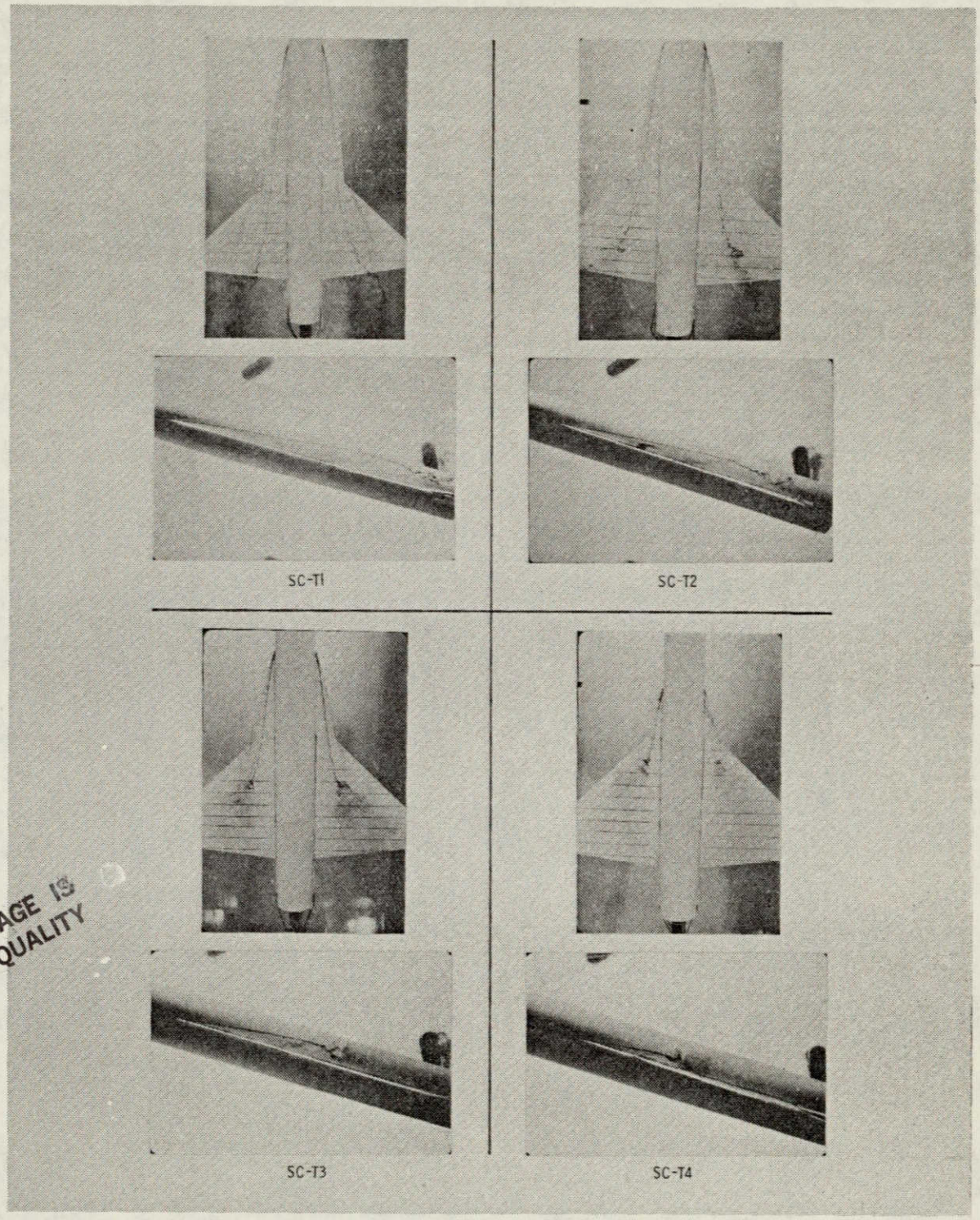

ORIGINAL PAGE IS
OF POOR QUALITY

(a) Strake and wing vortex patterns at $\alpha = 20^{\circ}$.

Figure 30.- Trailing edge cut series water tunnel photographs and strake vortex breakdown characteristics.

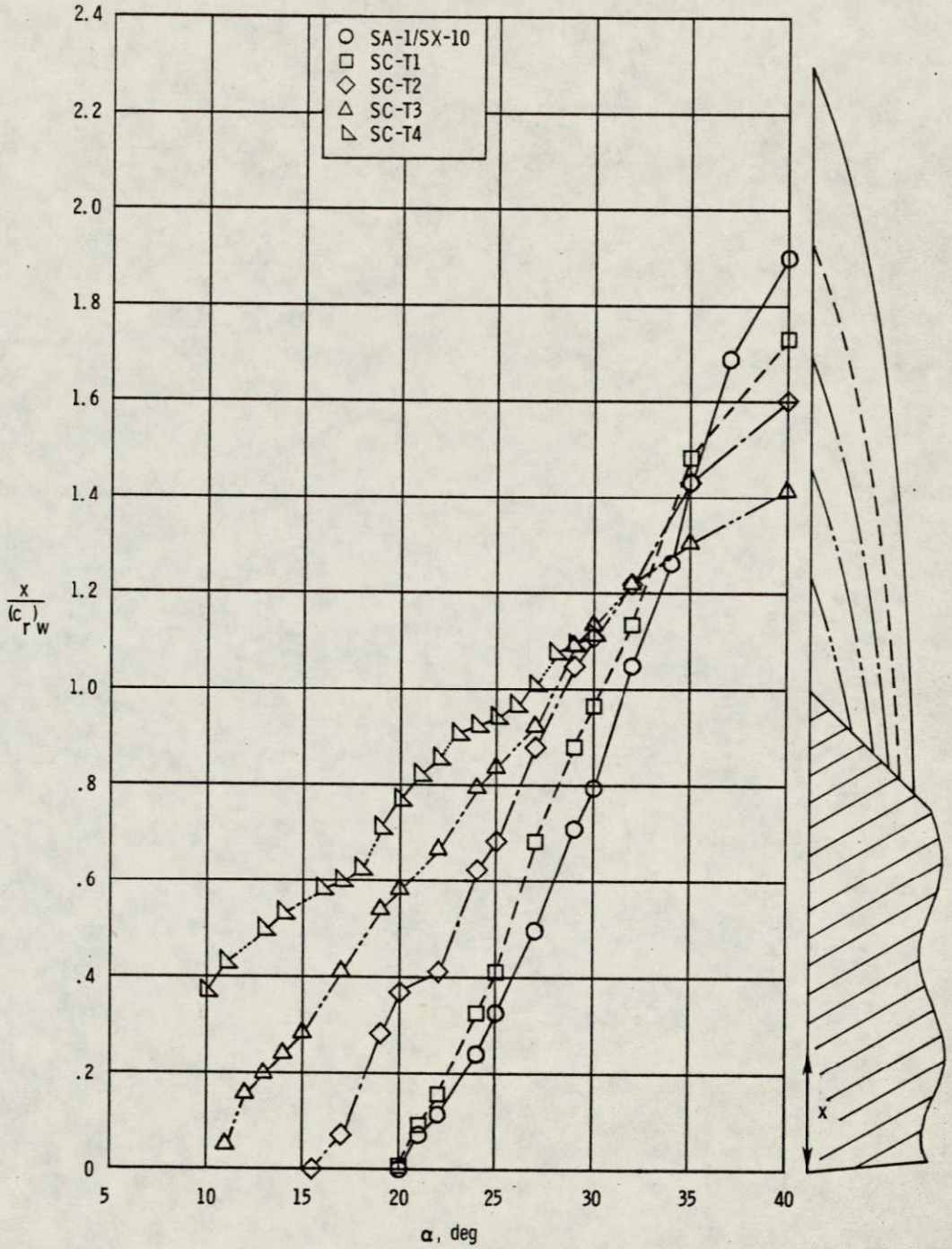

(b) Strake vortex breakdown position.

Figure 30.- Continued.

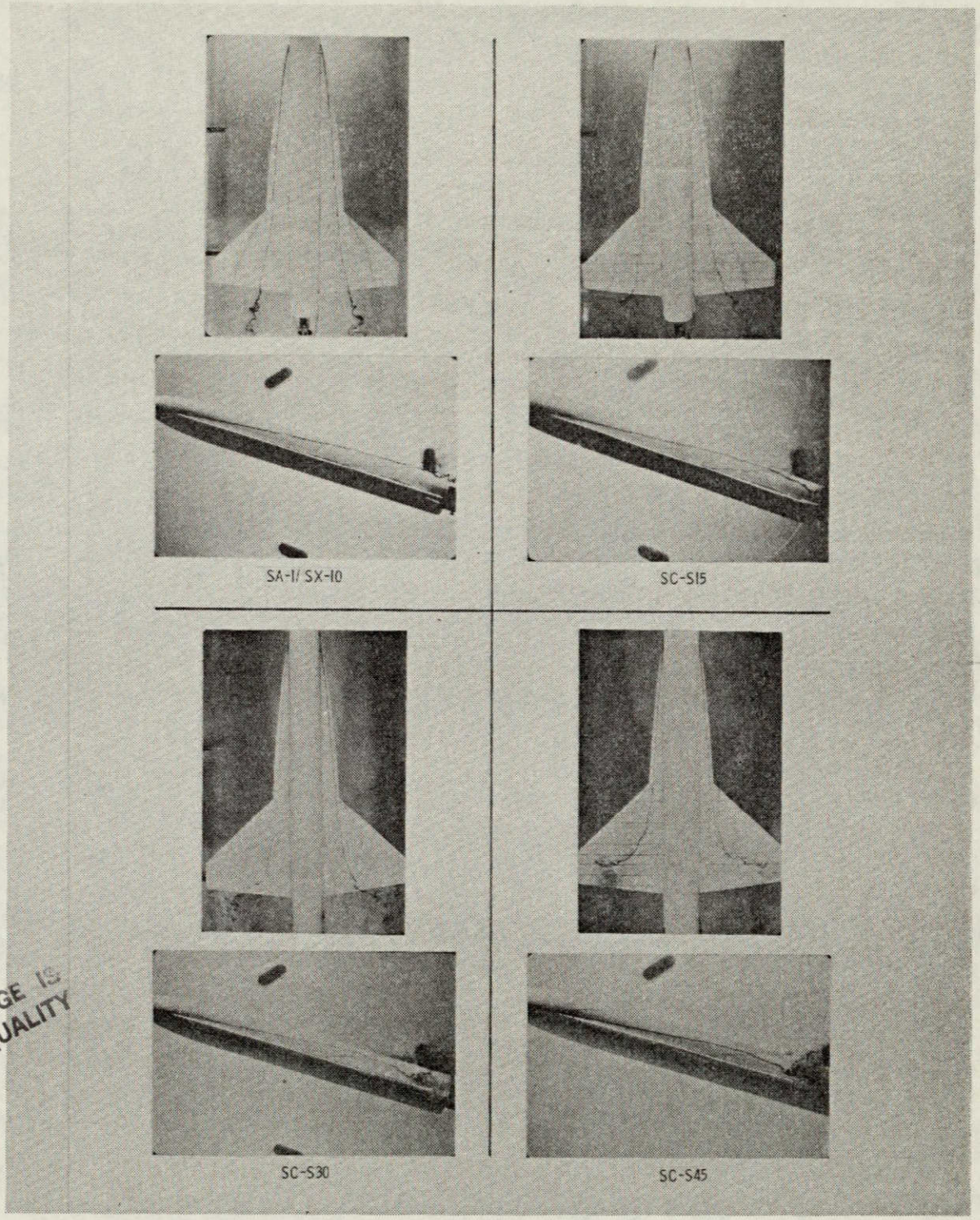

ORIGINAL PAGE IS
OF POOR QUALITY

(a) Strake and wing vortex patterns at $\alpha = 20^{\circ}$.

Figure 31.- Spanwise cut series water tunnel photographs and strake vortex breakdown characteristics.

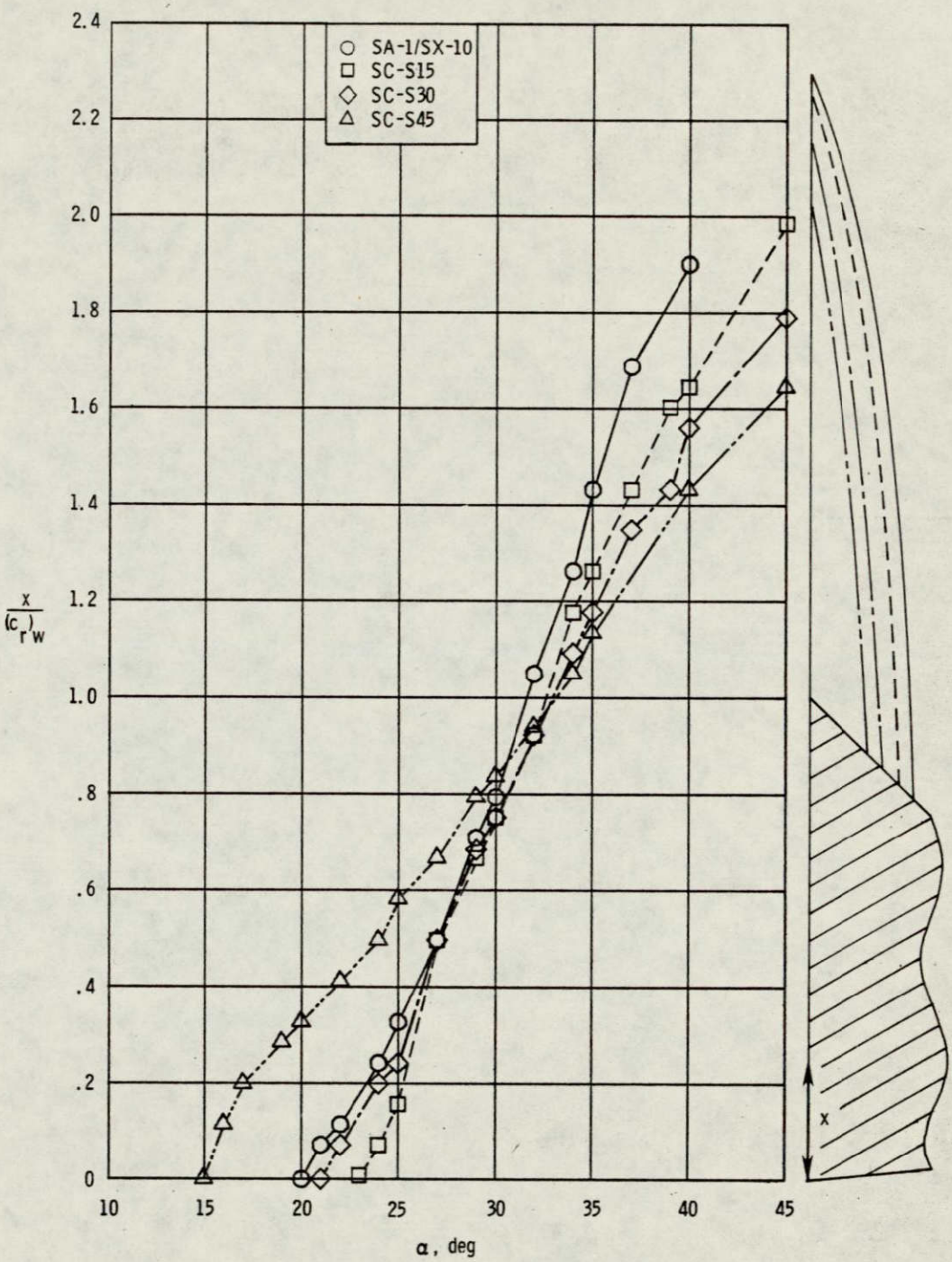

(b) Strake vortex breakdown position.

Figure 31.- Continued.

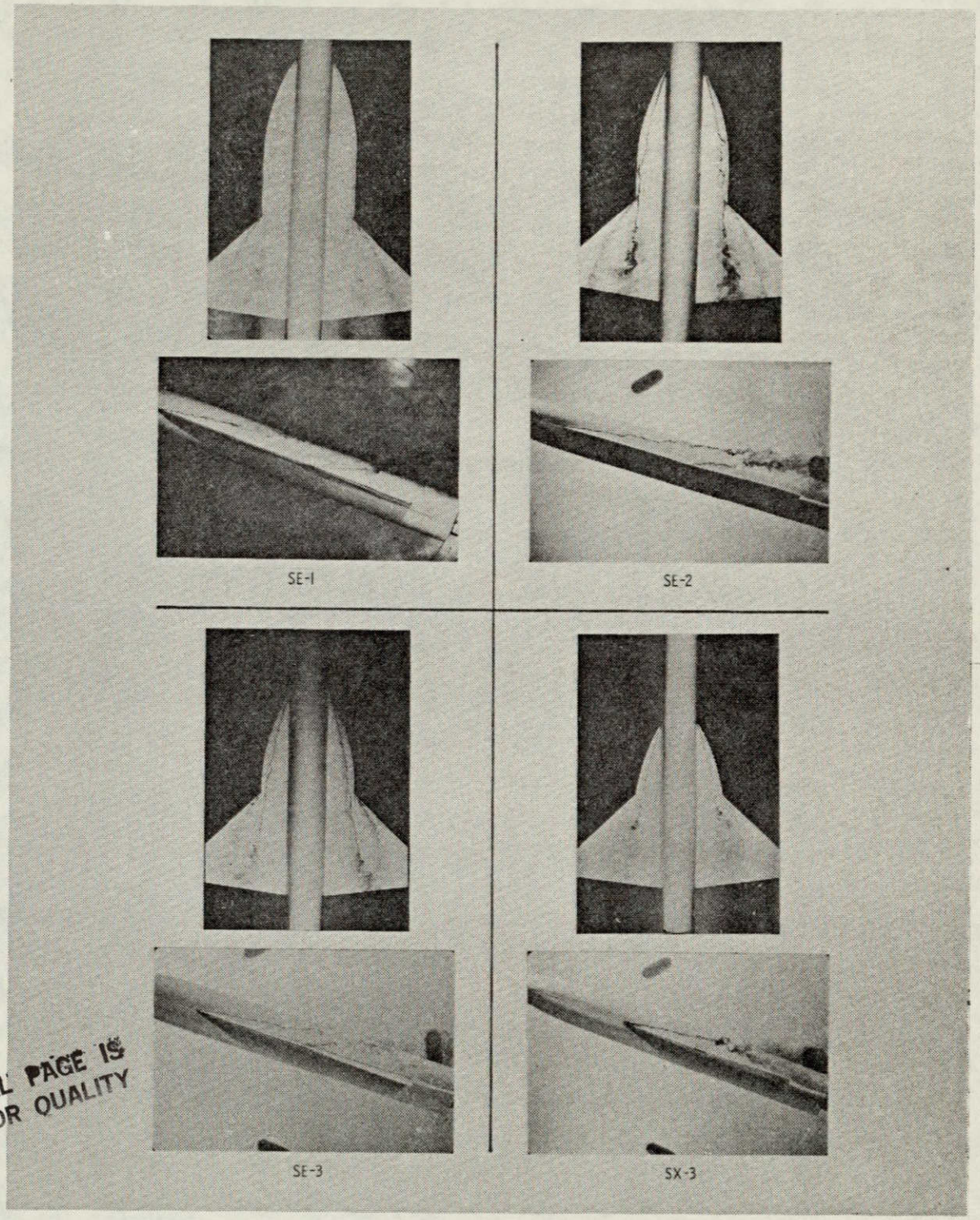

ORIGINAL PAGE IS
OF POOR QUALITY

(a) Strake and wing vortex patterns at $\alpha = 20^{\circ}$.

Figure 32.- SE series water tunnel photographs and strake vortex breakdown characteristics.

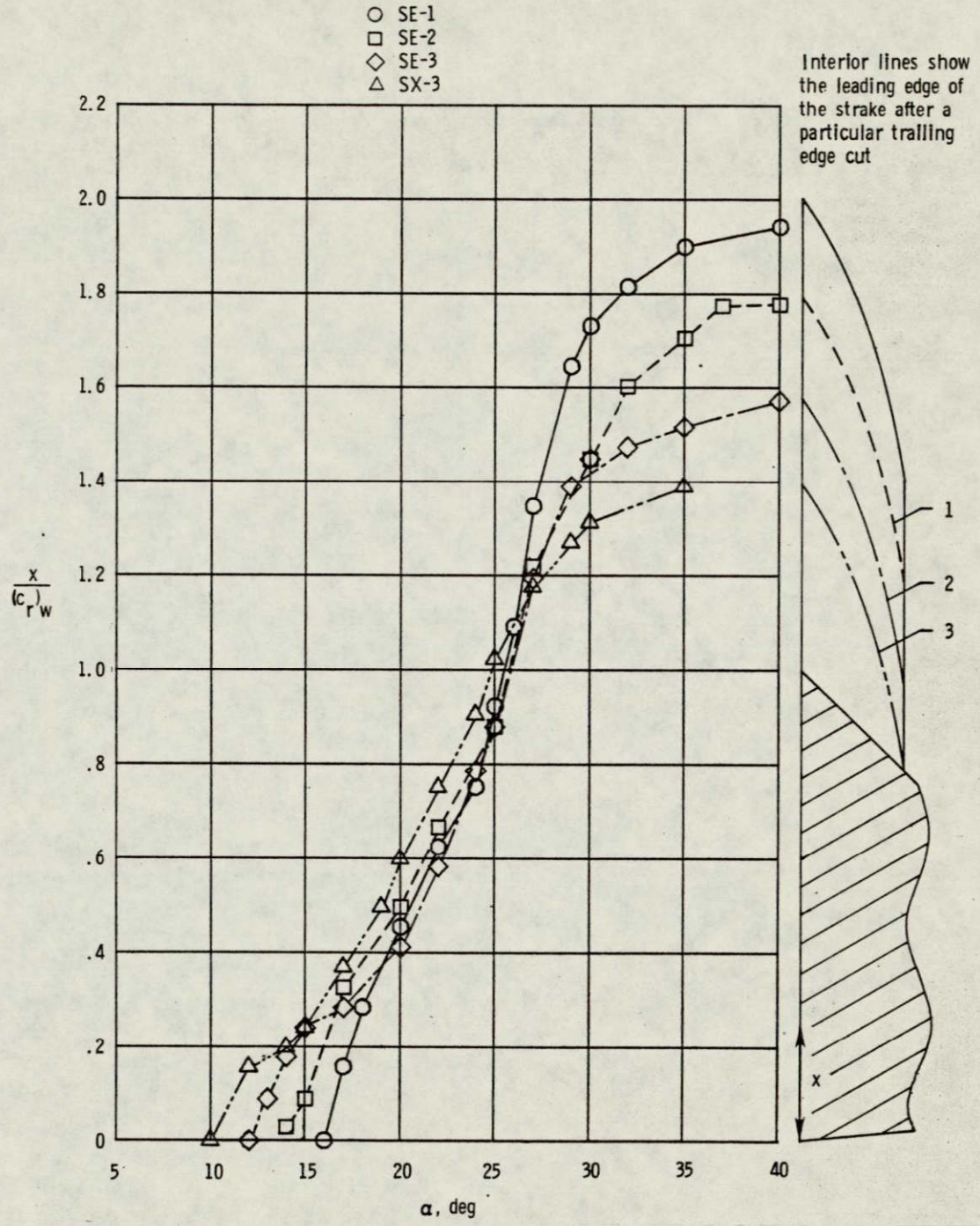

(b) Strake vortex breakdown position.

Figure 32. Continued.

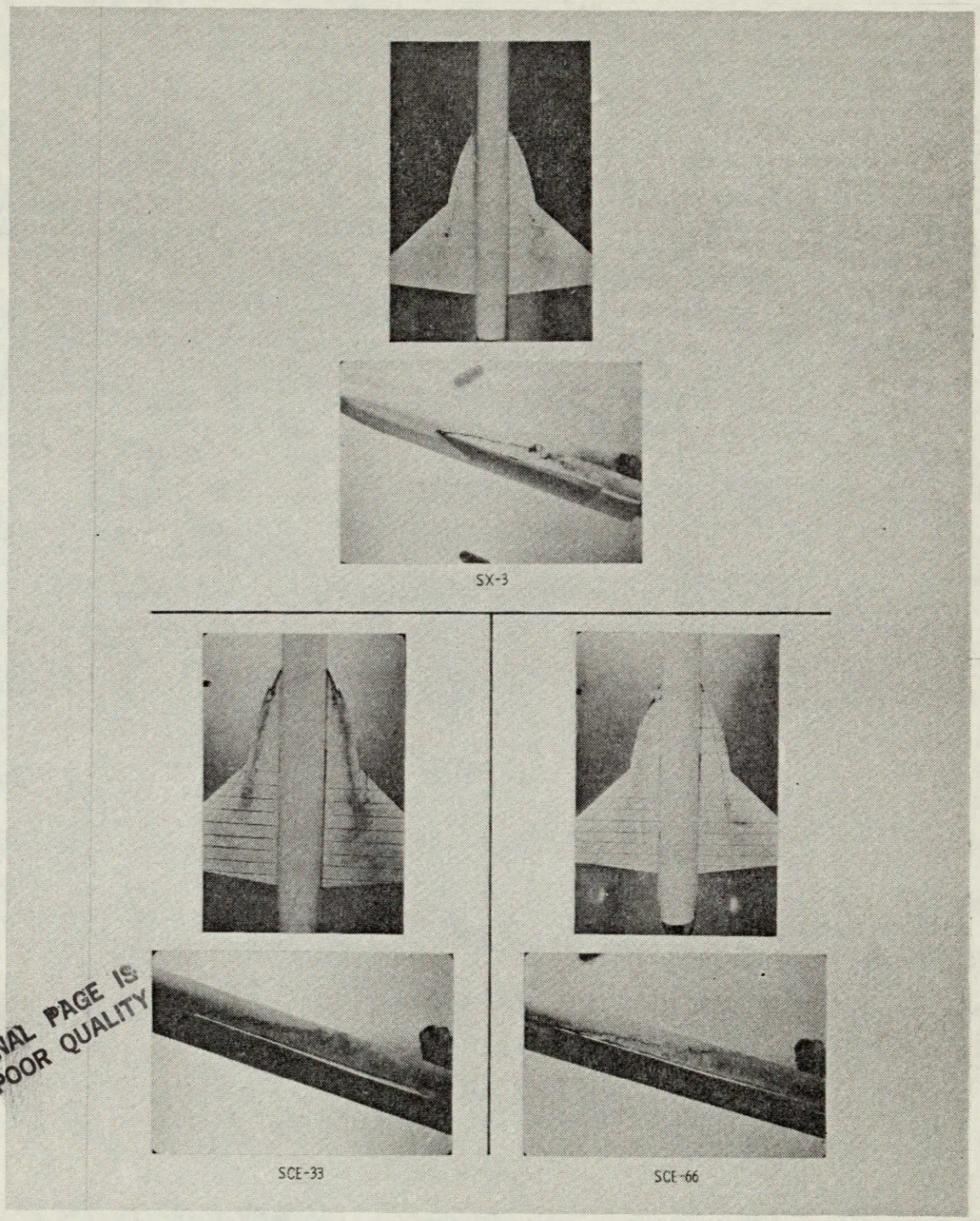

ORIGINAL PAGE IS
OF POOR QUALITY

(a) Strake and wing vortex patterns at $\alpha = 20^{\circ}$.

Figure 33.- Snagged strake series water tunnel photographs and strake vortex breakdown characteristics.

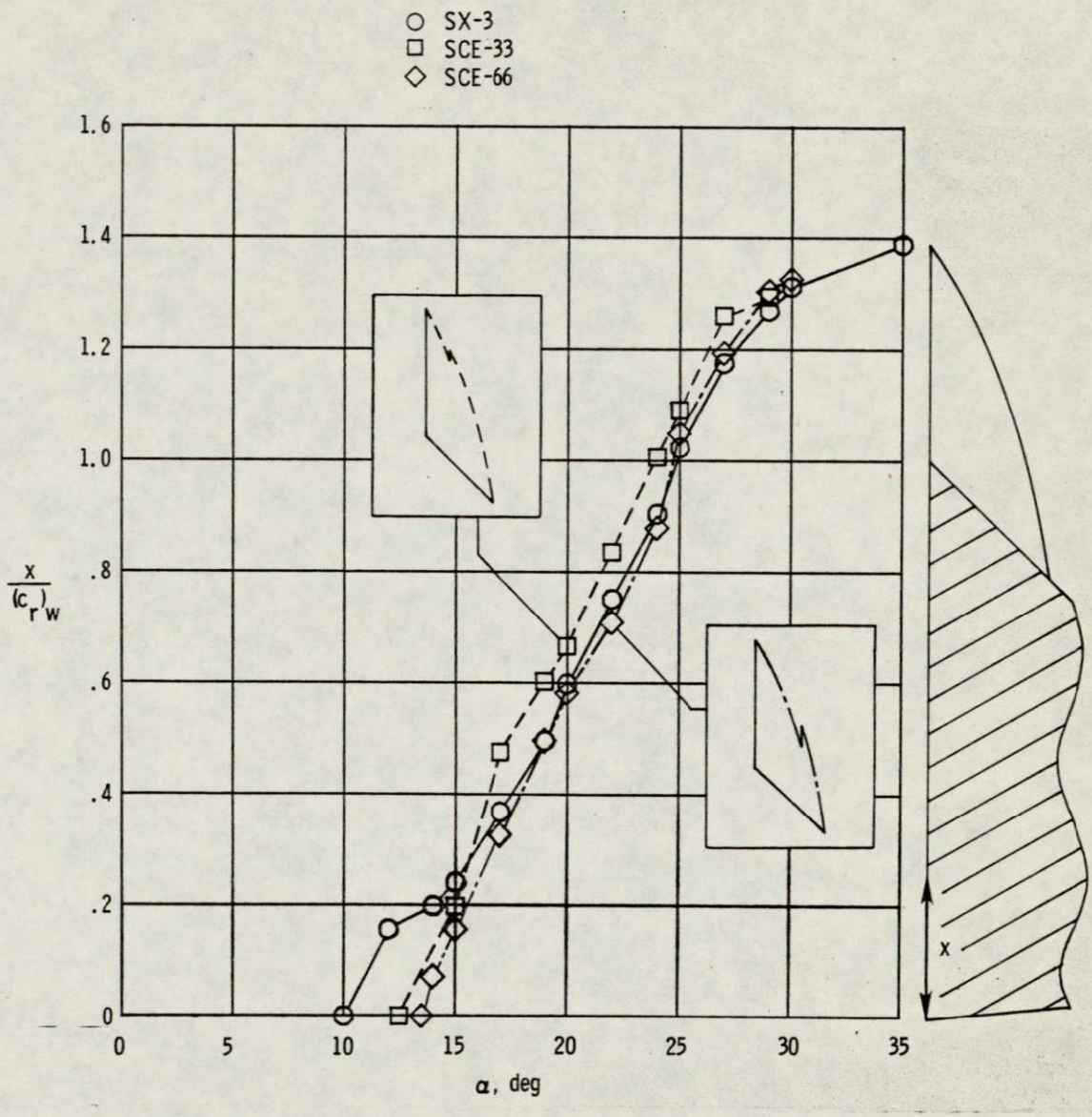

(b) Strake vortex breakdown position.

Figure 33.- Continued.

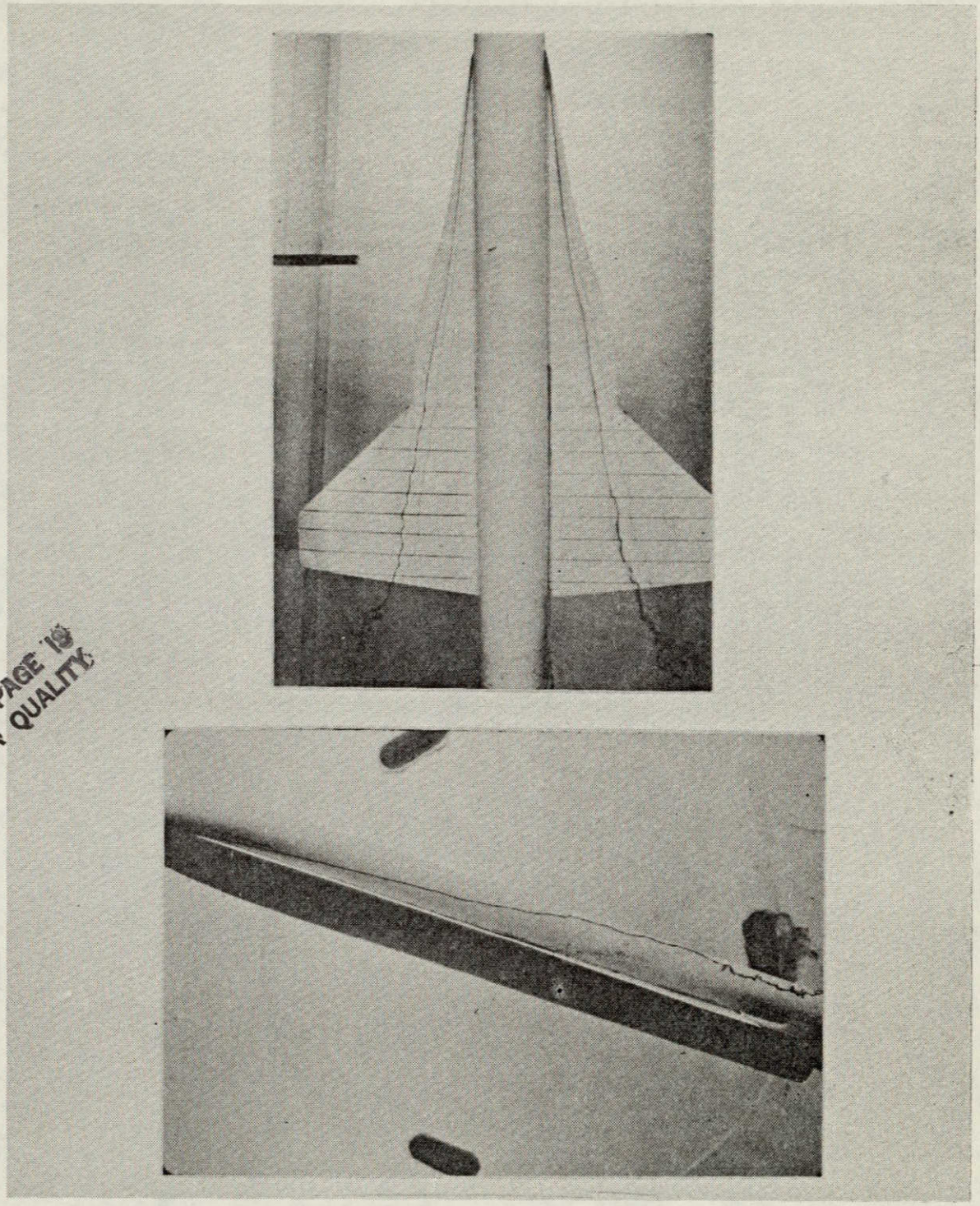

ORIGINAL PAGE IS
OF POOR QUALITY

(a) Strake and wing vortex patterns at $\alpha = 20^{\circ}$.

Figure 34.- Strake III of ref. 7 water tunnel photograph and strake vortex breakdown characteristics.

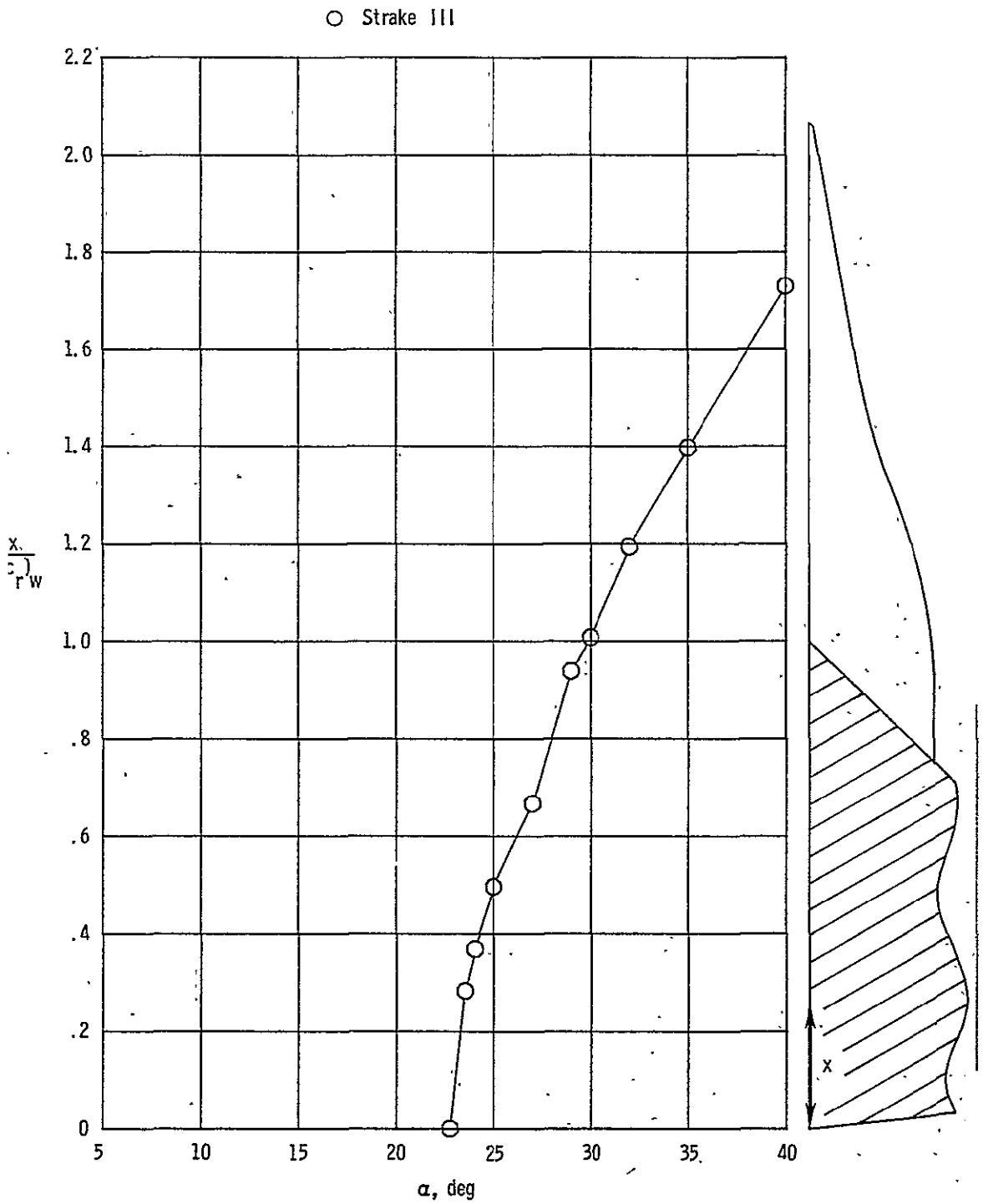

(b) Strake vortex breakdown position.

Figure 34.- Continued.

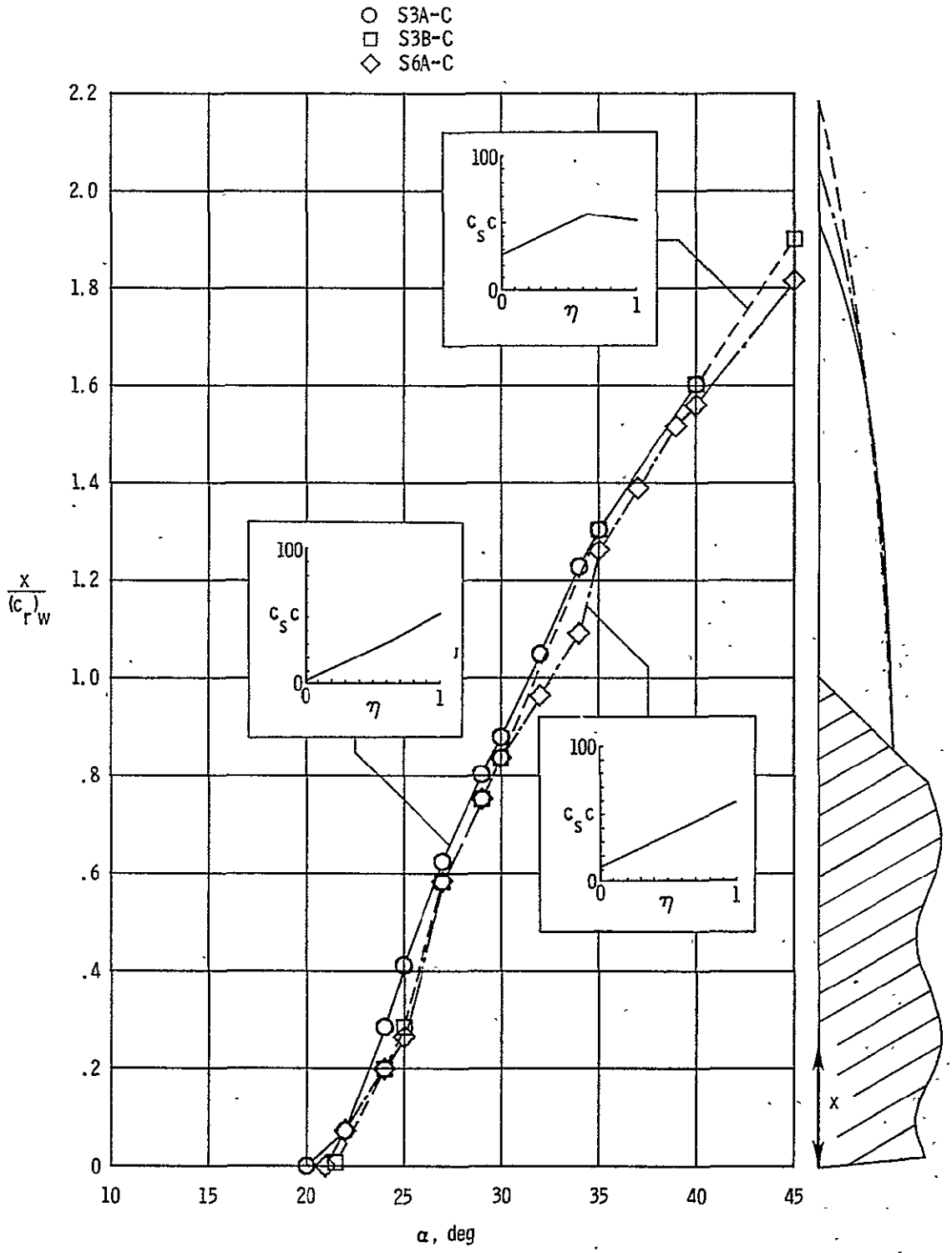

(a) Groups 3 and 6.

Figure 35.- Summary of strake vortex breakdown position for the "better" strakes from the suction distribution group study.

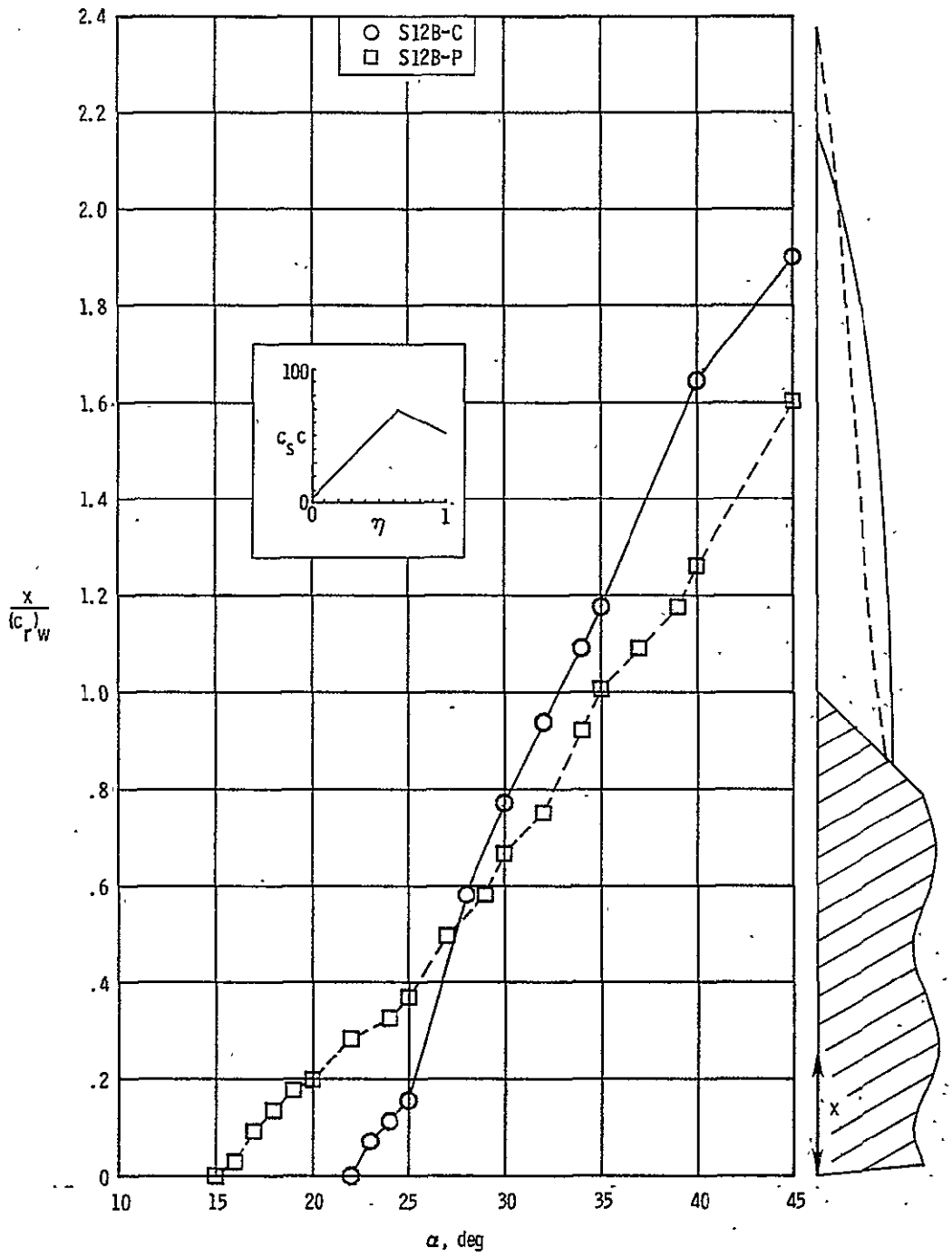

(b) Effect of pressure specification on group 12 strakes.

Figure 35.- Continued

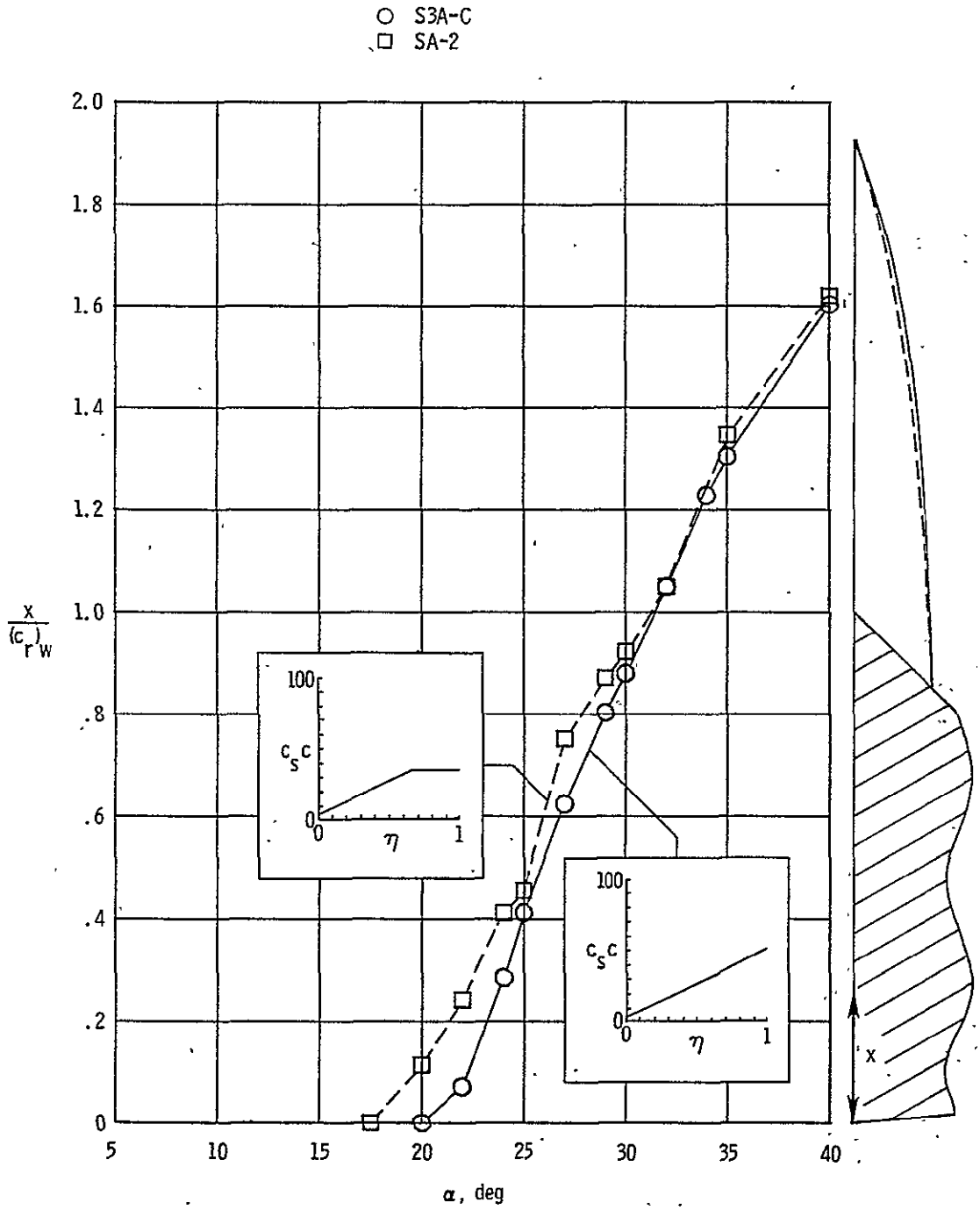

Figure 36.- Effect of suction distribution on vortex breakdown position for two strakes with $[\ell/(b/2)]_s = 7.0$ and $[(b/2)_s/(b/2)_w]_{exp} = 0.212$.

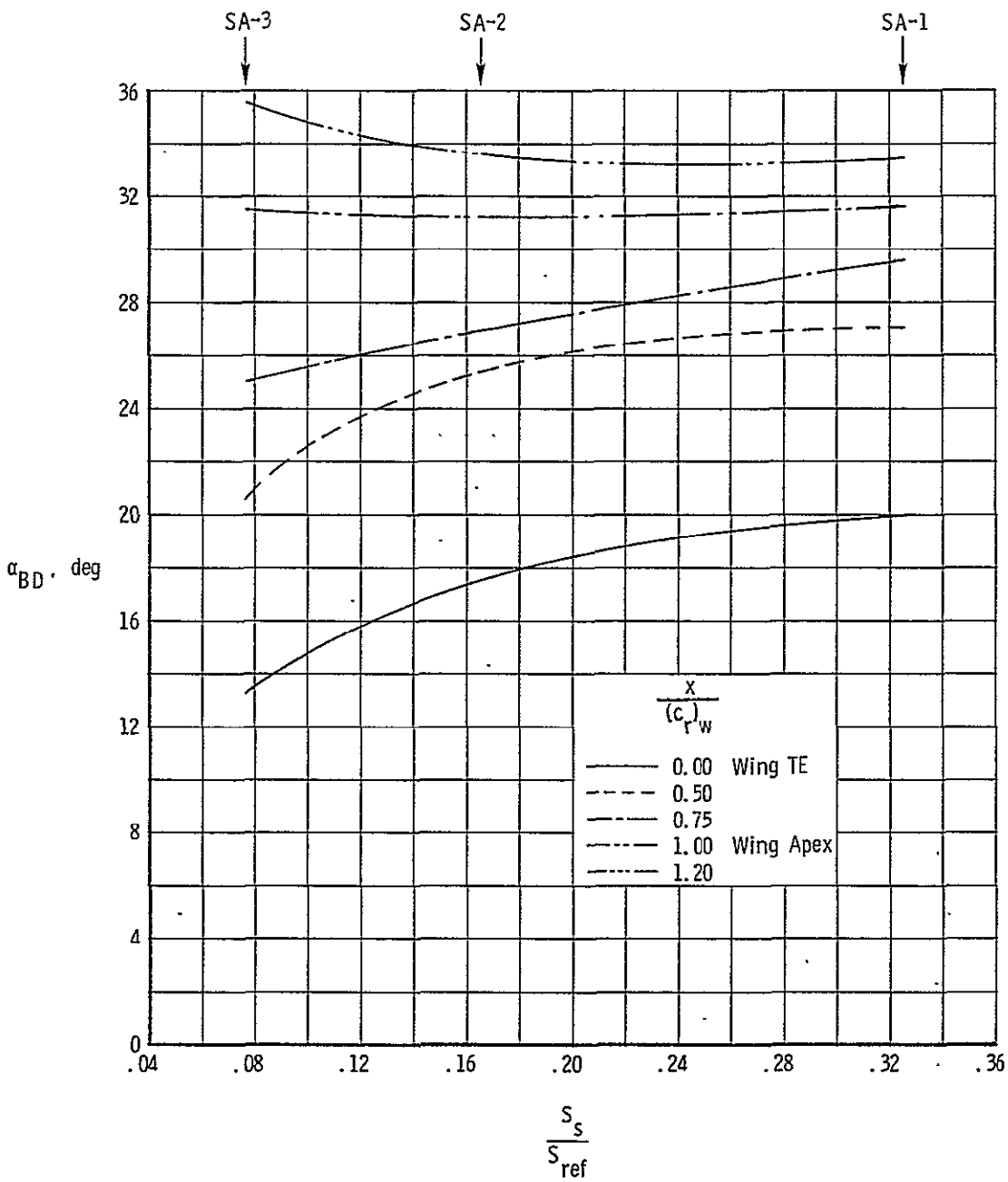

Figure 37.- Summary of vortex breakdown characteristics for area scaling: SA series.

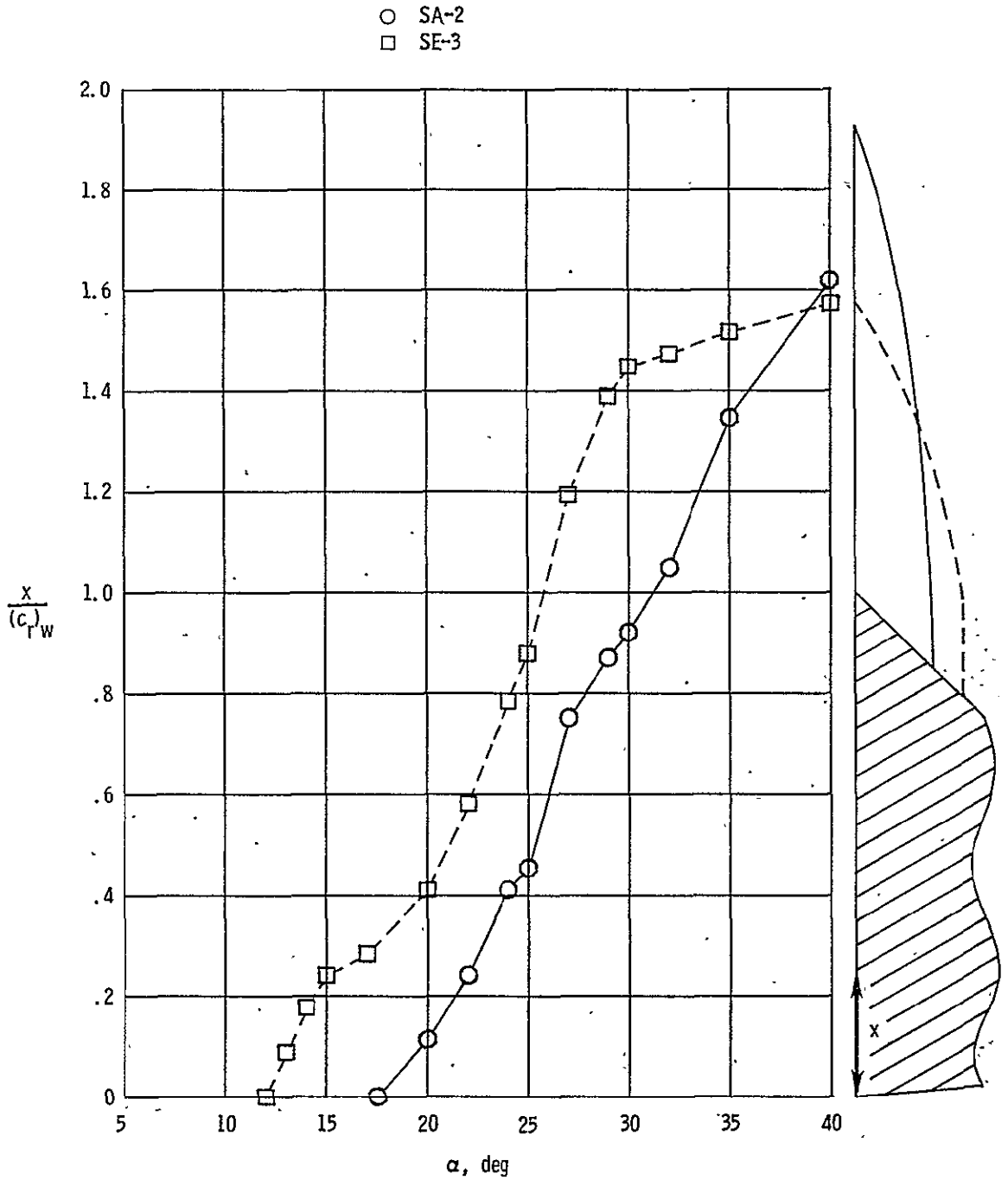

(a) $R_a = 0.166$.

Figure 38.- Effect of strake geometry on vortex breakdown position for a fixed ratio of strake area to wing reference area.

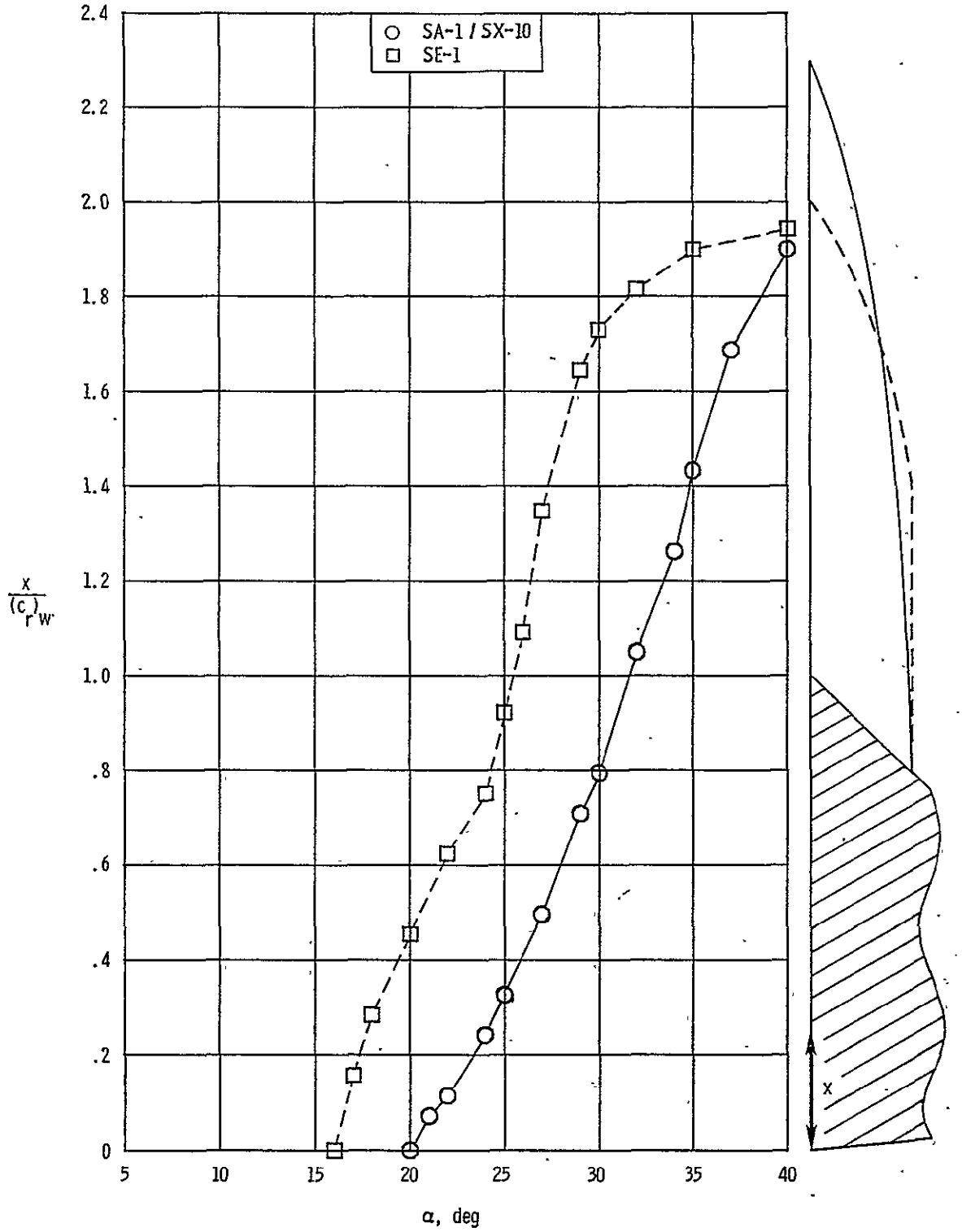

(b) $R_a = 0.325$

Figure 38.- Continued.

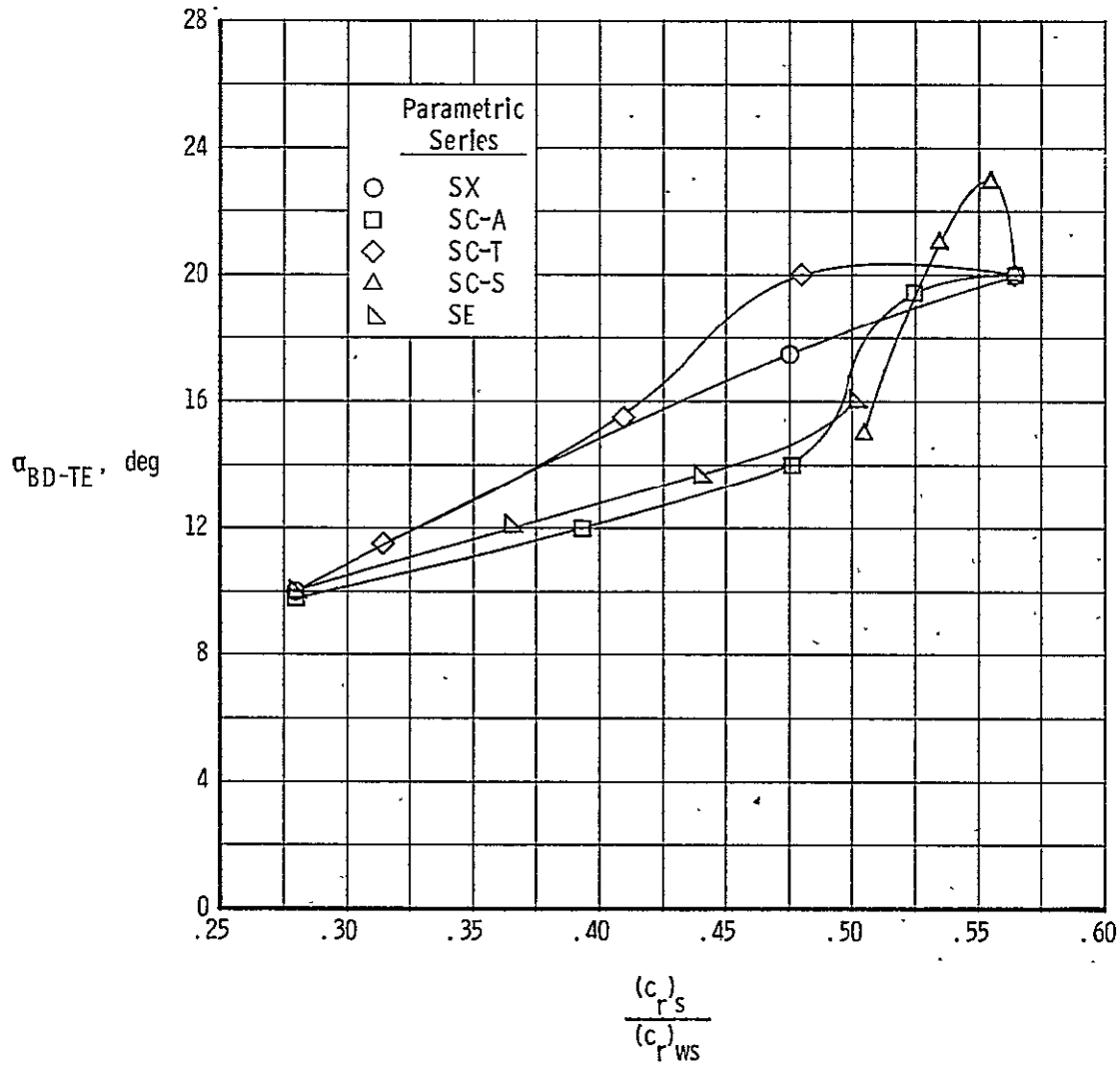

Figure 39.- Summary of trailing edge breakdown angle for the various chord modification techniques.

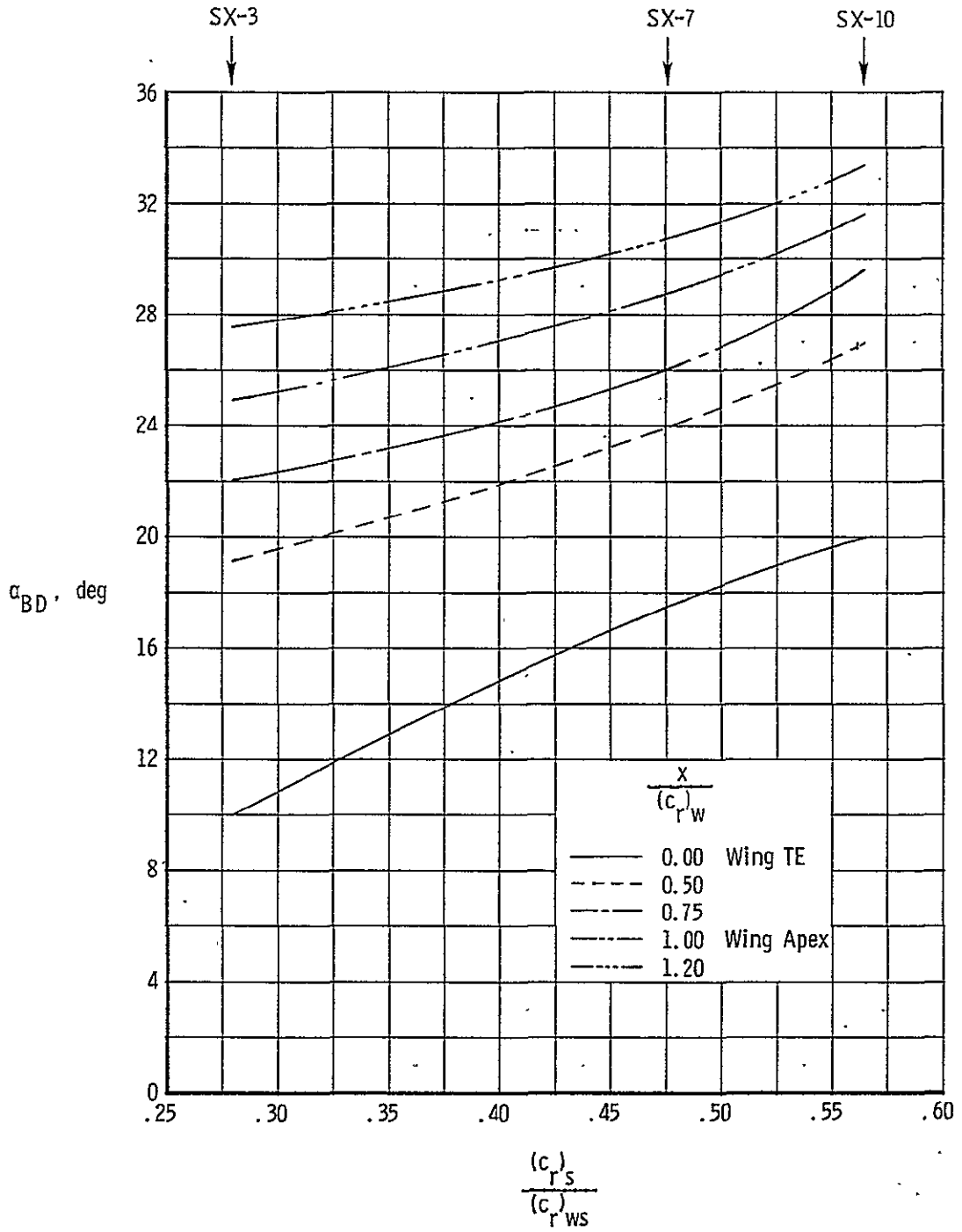

Figure 40.- Summary of strake vortex breakdown characteristics for chord modification by chordwise scaling: SX series.

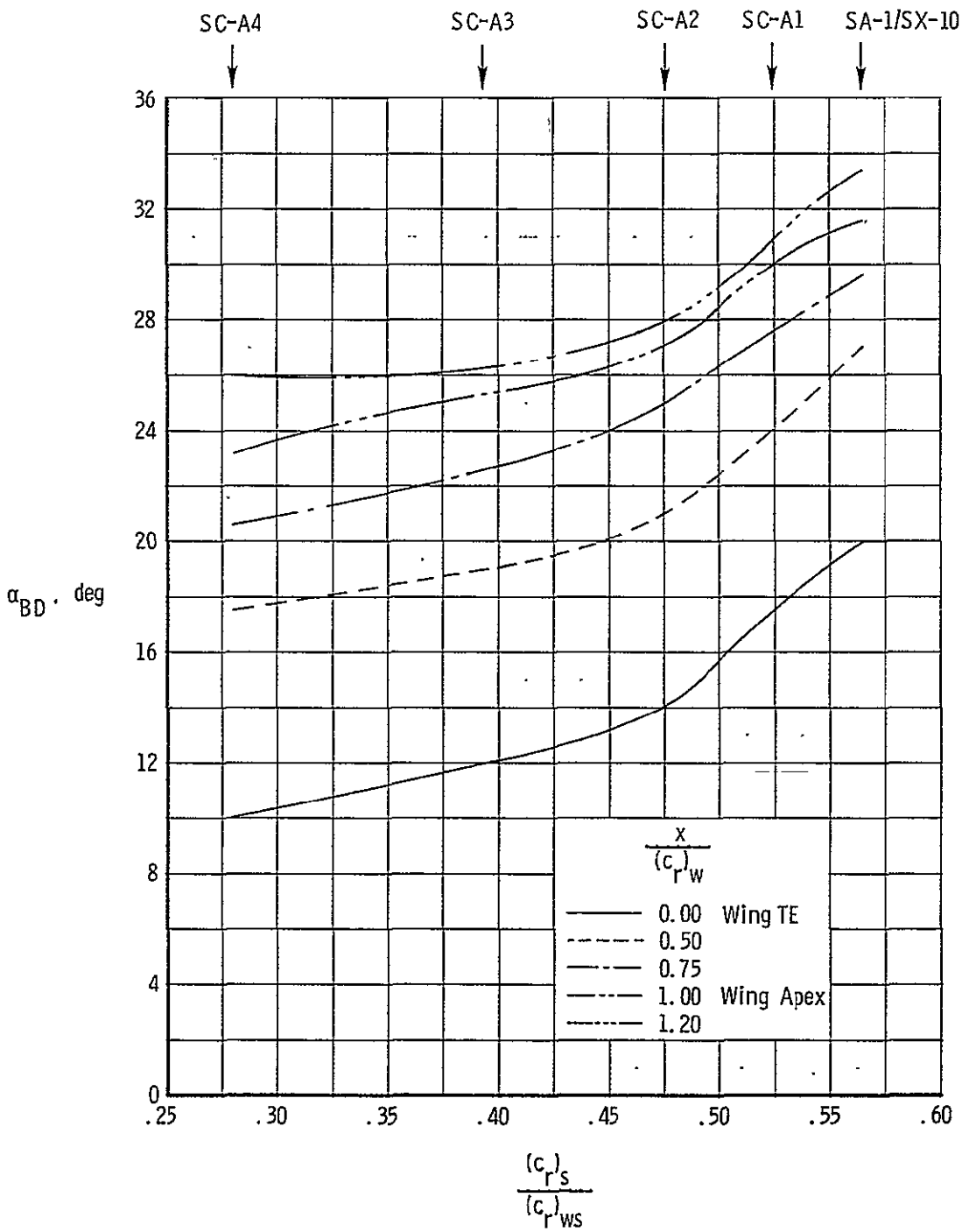

Figure 41.- Summary of strake vortex breakdown characteristics for chord modification by apex cutting: SC-A series.

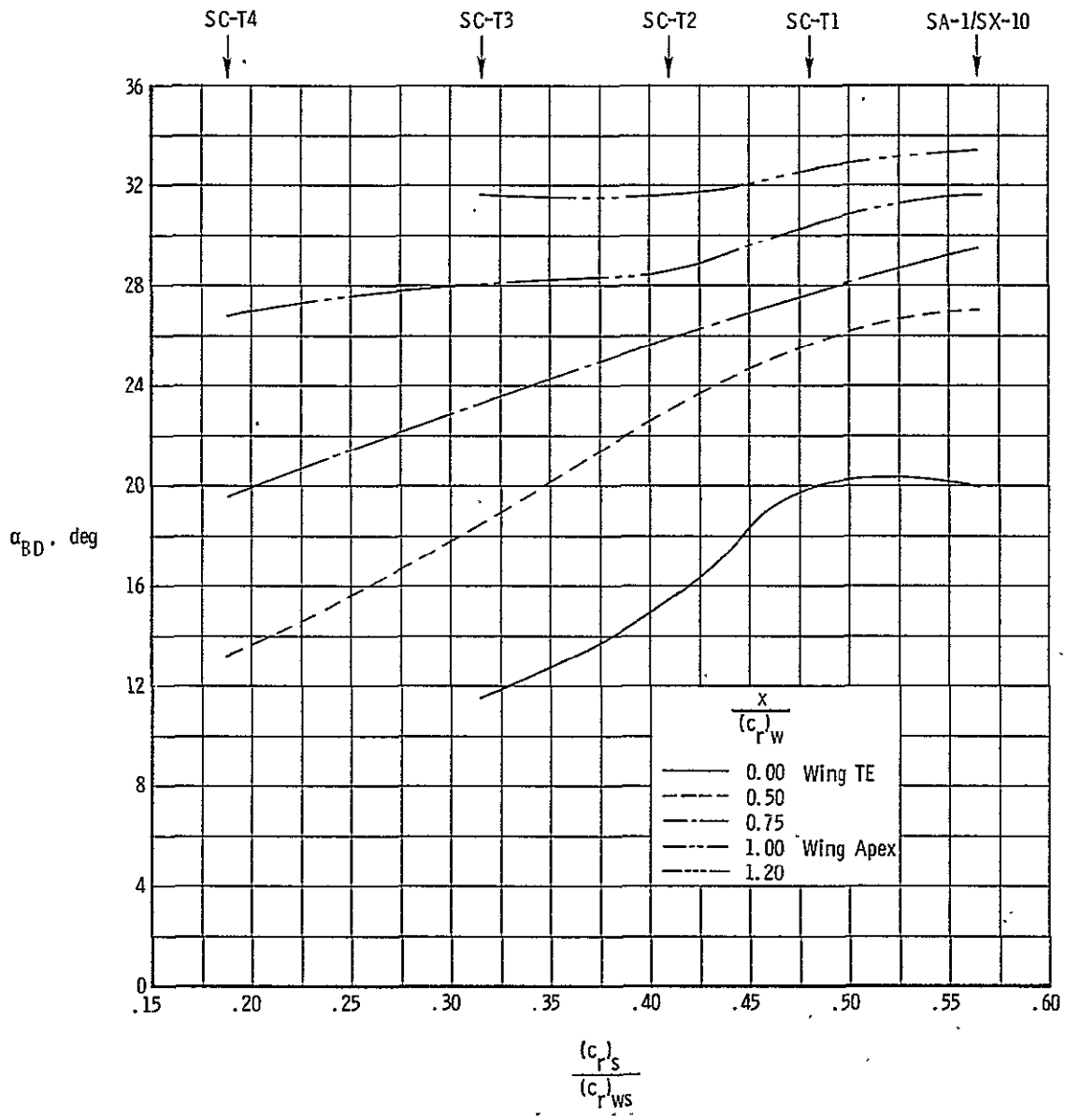

Figure 42.- Summary of strake vortex breakdown characteristics for chord modification by trailing edge cutting: SC-T series.

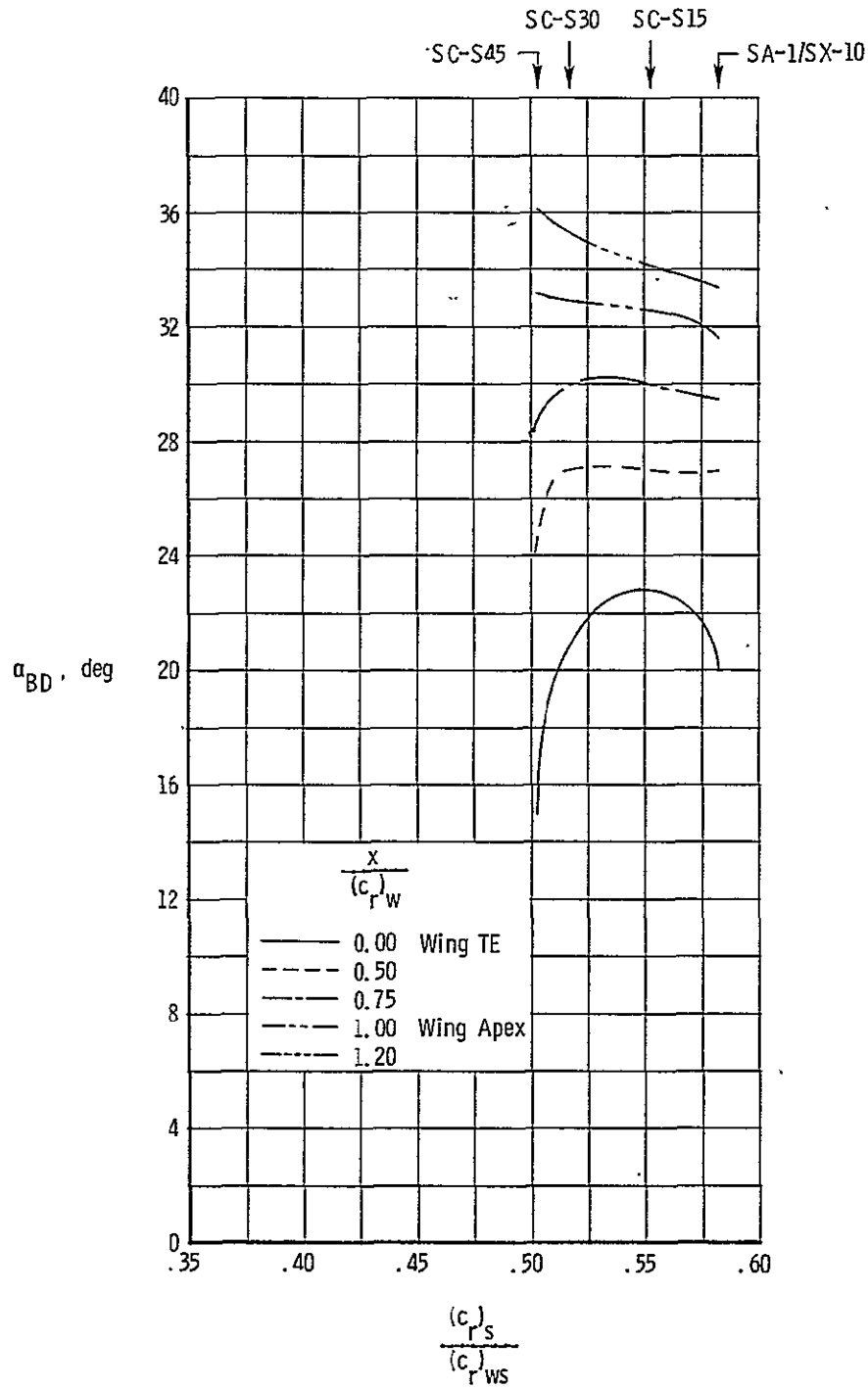

Figure 43.- Summary of strake vortex breakdown characteristics for chord modification by spanwise cutting: SC-S series.

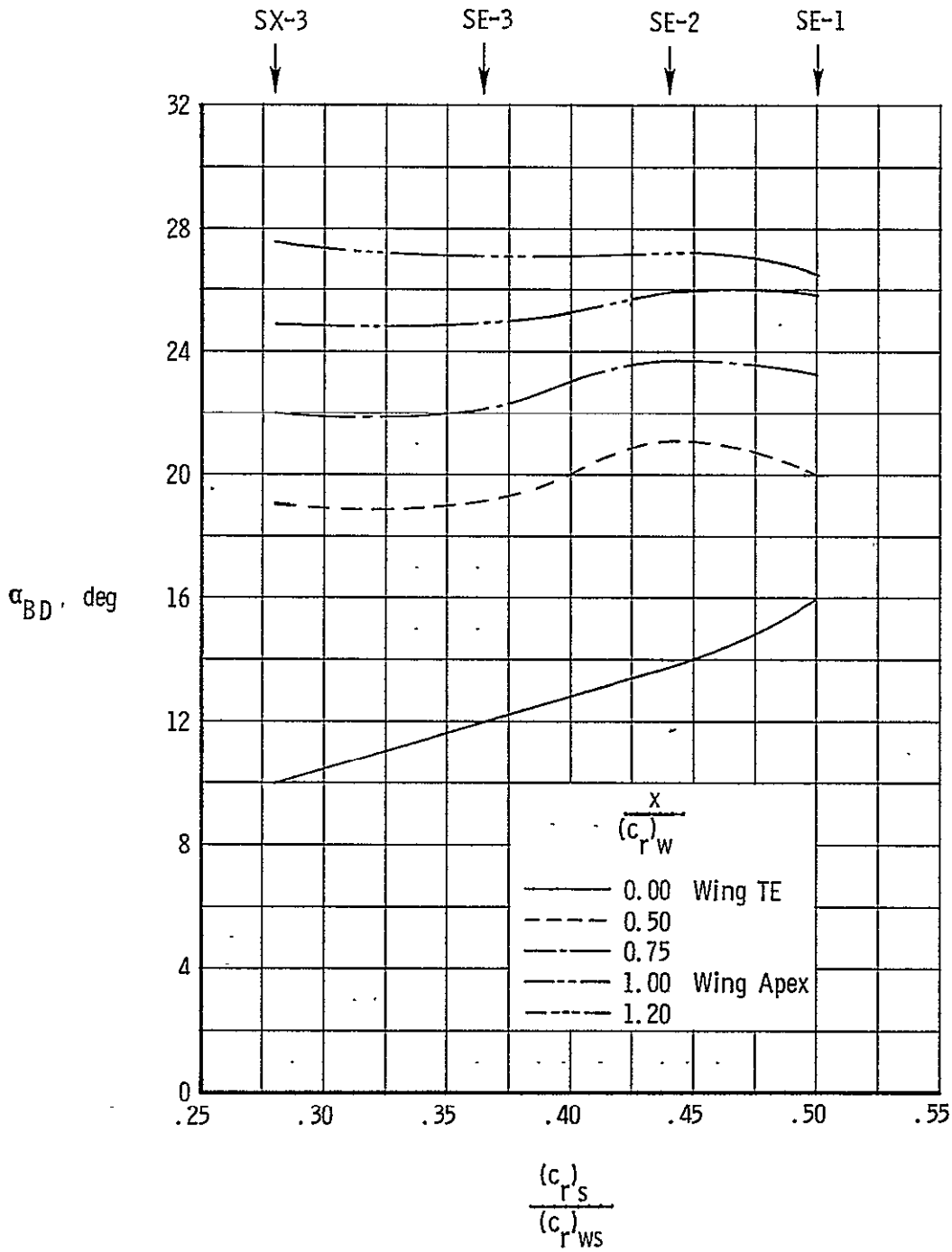

Figure 44.- Summary of strake vortex breakdown characteristics for chord modification by addition of trailing edge area/side edge length: SE series.

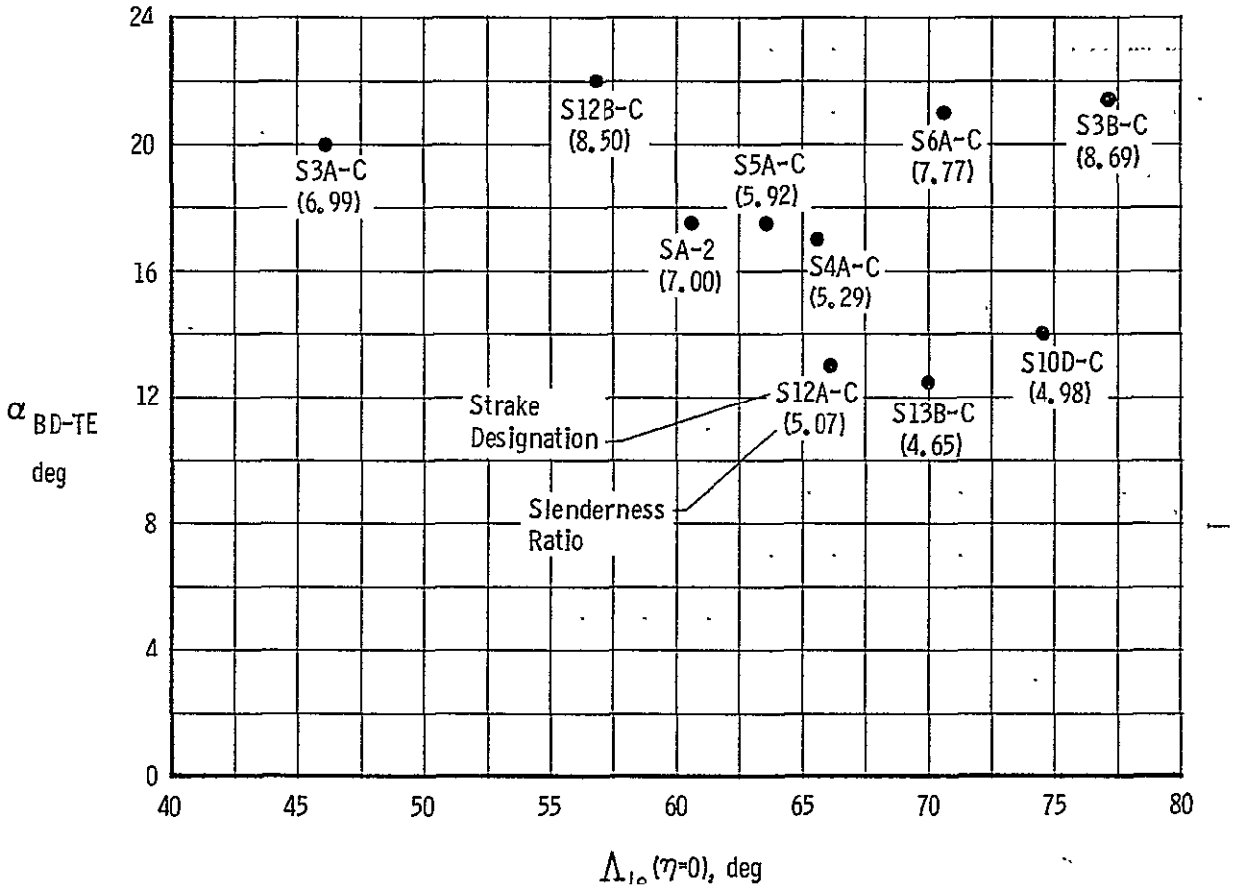

Figure 45.- Effect of slenderness ratio on wing trailing edge breakdown angle for gothic strakes with $[(b/2)_s/(b/2)_w]_{exp} = 0.212$.

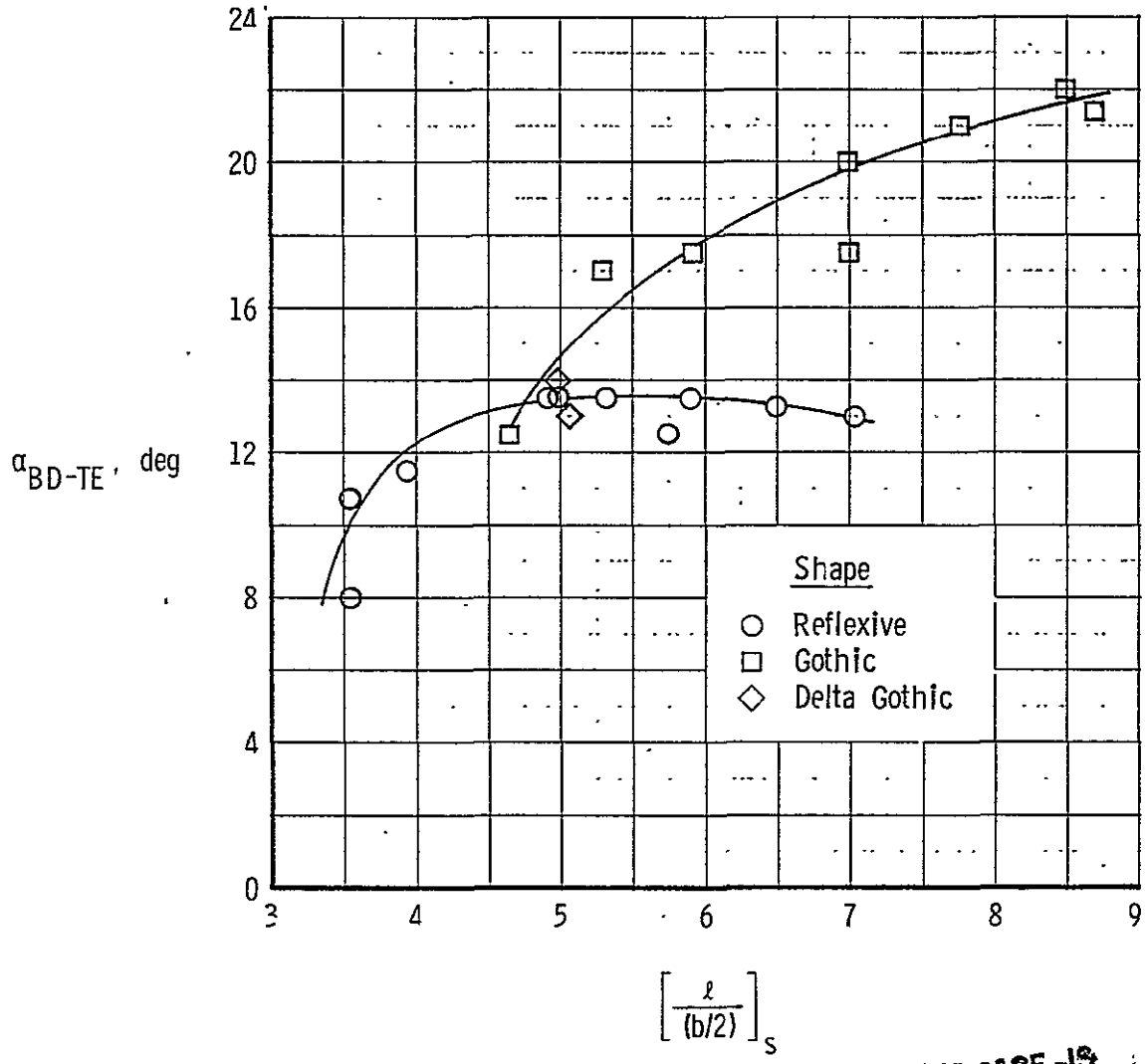

ORIGINAL PAGE IS
OF POOR QUALITY

Figure 46.- Effect of strake shape on wing trailing edge breakdown angle for a strake semispan of $[(b/2)_s/(b/2)_w]_{exp} = 0.212$.

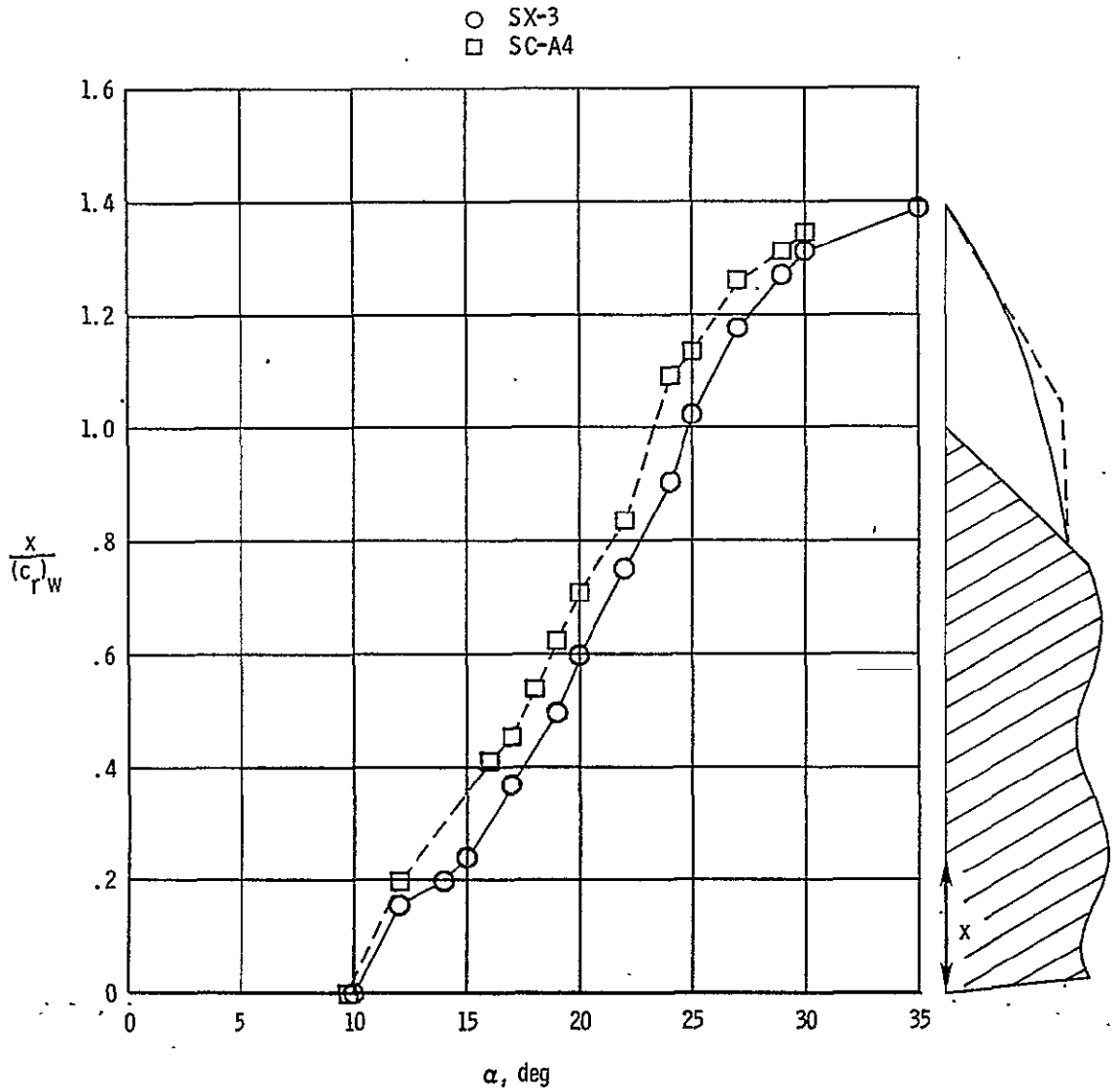

ORIGINAL PAGE IS
OF POOR QUALITY

(a) $\frac{\ell}{(b/2)} \approx 2.78$.

Figure 47.- Effect of strake geometry on vortex breakdown position for a fixed slenderness ratio.

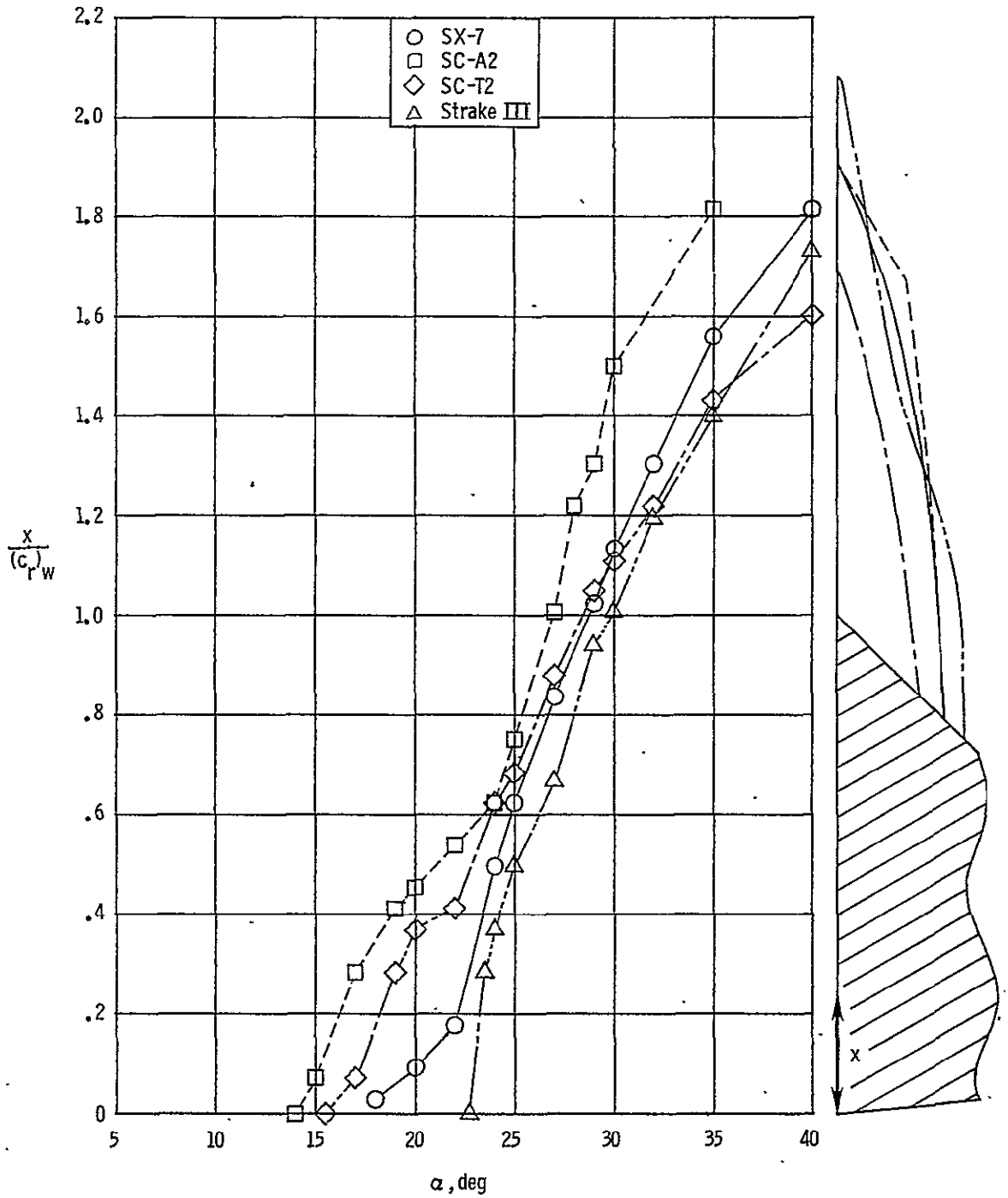

(b) $\frac{\ell}{(b/2)} \approx 5.2$.

Figure 47.- Continued.

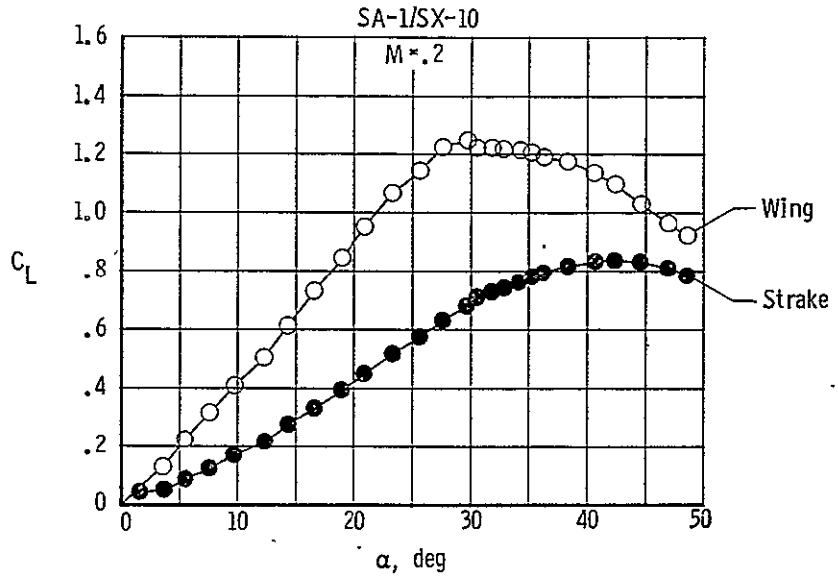

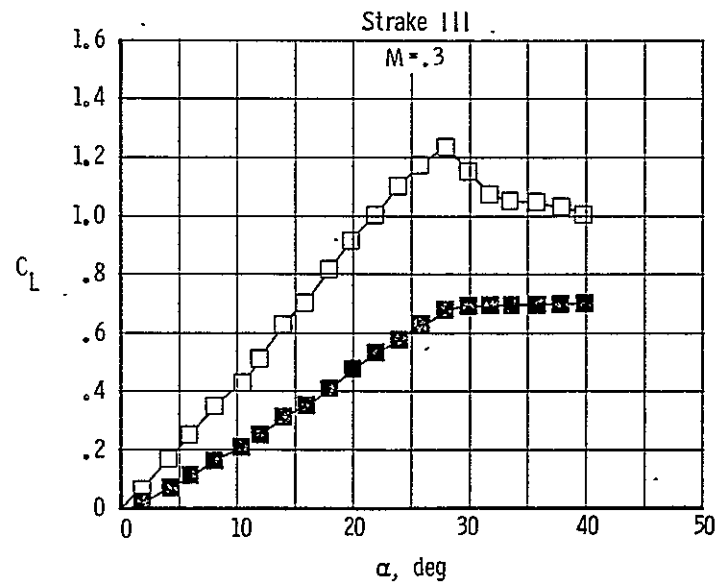

(a) Component loads for wing and strake

Figure 48.- Wind tunnel force and water tunnel vortex breakdown data for two wing-strake configurations; M = .2, .3 .

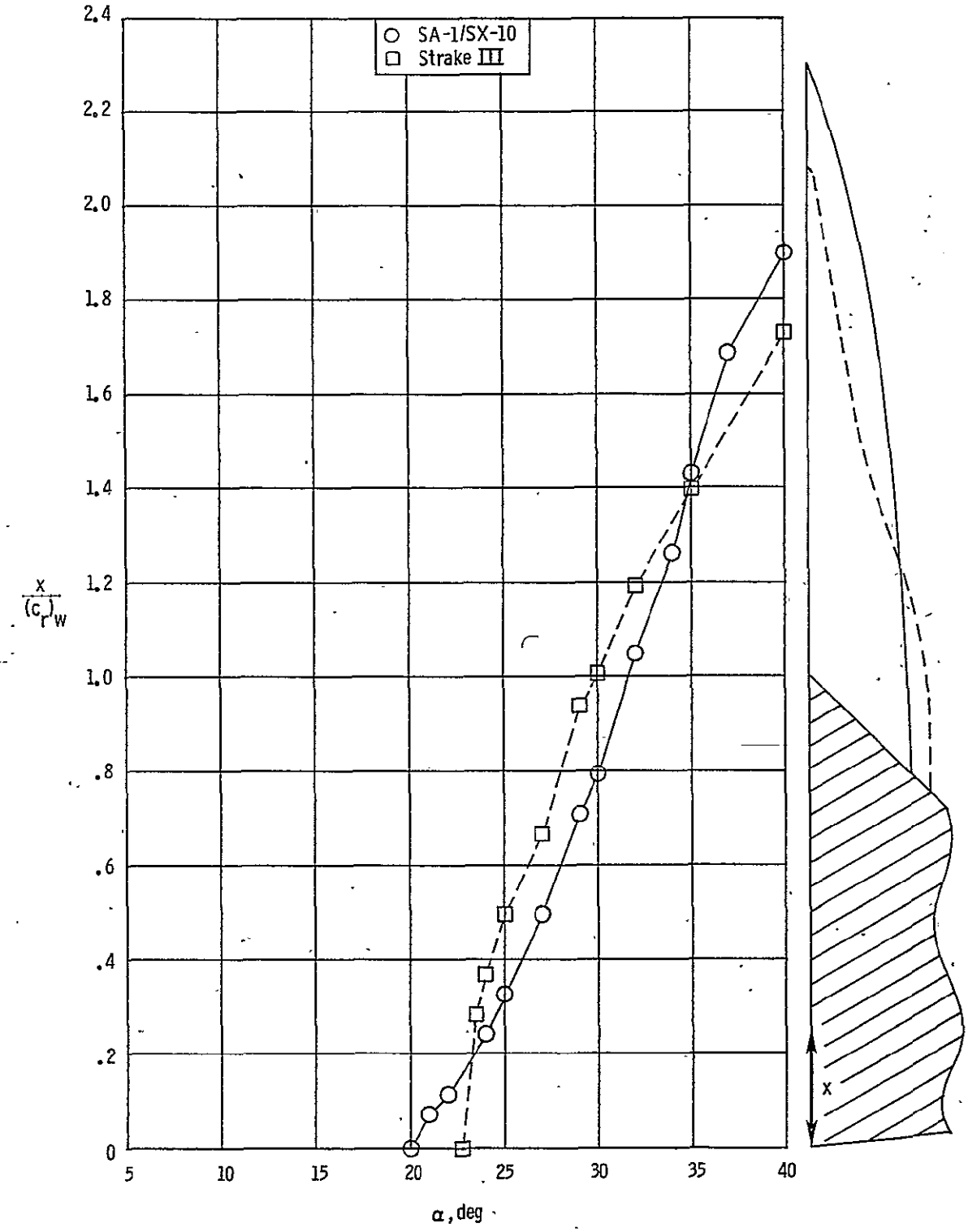

(b) Strake vortex breakdown position.

Figure 48.- Continued.